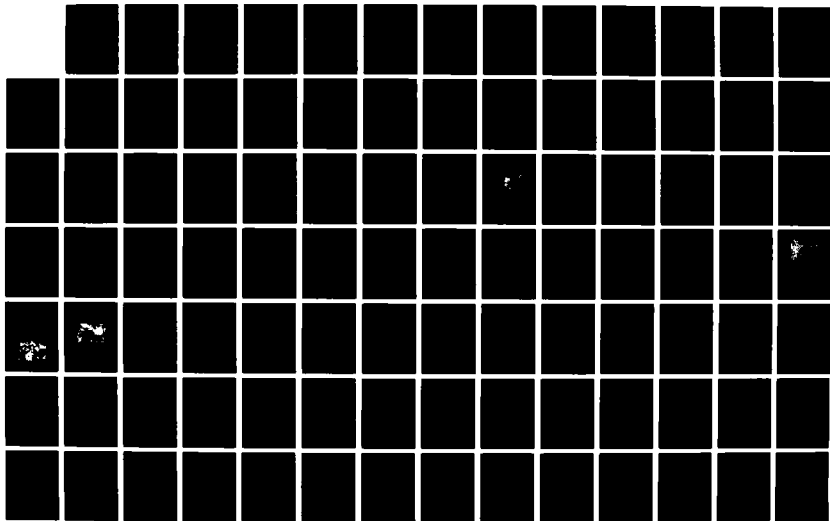
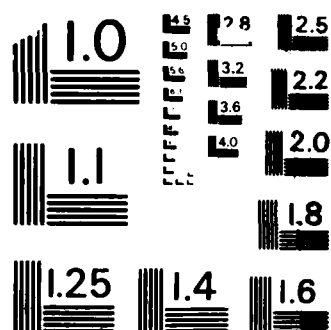


NO-A179 211 THE CATHODOLUMINESCENCE OF CLEARTRAN: A NOVEL FORM OF 1/2
POLYCRYSTALLINE ZNS(U) AIR FORCE INST OF TECH
WRIGHT-PATTERSON AFB OH SCHOOL OF ENGINEERING
UNCLASSIFIED J G VARNI DEC 86 AFIT/DS/ENP/86-2 F/G 28/12 NL





MICROCOPY RESOLUTION TEST CHART
NATIONAL BUREAU OF STANDARDS-1963-A

AD-A179 211



THE CATHODOLUMINESCENCE OF CLEARTRAN:
A NOVEL FORM OF POLYCRYSTALLINE ZnS

DISSERTATION

Jamie G. G. Varni
Captain, USAF

This document has been approved
for public release and sale; its
distribution is unlimited.

DEPARTMENT OF THE AIR FORCE
AIR UNIVERSITY

AIR FORCE INSTITUTE OF TECHNOLOGY

Wright-Patterson Air Force Base, Ohio

DTIC
ELECTE
APR 17 1987

87 4 16 06

AFIT/DS/ENP/86-2

THE CATHODOLUMINESCENCE OF CLEARTRAN:
A NOVEL FORM OF POLYCRYSTALLINE ZnS

DISSERTATION

Jamie G. G. Varni
Captain, USAF

AFIT/DS/ENP/86-2

APR 17 1987

Approved for public release; distribution unlimited

THE CATHODOLUMINESCENCE OF CLEARTRAN:
A NOVEL FORM OF POLYCRYSTALLINE ZnS

DISSERTATION

Presented to the Faculty of the School of Engineering
of the Air Force Institute of Technology
In Partial Fulfillment of the
Requirements for the Degree of
Doctor of Philosophy



Jamie G. G. Varni, B.S., M.S.
Captain, USAF

December 1986

THE CATHODOLUMINESCENCE OF CLEARTRAN:
A NOVEL FORM OF POLYCRYSTALLINE ZnS

Jamie G. G. Varni, B.S., M.S.

Captain, USAF

Approved:

<u>Robert L Hengshol</u>	<u>12/15/86</u>
Chairman	
<u>Don B. Roh</u>	<u>12/15/86</u>
<u>E. E. ...</u>	<u>12/15/86</u>
<u>John Jones Jr</u>	<u>12/15/86</u>

Accepted:

J. Strzemieniecki 15 Dec 86
Dean, School of Engineering

Preface

The purpose of the present work is to investigate a novel form of polycrystalline chemical-vapor-deposited ZnS: CleartranTM. The optical properties of Cleartran are vastly superior to conventional cvd ZnS. This suggests that the concentration of impurities in the individual crystals of which Cleartran is made must be very low and that the crystalline quality of the material must be high.

Many people helped me during the course of this work. I would like to thank Dr. Robert L. Hengehold, the chairman of my research committee, for holding my nose to the grindstone. I am grateful to Dr. Raymond L. Taylor and Mr. Mark Lefebvre of CVD Inc. for providing the samples of Cleartran I examined, and to Mr. Bud Graves and Mr. Douglas Wolf of the University of Dayton Research Institute for their invaluable aid in performing x-ray diffraction and spark-source mass spectrometry on my samples. I would like to thank Mr. Donald Evans of the Air Force Materials Laboratory and Dr. Won B. Roh of the Air Force Institute of Technology for many valuable discussions and comments. Last, but never least, I would like to offer my profoundest thanks to the Laboratory Staff of the Department of Engineering Physics: Mr. Curtis Atnipp, Mr. Ron Gabriel, and Mr. George Gergal. Without their constant aid none of this would have been possible.

Jamie G. G. Varni

Table of Contents

	Page
Preface.	iii
List of Figures.	vi
List of Tables	x
List of Symbols.	xi
Abstract	xiii
I. Introduction	1
Background	1
Problem Statement.	7
Sequence of Events	9
II. Theory and Summary of Previous Work.	11
Crystallography of ZnS	11
Crystal Growth Techniques.	15
The Energy Bands of ZnS.	20
Cathodoluminescence.	22
Effect of Temperature on the Band Gap.	27
Review of Topical Literature	31
III. Experimental	35
Sample Information	35
Photomicroscopy.	37
X-ray Diffraction.	41
Spark-source Mass Spectrometry	42
Experimental Systems	42
Overview	42
Vacuum System.	45
Cryogenic Transfer System.	47
Temperature Control System	48
Sample Handling.	49
Electron Gun	51
Optical System	54
Signal Detection and Processing System	55
IV. Results and Discussion	59
Sequence of Presentation	59
Single Crystal ZnS (Eagle-Picher).	59

Spot to Spot Variations.	63
Sample to Sample Variations.	64
Temperature Variation.	64
ZnS Platelets.	64
Spot to Spot Variations.	68
Sample to Sample Variations.	69
Temperature Variation.	69
Raytheon cvd ZnS	69
Spot to Spot Variations.	71
Sample to Sample Variations.	71
Temperature Variation.	71
CVD Inc. cvd ZnS	72
Spot to Spot Variations.	74
Sample to Sample Variations.	77
Temperature Variation.	77
Cleartran.	79
Spot to Spot Variations.	91
Sample to Sample Variations.	94
Temperature Variation.	98
Comparison of the Luminescent Response of the	
Forms of ZnS	103
Observed Emissions Between 300 nm and 800 nm .	107
Single Crystal ZnS (Eagle-Picher).	108
ZnS Platelets.	109
Raytheon cvd ZnS	110
CVD Inc. cvd ZnS	110
Cleartran.	111
Temperature Dependence of the Emission Edge. .	121
V. Conclusions and Recommendations.	126
Appendix: Data Manipulation Programs	130
Bibliography	145
Vita	159

List of Figures

Figure	Page
1. Transmittance of 5 mm thick sample of cvd ZnS . .	3
2. Transmission curves of Cleartran and cvd ZnS. . .	6
3. Effects of rain erosion on the transmission of Cleartran	8
4. The face-centered cubic lattice	12
5. The zincblende structure.	12
6. The close-packed hexagonal lattice.	13
7. The wurtzite structure.	13
8. Packing sequence of zincblende and wurtzite . . .	14
9. A reaction system for chemical vapor deposition of ZnS.	17
10. The schematic of a hot isostatic pressing (HIP) unit.	19
11. The energy band diagrams for the cubic and hexagonal forms of ZnS.	21
12. Possible radiant transitions in semiconductors. .	23
13. The Kanaya-Okayama range equation for 2 keV electrons in ZnS.	26
14. The surface of Raytheon1 at a magnification of 250	38
15. The surface of CVD1 at a magnification of 250 . .	38
16. The surface of CVD2 at a magnification of 250 . .	39
17. The surface of Cleartran1 at a magnification of 250	39
18. The surface of Cleartran2 at a magnification of 250	40
19. A schematic of the experiment	43
20. The main vacuum chamber	44

21.	The cryogenic transfer system	46
22.	The sample finger	50
23.	The Superior Electronics nude electron gun.	52
24.	The Faraday cup	53
25.	Spectral response of TN-6122 photodiode	56
26.	The 10 K cathodoluminescence of a sample of Eagle-Picher single crystal ZnS	60
27.	The variation of cathodoluminescence with position on the surface of a sample of Eagle-Picher single crystal ZnS	62
28.	The variation of cathodoluminescence with temperature for $10\text{ K} < T < 100\text{ K}$ on a sample of Eagle-Picher single crystal ZnS.	65
29.	The variation of cathodoluminescence with temperature for $125\text{ K} < T < 300\text{ K}$ on a sample of Eagle-Picher single crystal ZnS.	66
30.	The 10 K cathodoluminescence of a crystal platelet.	67
31.	The 10 K cathodoluminescence of a sample of Raytheon cvd ZnS.	72
32.	The 10 K cathodoluminescence of a sample from the first block of CVD Inc. cvd ZnS	73
33.	The 10 K cathodoluminescence of a sample from the second block of CVD Inc. cvd ZnS.	75
34.	Cathodoluminescence from a region where the visible bands were intense and the near band-edge luminescence was very weak	76
35.	The shift in energy position of the Cu-blue peak with position on the surface of a sample of CVD Inc. cvd ZnS	78
36.	The 10 K cathodoluminescence of an a) side view sample of Cleartran (WC5) and a b) end view sample of Cleartran (WC2)	80
37.	The 10 K cathodoluminescence of a sample of Cleartran showing the apparent dominance of a single donor bound-exciton line	82

38.	A typical 10 K cathodoluminescence spectrum of a sample of Cleartran (WC9) showing the level of detail in the region from 330 nm to 335 nm	84
39.	A typical 10 K cathodoluminescence spectrum of a sample of Cleartran (WC9) showing the level of detail in the region from 335 nm to 340 nm	85
40.	The donor-acceptor pair band labelled 'A' at 10 K in sample WC5	87
41.	The behavior of the SAL band under differing levels of excitation.	88
42.	The variation in the cathodoluminescence of a side view Cleartran sample (WC9) with position on the surface of the sample.	92
43.	The variation in the cathodoluminescence of an end view Cleartran sample (WC6) with position on the surface of the sample.	93
44.	The 10 K cathodoluminescence of a quenching region on the surface of Cleartran sample WC4	95
45.	The representative cathodoluminescence from high quality side view samples of Cleartran	96
46.	The representative cathodoluminescence from high quality end view samples of Cleartran.	97
47.	The 10 K cathodoluminescence of samples WC2, WC3, and WC4 after an oily film was deposited on these samples.	99
48.	The variation in the cathodoluminescence of a Cleartran sample (WC9) with temperature	100
49.	The full-width-at-half-maximum of a donor bound-exciton line in sample WC9 as a function of temperature.	102
50a.	A comparison of the cathodoluminescence of Cleartran sample WC9 with previous reports of cubic ZnS in the literature (Part 1).	104
50b.	A comparison of the cathodoluminescence of Cleartran sample WC9 with previous reports of cubic ZnS in the literature (Part 2).	105

51.	The average low temperature cathodoluminescence of each of the forms of ZnS examined during this effort.	106
52.	The temperature shift of the highest energy edge emission band for a) Cleartran and b) Eagle-Picher single crystal ZnS.	122
53.	The energy position of a single bound exciton line in Cleartran (+) and Eagle-Picher single crystal ZnS (\square) vs $\coth \frac{\hbar\omega_{LO}}{2kT}$	124
54.	The energy position of a single bound exciton line in Cleartran (+) and Eagle-Picher single crystal ZnS (\square) vs $\coth \frac{\hbar\omega_{LA}}{2kT}$	125
A1.	Program TNCOMM.	136
A2.	Program CANBCONV.	137
A3.	Program TNCONV.	139
A4.	Program NORMAL.	140
A5.	Program CALCDAT	141
A6.	Program DATARED	143

List of Tables

Table	Page
I. Selected Properties of cvd ZnS and cvd ZnSe. . .	4
II. The ZnS Samples and their Labels	36
III. Lattice Constants of the Polycrystalline ZnS Materials.	41
IV. Aging Schedule for BaO Cathode	51
V. Exciton Binding Energies and Donor Ionization Energies for Seven Unknown Donors in Cleartran .	90
VI. The Emissions of Single Crystal ZnS (Eagle-Picher)	113
VII. The Emissions of ZnS Platelets	114
VIII. The Emissions of Raytheon cvd ZnS.	115
IX. The Emissions of CVD Inc. cvd ZnS (Block 1 Samples).	116
X. The Emissions of CVD Inc. cvd ZnS (Block 2 Samples).	117
XI. The Emissions of Cleartran	118

List of Symbols

ABE	= Acceptor Bound-Exciton
BE	= Bound Exciton
$^{\circ}\text{C}$	= Degrees Centigrade
cm	= Centimeter
Cu-blue	= Copper-blue
Cu-green	= Copper-green
cvd	= Chemical-vapor-deposited
DA	= Donor-Acceptor
DBE	= Donor Bound-Exciton
eV	= Electron-Volt
FE	= Free Exciton
FTB	= Free-to-Bound
gm	= Gram
IR	= Infrared
K	= Degrees Kelvin
KeV	= Kilo Electron-Volt
KV	= Kilovolt
LA	= Longitudinal Acoustic
LO	= Longitudinal Optical
m	= Meter
meV	= Milli-Electron Volt
mm	= Millimeter
ppm	= Parts Per Million
psi	= Pounds Per Square Inch
SA	= Self-Activated

SAL = Self-Activated Low-Temperature
TO = Transverse Optical
UV = Ultraviolet
 μm = Micrometer

111602
Abstract

CLEARTRAN

Cathodoluminescence studies were carried out between 10 and 300 K on CleartranTM, a form of chemical-vapor-deposited (cvd) ZnS subjected to high temperature and pressure post-deposition processing. The results of these studies were compared to and contrasted with the cathodoluminescence of cvd ZnS samples grown by Raytheon and CVD Inc., with high quality crystal platelets of ZnS, and with bulk-grown cubic phase single crystal ZnS grown by Eagle-Picher Co. X-ray diffraction and spark-source mass spectrometry revealed that Cleartran was composed of high purity ($<10^{16}$ impurities/cm³) cubic phase crystals from 20 to 40 μm in size. The low temperature near band-edge luminescence of Cleartran was sharper (3-6 meV full width at half maximum) and more detailed than any previous reports of cubic phase ZnS. The intensity of near band-edge luminescence was unusually strong, generally eclipsing the familiar Cu-blue and -green and self-activated low-temperature (SAL) peaks of undoped ZnS. Direct observation of the recombination of the $n=1$ $T_6 - T_9$ free exciton led to an assignment of 35 meV for the free exciton binding energy. Exciton binding energies and ionization energies were also determined for seven unknown donors according to the theory of Sharma and Rodriguez [Phys. Rev. 159, 649 (1967)]. The measured energy shift of

CONFIDENTIAL

CLEARTRAN

several donor bound-exciton lines between 10 and 300 K was shown to agree with the Dow-Redfield theory of temperature-dependent phonon-generated microfields, although the 300 K near band-edge luminescence is probably due to free exciton-electron interaction rather than bound-exciton recombination. By comparison with previous reports in the literature, the Cleartran samples were shown to contain a significant concentration of copper, aluminum, chlorine, manganese, and oxygen impurities; and, with a smaller degree of confidence, iodine impurity and zinc vacancies.

I. Introduction

Background

In 1866, T. Sidot produced the first large artificial crystals of ZnS (2). Serendipity stepped into the picture when Sidot perceived that his crystals were phosphorescent. It was not until 1888 that Verneuil ascribed the phosphorescence to the presence of a "foreign luminogen impurity" (2:406). Since that time and until 1957, most II-VI compound research consisted of luminescence studies of ZnS (mostly phosphors) and photoconductivity studies of CdS (3). At that time, crystal growth techniques began to improve and single crystals of a variety of II-VI compounds became available for study. The principal use of ZnS in the 1950's was in the growing television industry, where it served as an efficient cathode ray tube phosphor (12:15). Since powdered ZnS could be made to glow blue in its pure form under electrical stimulation (self-activated or SA luminescence) or green and red when mixed with a small amount of a powdered metal (activated luminescence) it proved to be a versatile phosphor and is still in use today.

Although ZnS has excellent luminescent properties and has been the most widely researched II-VI compound, it is probably the least amenable to fundamental studies of luminescent properties (27). ZnS is so difficult to study because of its large direct band gap (3.84 eV in the cubic

or 3C phase at 4.2 K) and the extreme difficulty of growing high quality single crystals (51:1866). Recent studies of II-VI compounds have therefore tended to concentrate on more easily handled materials such as ZnSe, CdSe, CdS, and ZnTe (34, 36, 37, 104, 123, 195). Contemporary research into the properties of II-VI compounds centers primarily on the production of full-spectrum visible discrete diode and thin-film electroluminescent displays (139:2). The only p-n junction constructed from binary II-VI compounds was made from CdTe, a material basically uninteresting due to its low 1.5 eV bandgap. The production of a p-n junction from more interesting binary II-VI compounds has as yet escaped researchers because of the difficulty of making high conductivity p-type material (123).

The Air Force is interested in ZnS not only as a candidate for electronic and electro-optic devices, but also as a possible laser window material because its fundamental absorption edge lies in the near ultraviolet ($0.33 \mu\text{m}$). Figure 1 is a plot of the bulk transmittance of a 5 mm thick specimen of chemical vapor deposited (cvd) ZnS produced by CVD, Inc. (30). The high transmission window extending from over $10 \mu\text{m}$ to $0.5 \mu\text{m}$ makes ZnS an attractive material for use as a window for both IR and visible applications. The Air Force has also studied the feasibility of using ZnS or a ZnS/ZnSe sandwich material as an infrared missile dome (29,18:109).

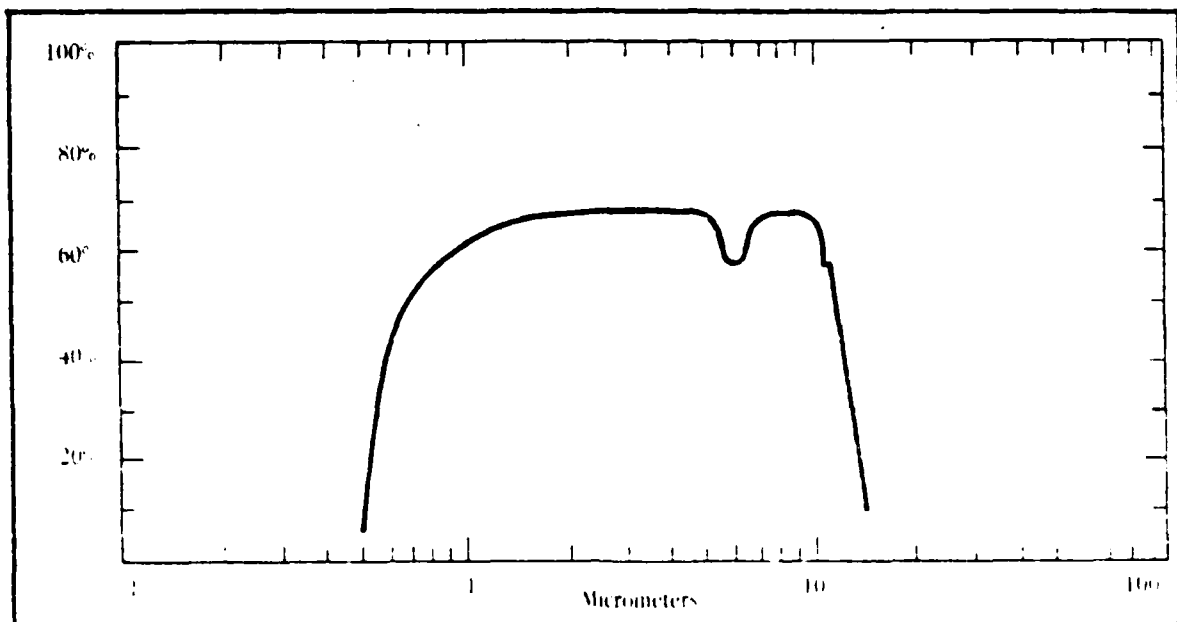


Fig. 1. Transmittance of 5 mm thick sample of cvd ZnS (30).

There are several inherent problems with using ZnS as a window material. The high refractive index of ZnS causes significant refractive losses at the surface (30). The long wavelength cutoff of ZnS, caused by multiphonon lattice absorption, occurs at 14 μm --- considerably below ZnSe's cutoff at about 20 μm (30). ZnS produced by Eastman Kodak's hot pressing process appears milky and transmits poorly in the visible (131:41). Standard cvd ZnS has a milky red-orange color and significant scattering in the near IR (131). ZnS is also relatively soft (Knoop hardness of 250) and is therefore subject to scratching by windblown grit (130).

ZnS does have a number of advantages over competing

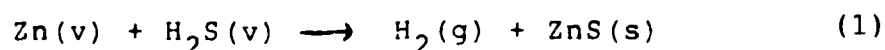
window materials such as ZnSe. ZnSe has an even higher refractive index than ZnS. The intrinsic absorption edge of ZnSe is at 0.5 μm . The flexural strength of ZnSe is 8000 psi while that of ZnS is 15000 psi (131:42) and the Knoop hardness of ZnSe is only 130. ZnS is also much less susceptible to rainwater erosion than is ZnSe (29). Selected optical, mechanical, and electrical properties of cvd ZnS and cvd ZnSe are listed in Table I.

TABLE I
Selected Properties of cvd ZnS and cvd ZnSe (131)

Property	cvd ZnSe	cvd ZnS
Transmission Limits	0.5-22 μm	1-12 μm
Refractive Index (1 μm)	2.489	2.292
Temperature Coefficient (dn/dT , 1/C at 10.6 μm)	6.1×10^{-5}	4.33×10^{-5}
Index of Refraction Inhomogeneity (ppm)	<3	<100
Density (gm/cm^3)	5.27	4.08
Flexural Strength (psi)	8,000	15,000
Young's Modulus (psi)	9.75×10^6	10.8×10^6
Hardness (Knoop, 50 gm)	130	250
Specific Heat ($\text{cal}/\text{gm}-\text{C}$)	0.081	0.112
Thermal Expansion (C)	7.57×10^{-6}	7.85×10^{-6}
Electrical Resistivity ($\text{ohm}-\text{cm}$)	10^{12}	10^{12}

In 1981, CVD Inc. first announced the creation of Cleartran, a "water-clear" form of polycrystalline cvd ZnS (131). Cleartran was unique because of its vastly improved visible transmittance, its low optical scatter, and the virtual elimination of the characteristic 6.3 μm absorption band, generally ascribed to the presence of ZnH_2 . Cleartran has a wider transmission band (0.3 μm - 12 μm), a low bulk absorption ($\sim 10^{-3} \text{ cm}^{-1}$), and a high damage threshold (40 MW/cm² at 1.06 μm for 15 minutes).

CVD Inc. produces cvd ZnS by reacting Zn vapor with H_2S gas:



The polycrystalline material is typically deposited at 670°C with a total pressure of 40 torr over a period of weeks. Plates of cvd ZnS have been produced by CVD Inc. up to 40 by 30 inches across and as much as one inch thick. Cleartran is created by subjecting pieces of this cvd ZnS to a hot isostatic pressing (HIP) process at high temperatures and pressures (129). This post-deposition processing leads to the enlargement of the grains and a subsequent weakening of the mechanical properties of the material.

Cleartran differs in several ways from the parent cvd ZnS. Primarily, the transmission curve of Cleartran is superior to that of the untreated material, especially in

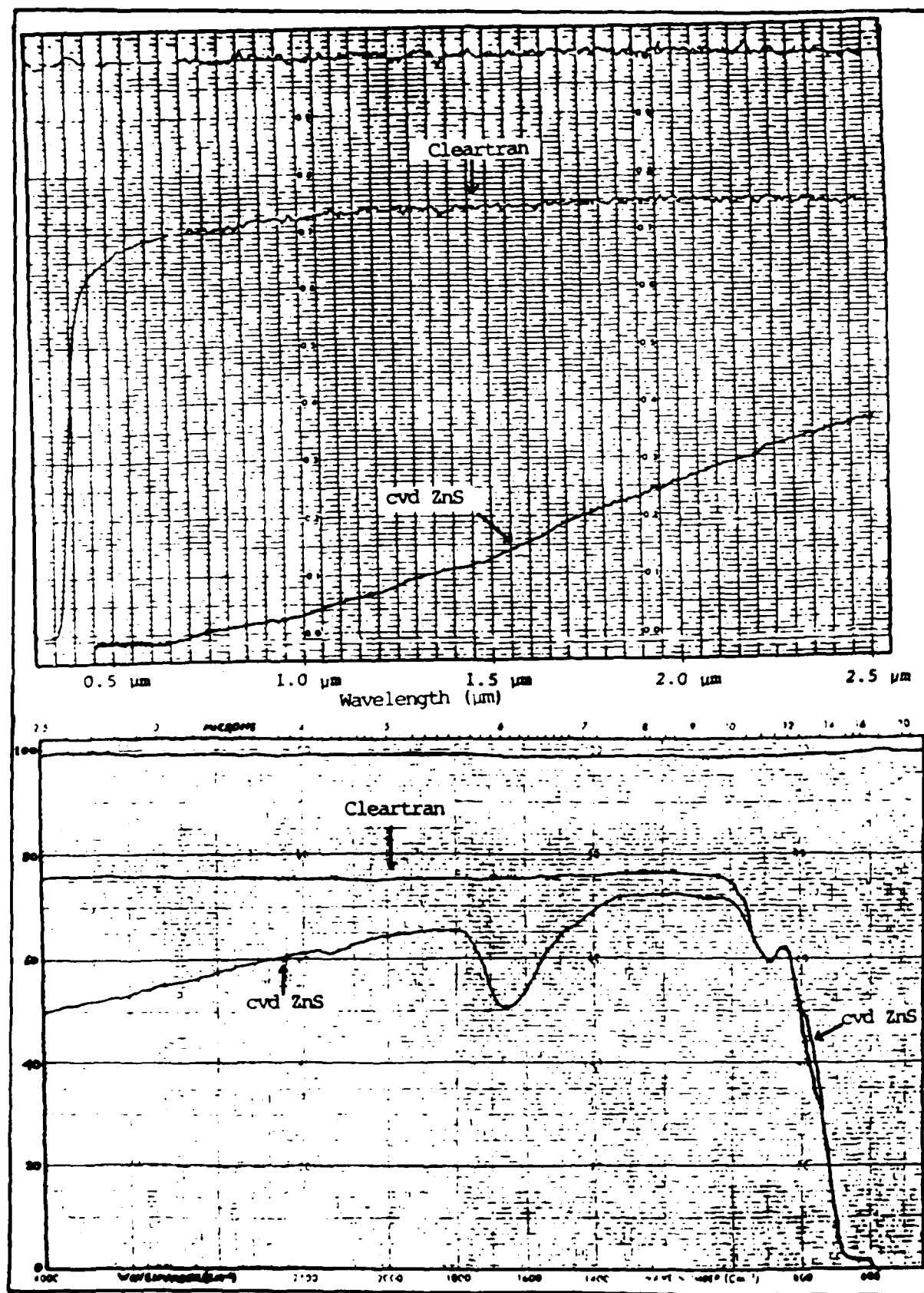


Fig. 2. Transmission curves of Cleartran and cvd ZnS (121).

the region from $0.33 \mu\text{m}$ to $0.5 \mu\text{m}$ (see Fig. 2). A poorly understood side effect of the HIP treatment reduces the Knoop hardness of Cleartran to 160 and the flexural strength to 9500 psi (129). Cleartran also suffers more severely from rain erosion than does untreated material (see Fig. 3).

The bulk optical, electrical, and mechanical properties of Cleartran have been measured by CVD Inc. and a research team from the University of Dayton Research Institute (UDRI) (129). The high bulk transmission, low index of refraction inhomogeneity, and large grain size of Cleartran suggest that the individual ZnS crystals may be of very high quality.

Problem Statement

High resolution luminescent spectroscopy has proven to be a sensitive technique for determining the purity and crystalline quality of semiconductor materials (100). However, the luminescence of polycrystalline materials has historically been heavily broadened and of low intensity so that little detailed luminescence spectroscopy has been done on this type of material (18, 32, 56, 83, 104, 139).

The spectral properties of ZnS have been shown to vary considerably with changes in the growth technique and in the structure of the material. At present, the spectral properties of the Cleartran form of ZnS are unknown. To improve the optical properties of Cleartran it is necessary

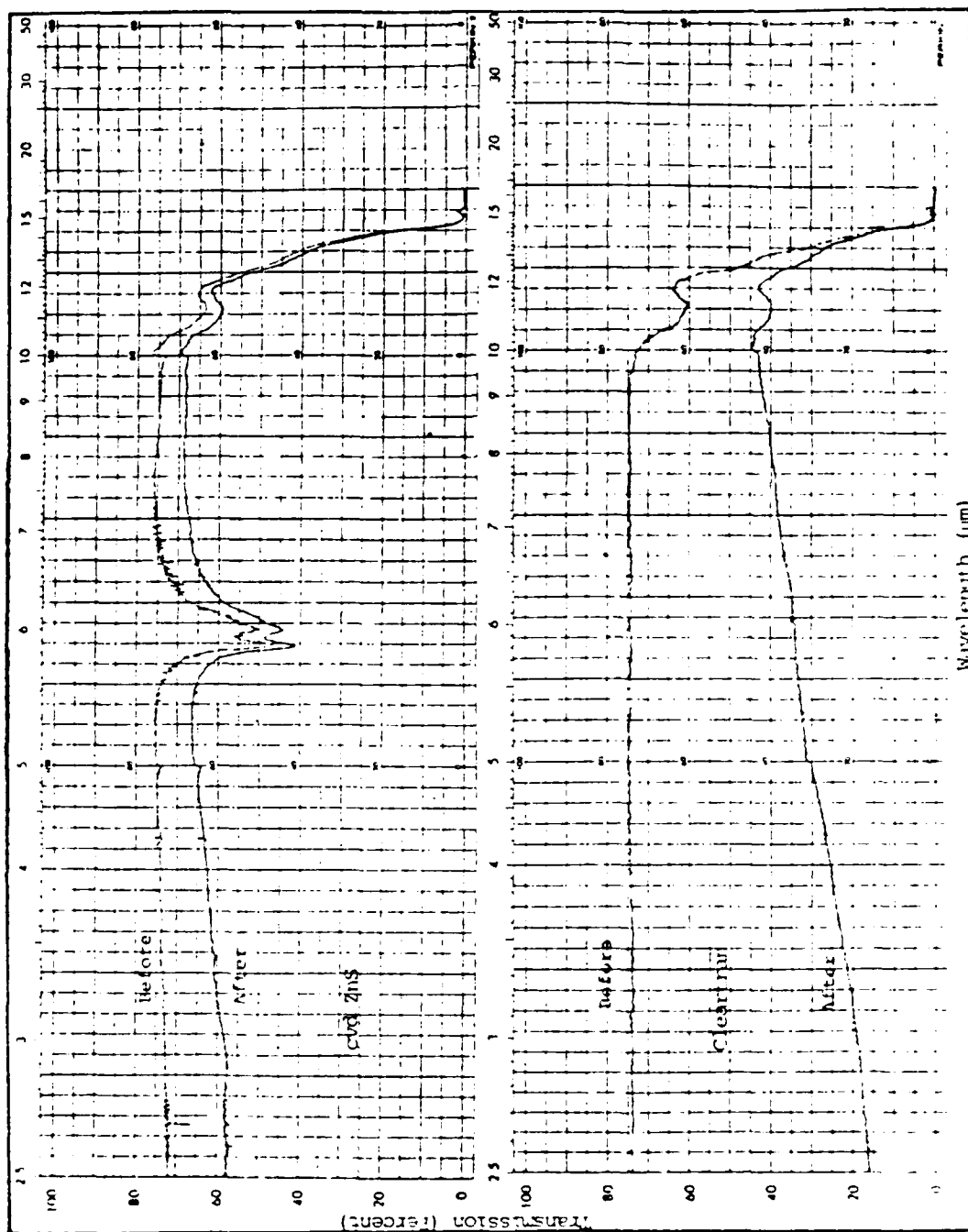


Fig. 3. Effects of rain erosion on the transmission of Cleartran. 475 mph, 90° impact, 1 inch/hour rainfall, 30 minute exposure (131).

to know something about the impurities which must remain in the crystal matrix. To produce a p-n junction from ZnS it is necessary to discover candidate impurities which may, by doping, allow us to produce high quality p-type ZnS.

The knowledge base on the nature and energy position of impurities in ZnS is very poor. A recent review of the optical spectroscopy of ZnS and ZnSe by R. N. Bhargava lists no more than 5 impurities as having well-known ionization energies in ZnS (12:20). Our knowledge of ionization energies could be quickly improved given ZnS of high purity and improved crystalline quality.

Since electron beam excitation leads to emission by all the luminescence mechanisms present in a semiconductor, I have chosen cathodoluminescence as my means of examining Cleartran. This report documents the results of low voltage cathodoluminescence of samples of Cleartran, cvd ZnS grown by two semiconductor companies, ZnS platelets, and cubic phase single crystal ZnS at temperatures ranging from 10 K to 300 K.

Sequence of Events

Before experimental results can be understood, it is necessary to have a solid background in the theory. Chapter II provides this background. After a brief discussion of the crystallography of the samples and the methods used to produce them, the basic concepts needed to understand the results are presented. This presentation

includes the band structure of cubic ZnS, the nature of known spectral emissions from semiconductors, the fundamentals of cathodoluminescence, and the effect of temperature on the band structure. The chapter ends with a brief review of the topical literature on the luminescence of ZnS.

Chapter III, "Experimental", documents the experimental apparatus and techniques used to measure the cathodoluminescence of the samples.

Chapter IV, "Results and Discussion", presents the experimental data. The cathodoluminescence of each type of sample is discussed in turn. Variations in the cathodoluminescence from sample to sample and even from spot to spot on the surface of a given sample are discussed. The various emission lines of each form of ZnS are summarized in Tables VI-XI, and the probable nature of each emission center is discussed. The ionization energies of a number of unknown but resolvable impurity centers are determined based on the theory of Sharma and Rodriguez (117). The energy shift of several donor bound-exciton (DBE) lines between 10 K and 300 K is then compared with predictions based on the Dow-Redfield theory of temperature-dependent phonon-generated electric microfields (41, 145-147).

In the final chapter, the results of all the measurements are summarized and recommendations are made for further work.

II. Theory and Summary of Previous Work

Crystallography of ZnS

ZnS crystals can be found with the hexagonal (wurtzite) or cubic (sphalerite or zincblende) crystal structures (122). The basic lattice for the zincblende structure is the face-centered cubic lattice shown in Figure 4. The zincblende structure is composed of two of these face-centered cubic lattices, one made of zinc (type A) atoms and one of sulfur (type B) atoms. The type B lattice is displaced from the type A lattice by one quarter of the body diagonal of the type A lattice. The zincblende structure is illustrated in Figure 5, where a complete face-centered cube of the type A atom is displayed. The wurtzite structure is composed of two close-packed hexagonal lattices, one of which is shown in Figure 6. When two of these lattices (types A and B again) with the same c-axis are interleaved with the type B lattice displaced a distance $3c/8$ from the type A lattice along the common c-axis, the wurtzite structure is formed (Figure 7).

Both the zincblende and wurtzite structures can be thought of in another way. Imagine the closest possible packing of spheres in a single plane: the hexagonal arrangement of Figure 8. A second hexagonally packed plane may be fit most tightly to the first plane by placing it above the first plane so that the atoms fall on the points labelled X in Figure 8. We now have a choice as to where

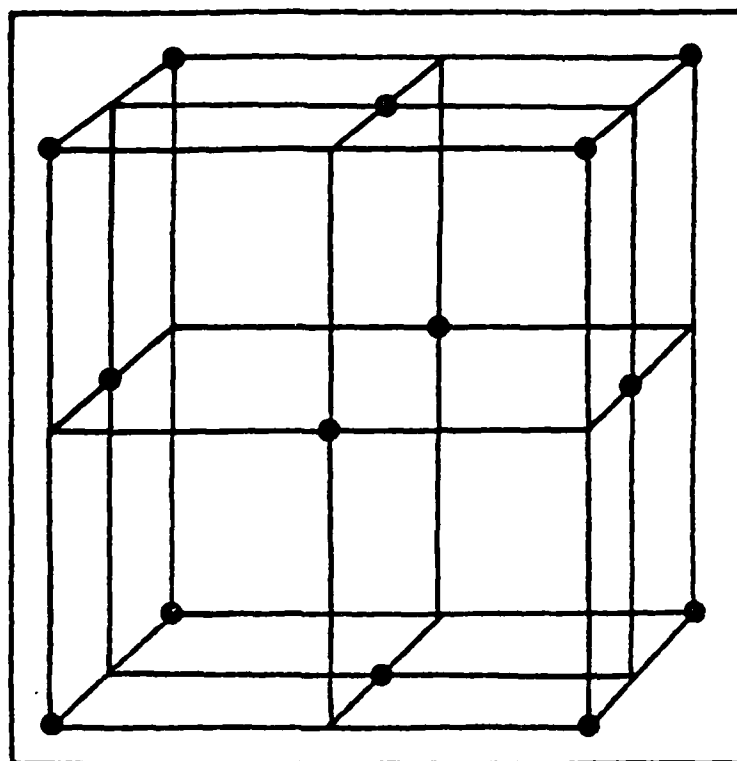


Fig. 4. The face-centered cubic lattice (122:86).

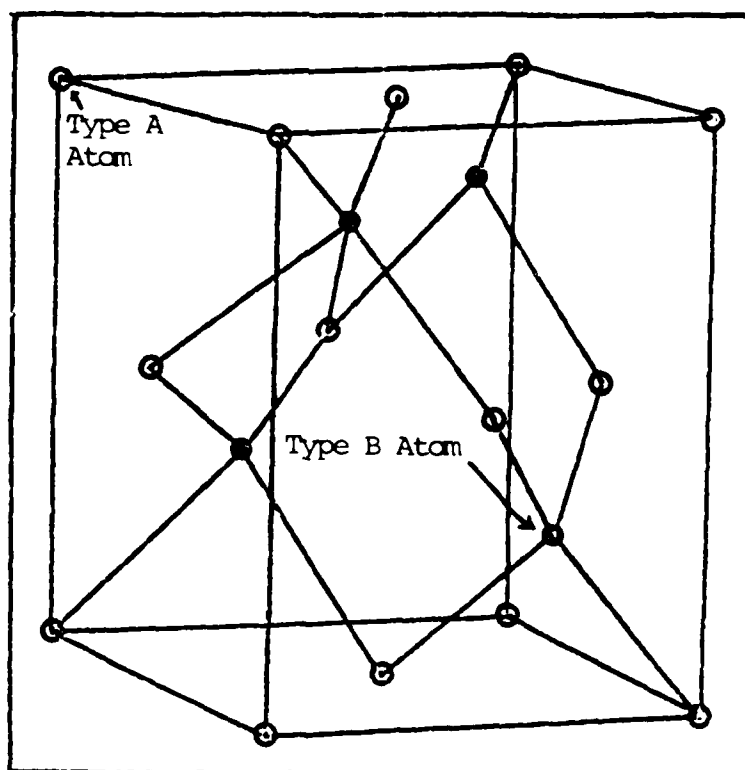


Fig. 5. The zincblende structure (122:87).

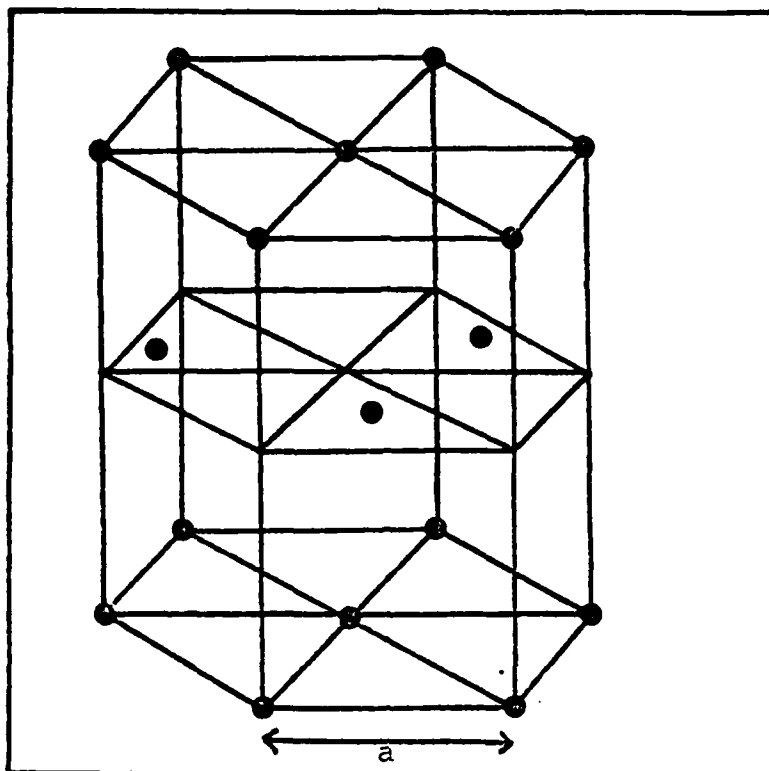


Fig. 6. The close-packed hexagonal lattice (122:89).

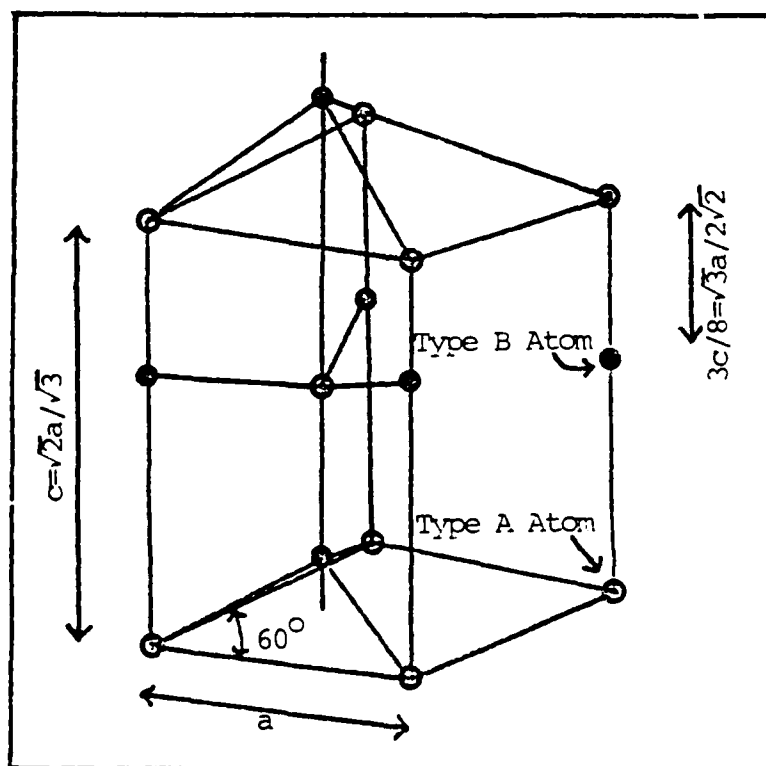


Fig. 7. The wurtzite structure (122:69).

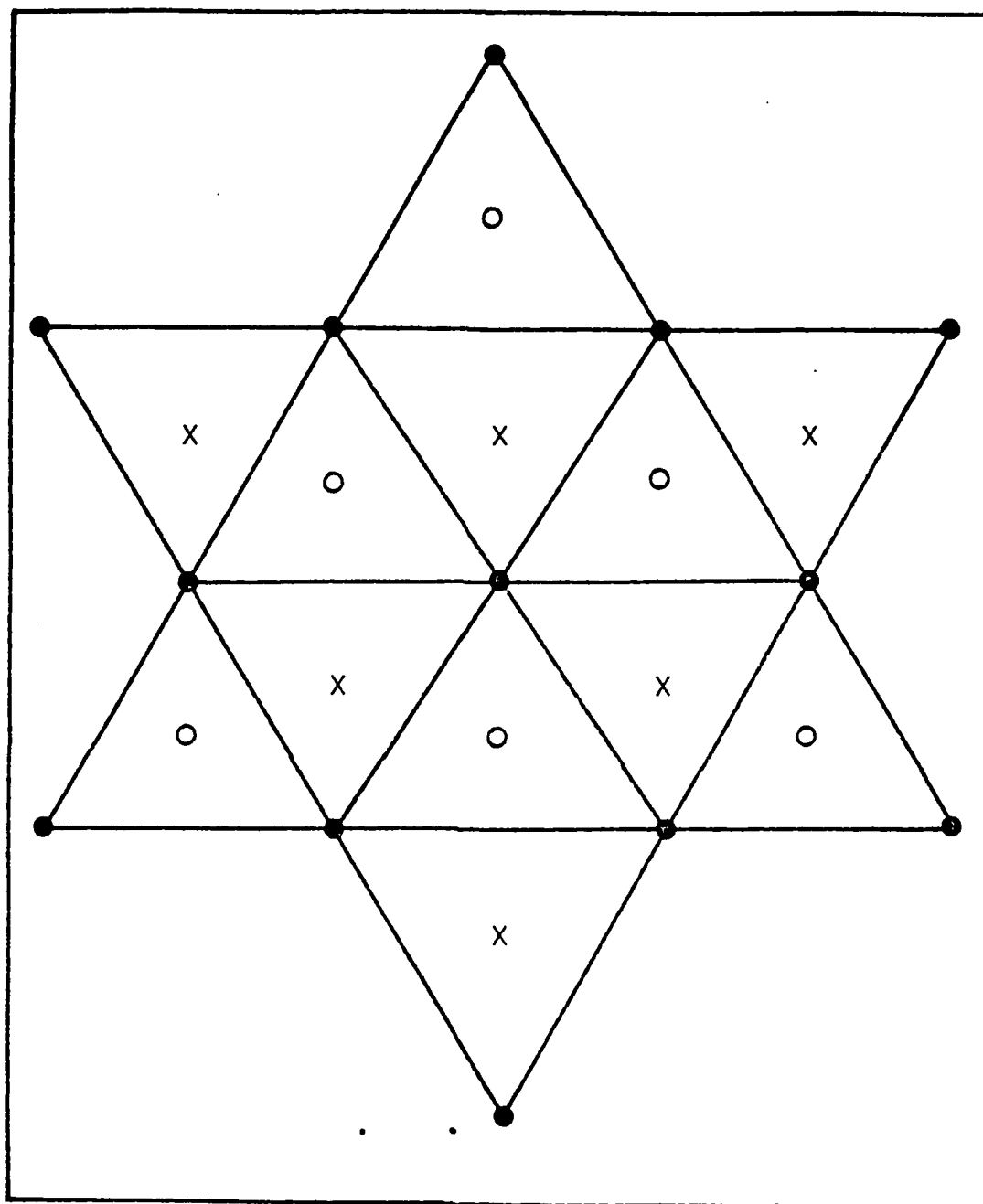


Fig. 8. Packing sequence of zincblende and wurtzite (122:88).

we place a third hexagonally packed plane above the first two. If the third plane is placed so that its atoms fall directly above the atoms in the first plane in Figure 8, we have created a wurtzite structure where the type A and B atoms are identical. If the third plane is placed so that its atoms fall above the 0 in Figure 8, we have created a zincblende structure with identical atoms---the so-called diamond structure.

All ZnS structures are thus built of alternating planes of zinc and sulfur atoms. The arrangement of each type of atom in the plane is that of hexagonally close-packed spheres. The structures differ from one another only in the sequence of stacking of the zinc and sulfur planes. It is possible to have a higher-order mixing of the zincblende and wurtzite structures to form what are called "polytypes" (99). It has long been known that, like SiC, ZnS is one of the few binary compounds that actually display polytypism (22:501). Unwanted polytypism is a frequent problem for those who wish to grow pure ZnS crystals. In fact, polytypism is often considered a form of macroscopic structural defect since a change in polytype is often accompanied by significant physical effects (61:553).

Crystal Growth Techniques

In this section, we summarize the methods used to grow cvd ZnS, Cleartran, and single crystal ZnS. The material in this section is condensed from three reports on crystal

growth techniques (12, 85, 131), an Air Force Technical Report (130), and personal discussions with Mr. Donald Evans of the Air Force Materials Laboratory (29).

Chemical vapor deposition (cvd) is a process in which the chemical reaction of vapors slowly forms a solid, polycrystalline material (130:1). This manufacturing technique is used whenever the material is difficult to form by the more conventional methods of crystal pulling, hot pressing, or casting. This technique is capable of producing very high purity material. Not only may high purity reactants be chosen, but a great deal of refining occurs during growth since involatile impurities tend to remain behind in the melt and volatile impurities tend to flow past the deposition region. It is possible to produce large pieces of high purity material in this fashion at a relatively low cost. Since the material is deposited upon a substrate (mandrel), any shape may be formed during the deposition process.

Figure 9 is a cross-sectional view of a cvd reaction system now in use at CVD Inc. The furnace is an electrically heated vacuum chamber equipped with a continuous gas flow system. The zinc vapor and H_2S gas are injected into the reaction chamber to mix and produce ZnS . The only limitations on the size of the cvd ZnS produced by this system are the size of the reaction chamber and the difficulty of monitoring and maintaining the necessary temperatures and pressures. To produce a one inch thick

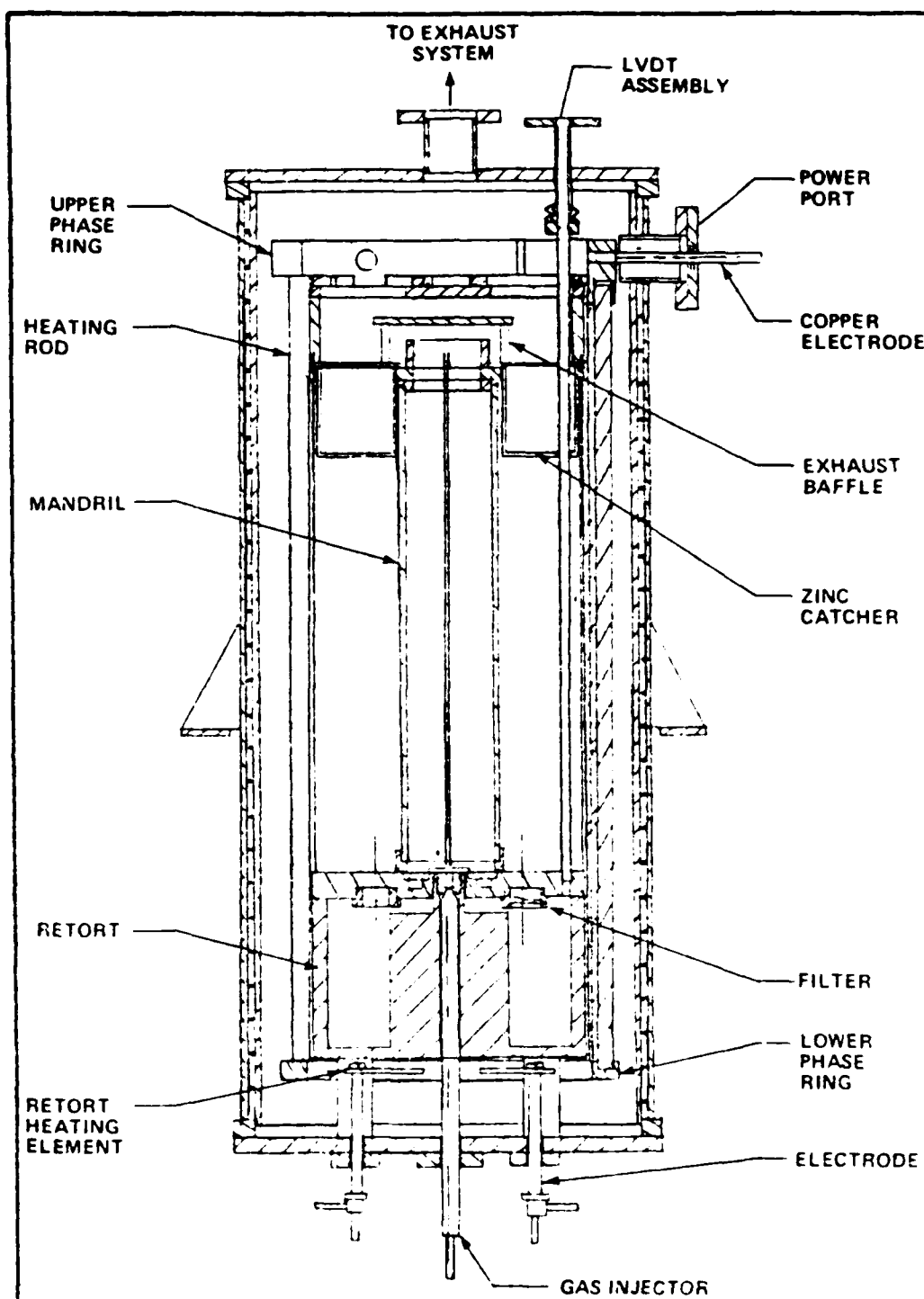


Fig. 9. A reaction system for chemical vapor deposition of ZnS (131).

sample of cvd ZnS, the reaction chamber must be continuously monitored and controlled for three weeks (130:1).

Cleartran is made from pieces of cvd ZnS grown by CVD Inc. The cvd ZnS is placed in containers which are enclosed in a heated high pressure vessel (130:10). The material is wrapped in a foil (generally platinum) to prevent contamination. The material can then be heated to temperatures as high as 2000°C in inert gas (typically argon) pressures of up to 30,000 psi. This HIP process is a proven technique previously used for creating high performance alloys from powder compacts. The HIP process has also been used to rejuvenate turbine blades and to densify castings (130:12). A schematic of a HIP unit used by IMT Inc. is shown in Figure 10.

Single crystal ZnS can be produced in a number of ways. Production of single crystal ZnS from the melt is accomplished by two basic methods: the sealed tube technique (47, 62), and the high pressure technique (72, 133). In the former technique, a sealed quartz ampoule serves as a liner to the traditional graphite crucible. Crystal growth occurs rapidly under controlled vapor pressures (9, 12, 21). In the latter technique, crystals are grown under a high pressure of an inert gas such as Ar or He to suppress outdiffusion of volatile substances. Growth from the melt often produces crystals which are of mixed hexagonal/cubic (wurtzite/zincblende) types due to

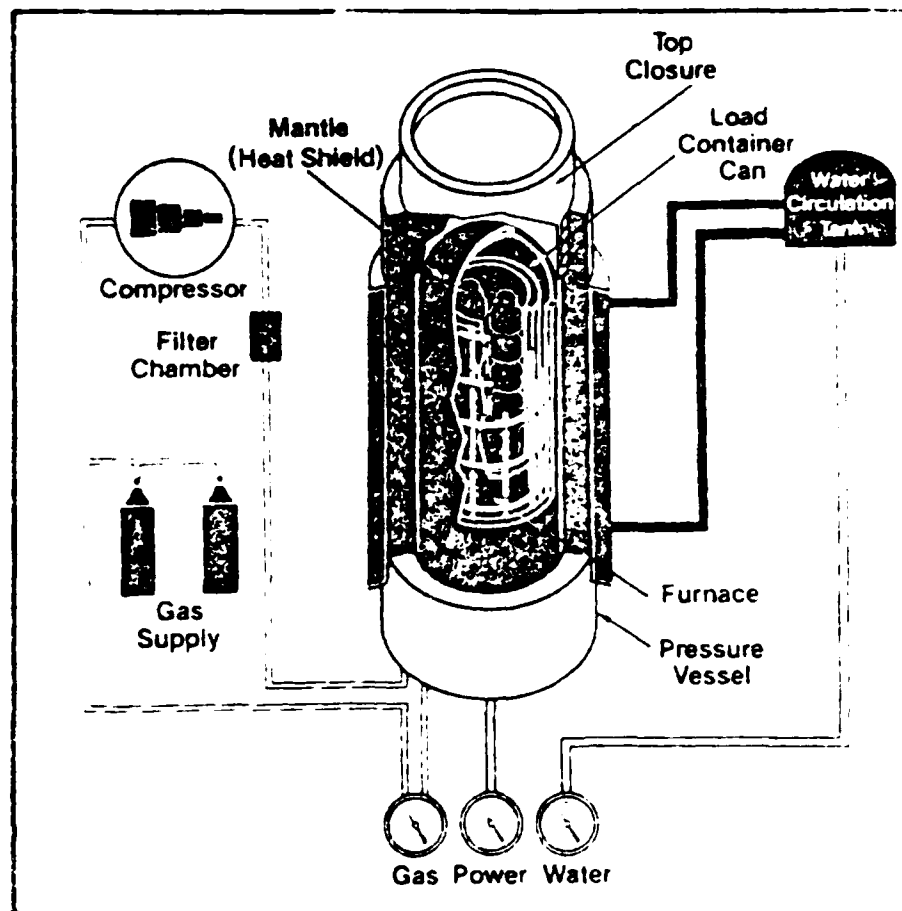


Fig. 10. The schematic of a hot isostatic pressing (HIP) unit (131:11).

inadvertent cooling through phase transition temperatures.

Single crystal ZnS may also be produced through vapor growth techniques at lower temperatures (and therefore lower background impurity concentrations). Once again, two basic techniques are employed: the closed tube vapor transport technique, and the Piper-Polich open tube vapor transport technique (12:16). In the former technique, halogens of the growth compounds are used as transport agents. In the latter technique, transport is provided by sublimation of the compound itself. Both of these techniques have produced crystals of relatively high perfection and low background impurity concentration (8, 106).

Other techniques used to create single crystal ZnS include vapor phase epitaxy on various substrates (11, 63, 87, 140, 141) and a cvd process employing organometallic precursors (34).

The Energy Bands of ZnS

The environment of the zinc and sulfur atoms in the wurtzite and zincblende structures of ZnS is virtually identical out to the second nearest neighbors (3:124). As a result, the crystal field potential of the wurtzite structure differs from that of the zincblende structure only by a small trigonal perturbation (3, 105).

The energy bands of the hexagonal structure at $k=0$ and in the k -direction parallel to the c -axis can be considered

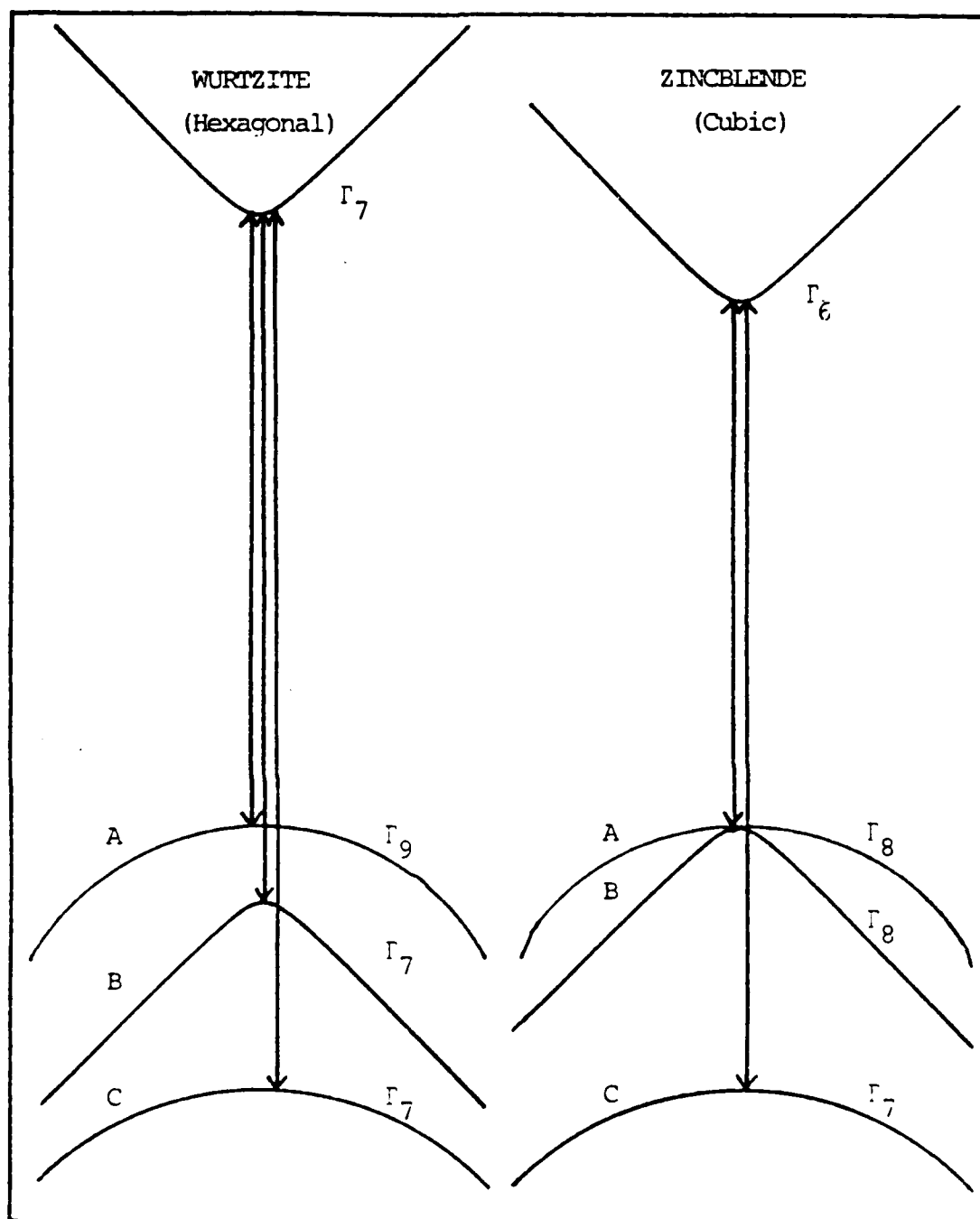


Fig. 11. The energy band diagram for the cubic and hexagonal forms of ZnS near $\vec{k}=0,0,0$ (3:424).

as slightly perturbed bands of the cubic structure. The perturbation splits the upper cubic valence band Γ_8 (formed from spin-orbit splitting of the anion 3p band) into two valence bands: the Γ_9 and Γ_7 . Figure 11 shows the energy band diagram of the two extreme structures of ZnS.

As is obvious from the energy band diagram, all possible structures of ZnS are direct gap materials. The energy gap for wurtzite ZnS is 3.91 eV (106:876). The energy gap for zincblende ZnS is 3.84 eV (51:1866). The work of Birman (15, 16) and of Brafman and Steinberger (22:501) shows that the band gap of polytypic ZnS varies linearly with the percentage of hexagonality of the polytype.

Cathodoluminescence

When keV electrons strike a semiconductor surface a variety of interactions occur. Some electrons are backscattered, secondary electrons are produced within the material, and characteristic photons are produced in the x-ray, ultraviolet, visible, and infrared regions of the spectrum. All of these fundamental processes can be used to characterize the semiconductor material (17, 82). Cathodoluminescent spectroscopy involves the production, detection, and interpretation of the ultraviolet, visible, and infrared photons produced during the electron-solid interaction.

The photons forming the cathodoluminescence signal are

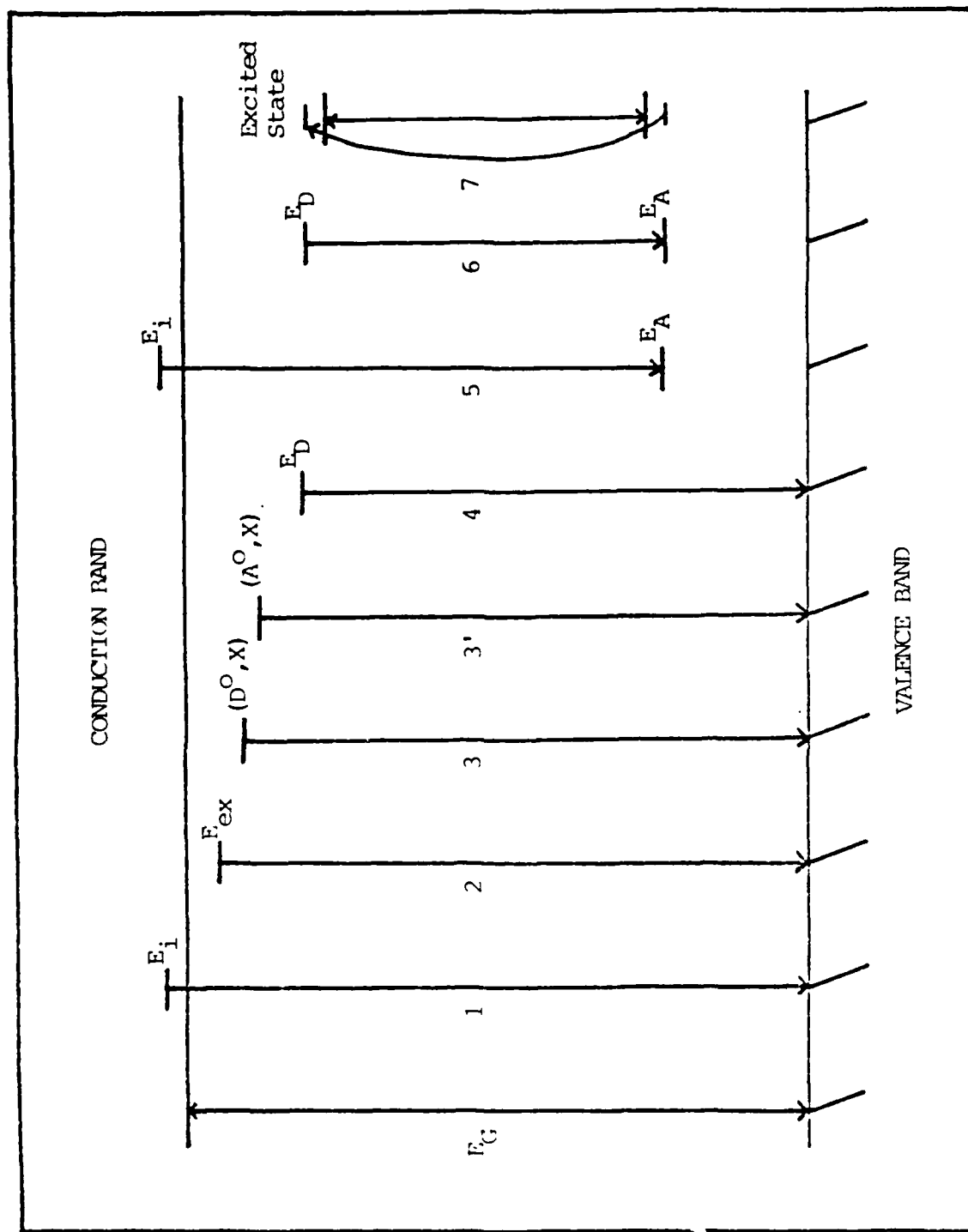


Fig. 12. Possible radiant transitions in semiconductors.

the result of electronic transitions between the conduction and valence bands of the semiconductor and levels (both impurity and defect type) lying in the band gap (see Figure 12). Only those semiconductor processes involving radiant transitions are detectable, but nonradiative recombination can be inferred from cathodoluminescent images of the surface provided the contrast between radiative and nonradiative sites is high (32, 59, 111). The nature of an impurity center can be determined by comparison with previous luminescence data in the literature. If no identification is present in the literature, a study must be done with intentionally doped samples.

Figure 12 shows the basic radiative transitions leading to emission in a semiconductor. Emission 1 is the intraband transition arising from electrons in the conduction band recombining with holes (unoccupied allowed electron energy states) in the valence band. Emission 2 is the result of the recombination of a free electron in close spatial association with a hole. This combination of entities is called a "free exciton". The free exciton exists at an energy level below that of the band gap because of the coulombic interaction between the hole and electron (modified by the dielectric constant of the semiconductor). The free exciton can only be seen at low temperatures such that kT is less than the binding energy of the exciton---a number ranging from a few tenths of an meV to several hundred meV depending on the material.

Excitonic states analogous to electronic states in hydrogen may also be seen at very low temperatures. Emissions 3 and 3' arise from excitons bound in the coulombic well near neutral impurity atoms in the semiconductor. Emissions 4 and 5 are due to radiative transitions that begin or end on localized impurity levels within the band gap (often called Free-to-Bound or FTB emissions). Emission 6 is the so-called Donor-Acceptor or DA emission arising from electronic transitions beginning on donor impurities and ending on acceptor impurities. Due to the wide range of possible separations between donor and acceptor impurity atoms, the DA emission is usually seen as a broad, asymmetric continuum. Since the range of possible separations for substitutional impurities consists of a set of discrete, easily computable values it is theoretically possible for many semiconductors to see a DA emission band consisting of a large set of narrow emission lines (35). Emission 7 arises from radiative transitions in a deep center such as a rare-earth ion (10, 75).

Individual electrons in the electron beam undergo a series of elastic and inelastic scattering events in the semiconductor. These scattering events eventually randomize the electron trajectories. The range of penetration of the electrons is an important number for the spectroscopist, since it is frequently his only measure of spatial resolution. The range of penetration must depend on the electron energy E_b :

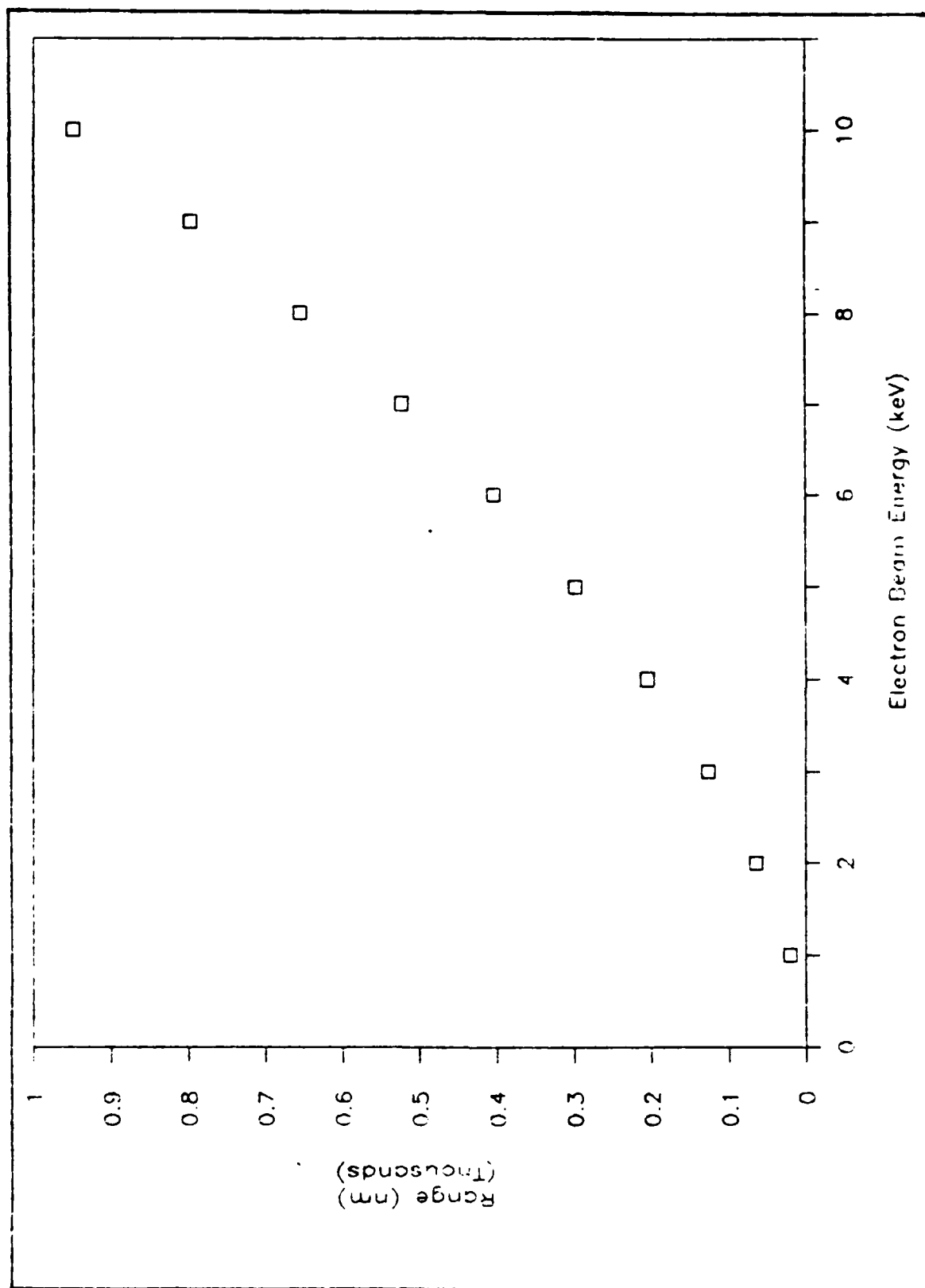


Fig. 13. The Kanaya-Rokayama range equation for electrons in SnS.

$$R_e = (0.0276 A/\rho Z^{0.889}) E_b^{1.67} \quad (2)$$

where R_e is in μm , E_b is in keV, A is the atomic weight in g/mol, ρ is in g/cm^3 , and Z is the atomic number. This general expression for electron range was developed by Kanaya and Okayama (69) and agrees well with experimental data for a wide range of atomic numbers (53). The Kanaya-Okayama range equation is plotted for 1 to 10 keV electrons in ZnS in Figure 13.

Cathodoluminescence is recognized as one of the most valuable tools for semiconductor research. There have been a number of excellent reviews on this subject in recent years, particularly in the area of scanning electron microscope cathodoluminescence (SEM-CL) (33, 60, 84, 145).

Effect of Temperature on the Band Gap

There are two main reasons for the shift of band gap with temperature. Since the band structure is a function of lattice spacing, dilatation of the lattice must affect the band gap. The second reason is the interaction that occurs between lattice phonons and electrons. By considering data on the variation of band gap with pressure, Yacobi (146) has determined that the dilatation effect contributes at most 10-20% of the temperature dependence of the band gap in cubic (zincblende) ZnS.

There are at least two ways to take the remaining

temperature dependence into account. Historically, the strictly empirical relationship of Varshni has had some success (145). A recent attempt to quantify the electron-phonon interaction more directly is based on the early work of Dow and Redfield (41). Dow and Redfield calculated the mean-square field generated by quantized lattice vibrations (the LO phonon in equation 3) assuming weak fields ($10^4 - 10^6$ V/cm) to avoid a substantial perturbation of lattice atoms, a Gaussian distribution of these fields, and a near-uniform electric field strength in crystal volumes commensurate with the excitonic radius (147:1007)

$$F^2 = [\hbar\omega_{LO}q_c(\epsilon_0 - \epsilon_\infty)/3\pi\epsilon_0\epsilon_\infty] \coth(\hbar\omega_{LO}/2kT) \quad (3)$$

$$= \beta \coth(\hbar\omega_{LO}/2kT)$$

where ϵ_0 and ϵ_∞ are the static and high frequency dielectric constants, respectively; q_c is the polaron cutoff wave vector; and $\hbar\omega_{LO}$ is the energy of the LO phonon. The quantity q_c selects the phonons whose wave vectors provide a near-uniform electric field strength across the excitonic radius, therefore $q_c \leq \pi/a$ where a is the excitonic radius.

Equation 3 is based on the observation that ZnS crystals obey Urbach's rule for exponential absorption edges (136)

$$\mu = \mu_0 \exp[\sigma(\hbar\omega - \hbar\omega_0)/kT] \quad (4)$$

where μ is the absorption coefficient; ω is the photon frequency; and μ_0 , ω_0 , and σ are material-dependent constants. The constant σ is called the slope constant. The slope constant for some ionic crystals is known to depend on an effective phonon energy, $\hbar\omega_0$ (86)

$$\sigma = \sigma_0 (2kT/\hbar\omega_0) \tanh(\hbar\omega_0/2kT) \quad (5)$$

where σ_0 is another material-dependent constant.

The Dow-Redfield theory explains the exponential absorption edge as an effect produced by electric field ionization of the exciton. The theory is based on an internally generated Franz-Keldysh effect (101) and Dexter's work on Stark shifting in the excitonic system (40). The probable sources of these electric fields include not only phonons, but also impurities and dislocations (147).

This model has been successfully employed to explain the shift of the absorption edge with temperature in single crystal ZnS with the 3C (cubic), 4H, and 2H (hexagonal) structures by B. G. Yacobi (147). Yacobi has also shown that the model can be extended to the case of emission, at least for direct band-gap semiconductors (146). Yacobi showed that the model explained the temperature shift of the acceptor-to-band emission in ZnS(Cu,Cl) single crystals.

Franz (49) originally determined, in the weak-field approximation to Franz-Keldysh theory, that the Franz-Keldysh shift of the absorption edge was proportional to F^2 . Assuming that only one type of phonon is responsible for the temperature shift of the emission, and that the Franz-Keldysh shift of the emission peak ΔE_p is also proportional to F^2 , Yacobi obtained (146:1008)

$$\Delta E_p = -\gamma' F_{rms} \quad (6)$$

where γ' is the Franz-Keldysh coefficient for the emission band, and F_{rms} is the root-mean-square phonon-generated microfield. Combining equations 3 and 6, we find

$$E_p = E_p(T_1) - E_p(T_2) = S'_{LO} [\coth(\hbar\omega_{LO}/2kT_1) - \coth(\hbar\omega_{LO}/2kT_2)] \quad (7)$$

where $S'_{LO} = \gamma'\beta$, $T_2 > T_1$, and we have implicitly assumed that γ' is not temperature dependent.

We have assumed throughout these calculations that it is the LO phonon that is primarily responsible for the electron-phonon interaction which causes the band shift. At temperatures below about 100 K, it is likely that other phonons (in particular the longitudinal acoustic or LA phonon in cubic ZnS) provide the dominant electric field. Yacobi also emphasizes that for temperatures such that the electric field strength exceeds about 10^6 V/cm there is a strictly linear relationship between temperature and absorption edge (147:2991,137).

Review of Topical Literature

Historically, the bulk of ZnS studies have been performed on phosphors (2, 42, 70, 71, 76, 78, 89, 94, 96, 97, 102, 103, 107, 121, 128, 132). These studies have concentrated on the search for efficient activator impurities for producing a full spectrum of colors from ZnS LEDs. The study of single crystal ZnS in the cubic and hexagonal phases has been both basic and device-oriented (4, 15, 17, 31, 32, 34, 51, 54, 64, 67, 73, 77, 79, 81, 90, 91, 92, 108, 113, 127, 143). The seminal study of single crystal hexagonal phase ZnS was done by R. Wheeler and J. Miklosz in 1963/4 (142). Their luminescence data on hexagonal ZnS was detailed and complex---to date, no comparable work has been done with cubic ZnS due to the difficulty of growing fine cubic crystals. Thin film work has also been limited (88, 104, 114, 139). Very few attempts have been made to excite and study the luminescence of cvd ZnS (18, 32, 34, 56, 104, 114, 139), and there have only been two cursory attempts to measure the luminescence of Cleartran---an unpublished study of band-edge cathodoluminescence by Varni (139) and an unpublished master's thesis by Blessinger (18).

The luminescence produced by II-VI compounds in the visible and ultraviolet regions of the spectrum falls into two broad categories: the "edge" or "near band-edge" luminescence, and the "self-activated" or "SA"

luminescence. The near band-edge luminescence has been variously defined as "radiative recombination processes occurring within several tenths of an electron volt of the band gap energy" (2:385) and "the interimpurity, donor-acceptor transitions which constitute the true 'edge luminescence' first defined in a direct gap semiconductor" (36:4888). In this report, the first definition will be assumed to be the correct one. Near band-edge emission then includes both the sharp low-temperature luminescence lines and their satellites (called "two-electron" transitions) and the donor-acceptor pair bands just below these lines. The self-activated region includes those broad, featureless emission peaks lying typically (for ZnS) in the visible region of the spectrum. The term "self-activated" arises from our inability to produce ZnS without SA emission peaks.

The low temperature near band-edge luminescence lines in ZnS are generally due to bound excitons and their phonon replicas (8, 34, 48, 51, 57, 70, 73, 94, 108, 113, 114, 121, 127); FTB radiative recombination (51, 70); and DA radiative recombination (17, 34, 48, 51, 54, 71, 81, 91, 108, 113, 114). Excitons may be bound to neutral donor impurity atoms or to ionized donor impurity atoms (36). Recombination by excitons bound to neutral donors is designated " (D^0, X) " or " I_2 " in the literature. Recombination by excitons bound to ionized donors is designated " (D^+, X) " or " I_3 " in the literature.

Additionally, two-electron satellite transitions created when bound excitons leave the formerly neutral donor in an excited state are also possible (P35). The designations " (A^0, X) " or " I_1 " are reserved for recombination due to excitons bound to neutral acceptors. Neither I_3 nor two-electron satellite lines have ever been seen in any form of ZnS. Donor bound-exciton (DBE) and acceptor bound-exciton (ABE) lines have only been imperfectly observed in ZnS, and few assignments of impurity type have ever been made (9, 20, 39, 48, 50, 57, 66, 73, 92, 106, 108, 113, 115, 116, 124, 142).

It is difficult to observe the discrete pair lines which compose the DA recombination bands in direct gap semiconductors, because it is so difficult to saturate the distant pairs to increase the relative luminescent strength of the resolvable near pairs (39:81). Despite this difficulty, discrete pair lines have been observed in such direct gap materials as CdS, CdSe, and ZnO; but only under extremely high excitation and with the highest resolution equipment. While discrete pair lines have never been observed in ZnS, several authors have reported the discovery of probable DA bands in the near band-edge region. Gezci and Woods (51) reported two possible DA bands called P and Q at 339.5 nm and 336 nm. Samelson and Lempicki (108) saw a possible DA band they labelled "SA" in the region of 459-465 nm. An unlabelled band at 345 nm has been called a DA band and associated with both zinc and

sulfur interstitials and zinc and sulfur vacancies (68). A DA band outside the near band-edge region at 520 nm has been called the "copper-green" or "Cu-green" band and is due to copper substituted at zinc sites and substitutional chlorine atoms (102, 118, 119, 120, 138).

Emission peaks in the SA region (visible) are generally agreed to arise from FTB recombination at deep centers; DA recombination; and recombination at isoelectronic impurities, deep defects, or rare-earth ions. A persistent emission band occurring near 390-420 nm at low temperatures ($T \leq 50$ K) has been called the "SAL" band. The SAL band has been variously attributed to zinc vacancies (52), chlorine substituted at sulfur sites (108), and oxygen vacancies in ZnSO precipitates within the ZnS lattice (90). A strong blue emission band labelled "copper-blue" or "Cu-blue" is often seen between 430-450 nm. This Cu-blue band probably arises from recombination between substitutional copper atoms and interstitial copper atoms (98, 134, 135). A band also labelled "SA" is frequently reported near 455-475 nm. This SA recombination band has been confirmed by optical paramagnetic resonance (OPMR) to be yet another DA band associated with an A-center composed of a zinc vacancy and a chlorine impurity atom (17, 148). These are the most frequently reported visible emission bands. Many other visible emission bands have been reported in the literature (17, 21, 25, 26, 31, 42, 54, 64, 67, 71, 76, 78, 79, 89, 96, 102, 109, 110, 112, 125, 128, 132).

III. Experimental

In this chapter, I describe the equipment and experimental procedures used in my research and the semiconductor samples I studied.

Sample Information

Polycrystalline ZnS obtained from Dr. Raymond L. Taylor of CVD Inc. was grown by cvd from molten zinc and hydrogen sulfide gas in large temperature- and pressure-controlled reaction ovens. This material was grown at 670°C and 40 torr. CVD Inc. also provided samples of Cleartran produced by the HIP process at 990°C and 30,000 psi from the parent cvd ZnS. The Raytheon cvd material studied here was obtained from the sample bins of the Department of Engineering Physics, Air Force Institute of Technology. Two types of single crystal ZnS were examined during this effort. The first type was grown in the early to mid 1970's by D. C. Reynolds at Wright-Patterson AFB, Ohio, by the closed tube vapor transport technique. This technique produces thin, fragile crystal platelets. The second type of single crystal ZnS was grown from the melt under a high pressure of Ar gas by Eagle-Picher Co. Large pieces of the cvd materials were cut into a manageable sample size of 5 mm by 5 mm by 1.6 mm. These smaller samples were then successively lapped with 1 μm , 0.3 μm , and 0.05 μm alumina powder and Buehler's micro-cloth. The cvd samples were

Table II

The ZnS Samples and Their Labels

Material	Designation	Origin	Orientation at Surface
Cleartran	WC1	Cleartran4	Unknown
	WC2	Cleartran1	(311)
	WC3	Cleartran2	(220)
	WC4	Cleartran2	(220)
	WC5	Cleartran2	(220)
	WC6	Cleartran1	(311)
	WC7	Cleartran1	(311)
	WC8	Cleartran1	(311)
	WC9	Cleartran2	(220)
	WC10	Cleartran1	(311)
	WC11	Cleartran1	(311)
cvd ZnS	Yellow1	CVD3	Unknown
	Yellow2	CVD1	(220)
	Yellow3	CVD2	Mixed
	Raytheon1	Raytheon1	Random
	Raytheon2	Raytheon2	Random
Single Crystal (Eagle-Picher)	SC1	*Lot 14007B	Unknown
	SC2	*Lot 14007B	Unknown
	SC3	*Lot Z1349	Unknown
Crystal Platelet	P1	#ZnS1	N/A
	P2	#ZnS7	N/A

*Eagle-Picher Co. lot numbers.

#Designations listed on sample containers.

etched in a mild solution of H_2SO_4 to remove surface damage caused by polishing. The Eagle-Picher single crystal samples were cleaved from the center of melt-grown boules. The single crystal platelets were studied in their pristine state. A list of the samples studied during this effort is contained in Table II.

Photomicroscopy. Photographs were taken at a magnification of 250 of the surface of each large piece of cvd ZnS and Cleartran from which samples were cut. Samples of cvd ZnS grown by Raytheon were cut from a single large piece, labelled Raytheon1 in Table III. Samples of cvd ZnS grown by CVD Inc. were cut from two large pieces, labelled CVD1 and CVD2 in Table III. Samples of Cleartran were also cut from two large pieces, labelled Cleartran1 and Cleartran2 in Table III. Photographs of the surface of each of these five large pieces of polycrystalline material are contained in Figures 14 through 18.

The photographs show that the Raytheon cvd ZnS is composed of very small, irregular crystals of about 1-3 μm in size. The cvd ZnS grown by CVD Inc. was also composed of irregularly shaped crystals, but these crystals were 1-10 μm large---the pictures of this type of material give the general impression of a larger-sized grain structure. It is also evident from Figures 15 and 16 that the grain size in CVD2 is definitely smaller on the average than the grain size in CVD1. The crystals of which the two pieces of Cleartran are composed are very large (roughly 20-40 μm)

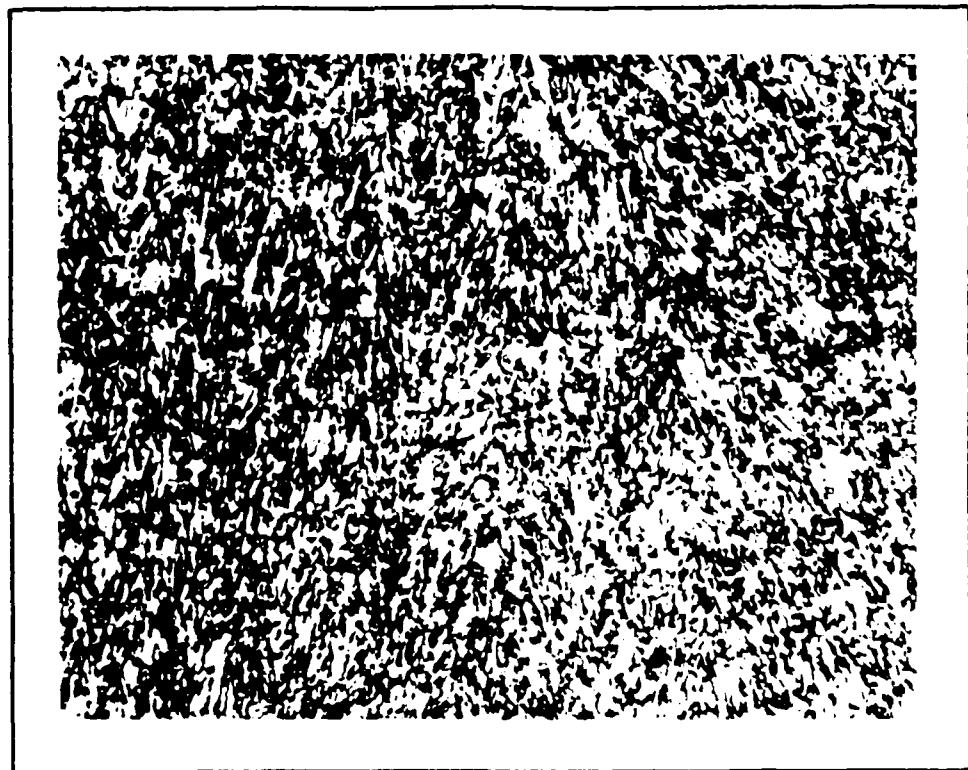


Fig. 14. The surface of Raytheonol at a magnification of 250.



Fig. 15. The surface of CVD1 at a magnification of 250.

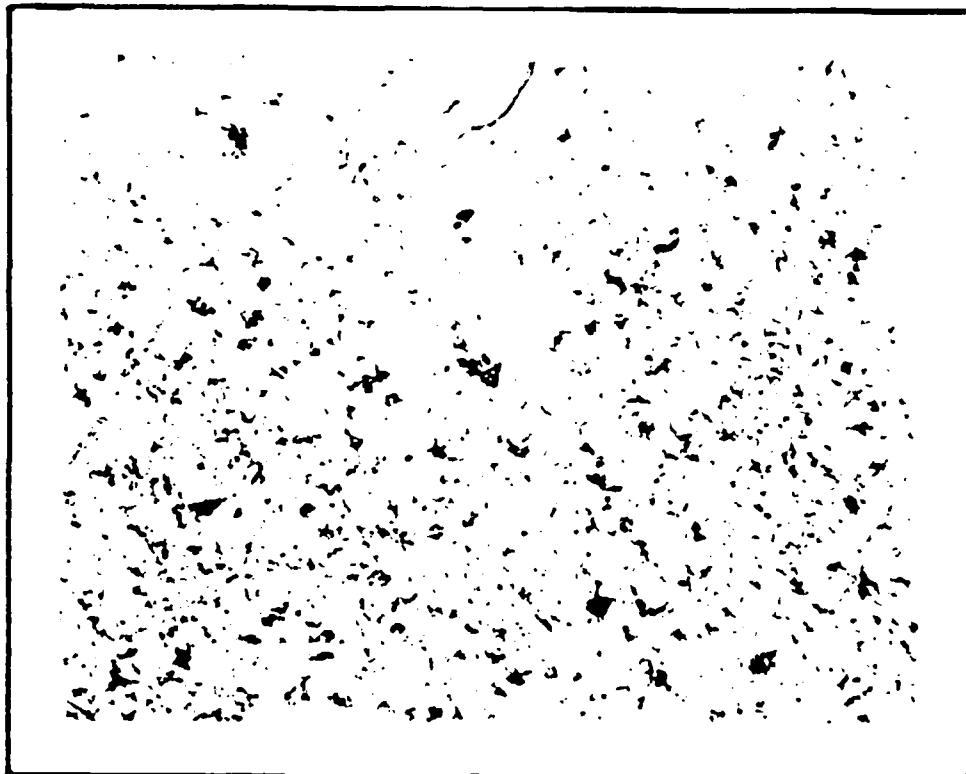


Fig. 16. The surface of CVD2 at a magnification of 250.

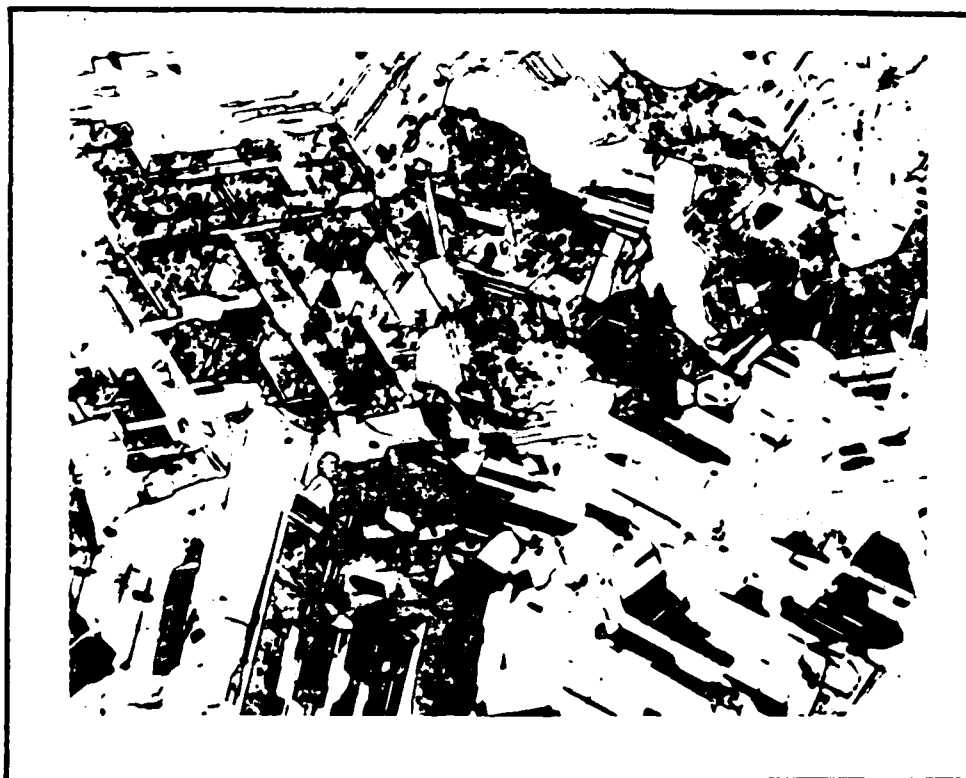


Fig. 17. The surface of Cleartran1 at a magnification of 250.



Fig. 18. The surface of Cleartran2 at a magnification of 250.

and even more irregularly shaped than the crystals in the unprocessed cvd material. Examination of Figures 17 and 18 reveals that there are many more cracks and crevices in Cleartran1 (Figure 17). A previous, larger scale investigation of the size of individual crystals in Cleartran by Taylor and Lefebvre (130) also concluded that the grain size in Cleartran is roughly 20-40 μm .

X-ray diffraction. The polycrystalline samples were examined by x-ray diffraction in both the flat surface and powdered forms. The relative intensities of the x-ray peaks corresponded in all cases to the cubic (3C) phase. There was no indication of the presence of the hexagonal (2H) phase or of any of the many polytype phases of ZnS. The precision lattice constants for each of the five large pieces of polycrystalline ZnS are listed in Table III.

TABLE III

Lattice Constants of the Polycrystalline ZnS Samples

Material	Designation of Block	Lattice Constant (Angstrom)
Cleartran	Cleartran1	5.410 \pm 0.001
Cleartran	Cleartran2	5.4120 \pm 0.0006
cvd ZnS	CVD1	5.408 \pm 0.001
cvd ZnS	CVD2	5.4138 \pm 0.0007
cvd ZnS	Raytheon1	5.4128 \pm 0.0004

The crystals in Raytheon1 were randomly oriented. The crystals in CVD1 were preferentially ordered along the primary growth direction of the crystals with the face of CVD1 containing mostly the side or (220) planar view of the zincblende lattice. The crystals in CVD2 revealed a mixed orientation: 30% of the crystals in the surface displayed the (220) or side view, and 70% displayed the (311) or end view of the zincblende lattice. The surface of Cleartran1 showed only the (311) or end view of the zincblende lattice. The surface of Cleartran2 showed only the (220) or side view of the zincblende lattice. The surface orientation of the crystals in each of the samples studied during this effort is included in Table II, along with the designation of the parent block of material from which each sample was cut.

Spark-source mass spectrometry. Each of the five parent blocks of polycrystalline material were examined by spark-source mass spectrometry with a sensitivity of 5 ppm. Only Raytheon1 showed any indication of impurities, revealing a trace amount of aluminum.

Experimental Systems

Overview. Figure 19 is a schematic of the experimental system. The samples were affixed to the end of a Helitran cold finger by a copper mask and suspended in a high vacuum (10^{-9} torr) chamber. The vacuum was achieved using a

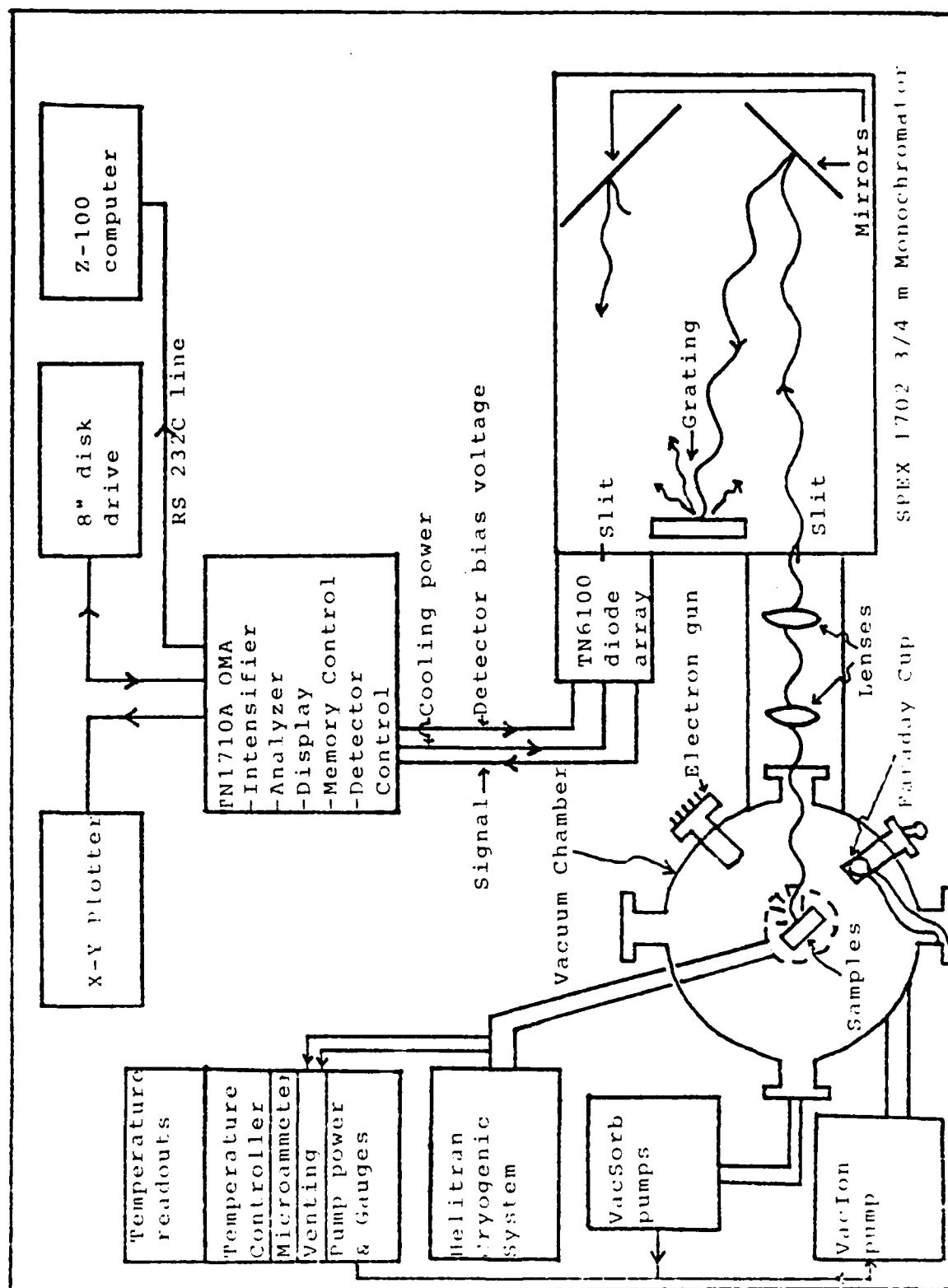


Fig. 19. A schematic of the experiment.

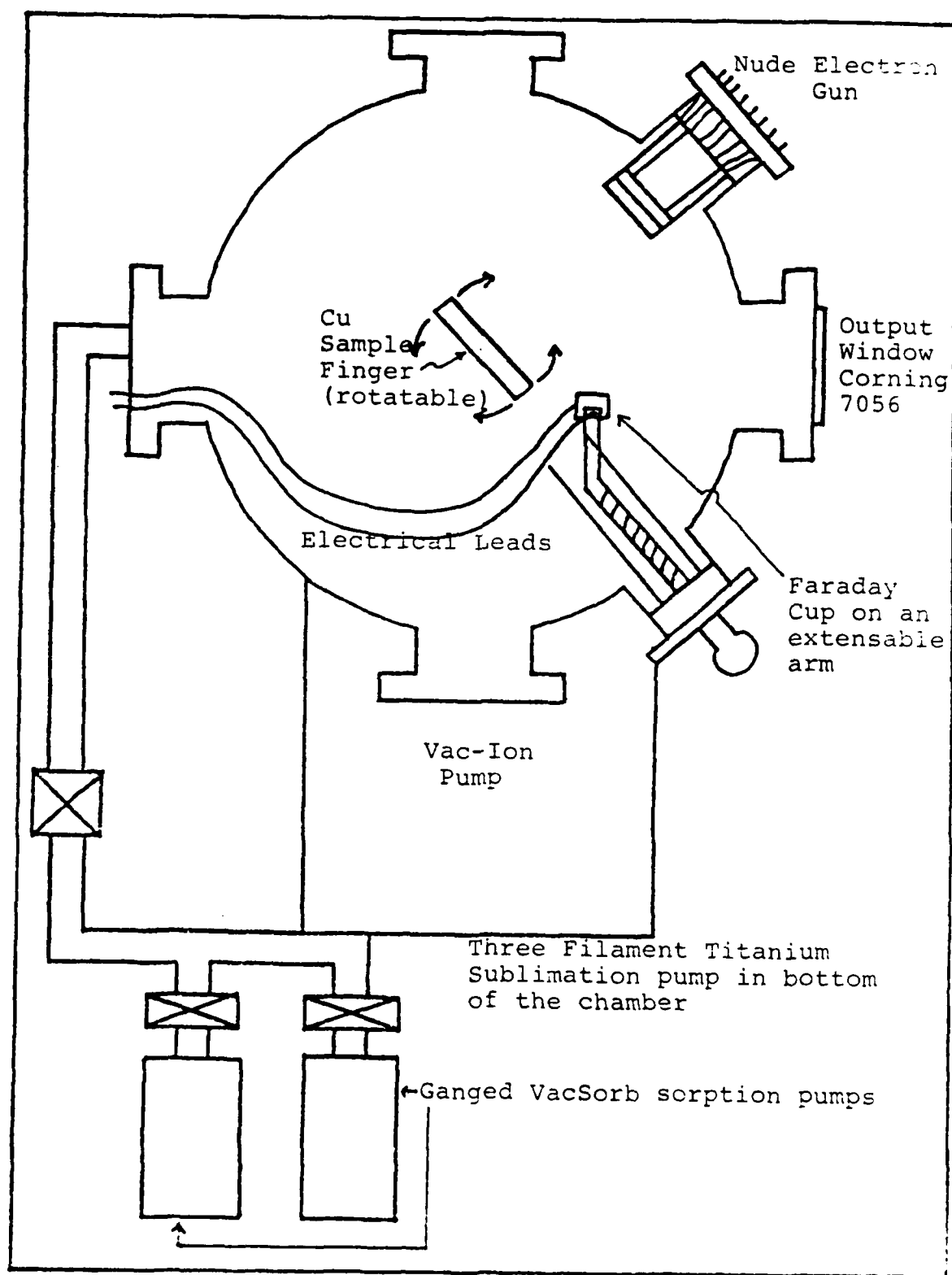


Fig. 20. The main vacuum chamber.

ganged assembly of two sorption pumps and a vac-ion pump. Cathodoluminescence was excited with a Superior Electronics BaO cathode electron gun. Beam currents were measured with a Faraday cup mounted on the side of the cold finger. Sample luminescence was focussed by two quartz lenses onto the entrance slit of a monochromator equipped with a 1200 line/mm grating and a Tracor Northern 6100 1024-diode detector array. A HeNe laser and a mechanical iris on a bi-directional traversing mount were used to align the optics. Signals from the diode array were processed by a Tracor Northern 1710A OMA system. Occasionally, an RCA 8850 photomultiplier tube was attached to the monochromator to record spectral data from larger regions of the spectrum than the 27 nm covered by the diode array. Signals from the RCA 8850 photomultiplier were sampled by an EG G/PAR Model 1112/1121A photon counting system or a Canberra 8100 OMA.

Vacuum System. The main vacuum chamber was cylindrical in shape with a diameter of 0.3 m and a height of 0.67 m (Figure 20). The chamber was equipped with four 8-inch vacuum ports equally spaced around the circumference of the chamber. There were also four 2.75-inch ports placed directly between the 8-inch ports. Three of the 8-inch ports were sealed with Varian plates, the fourth was covered with a vacuum-tight window of Corning 7056. The electron gun was mounted at 45° to the right of the exit window in one of the 2.75-inch ports. An auxiliary Faraday

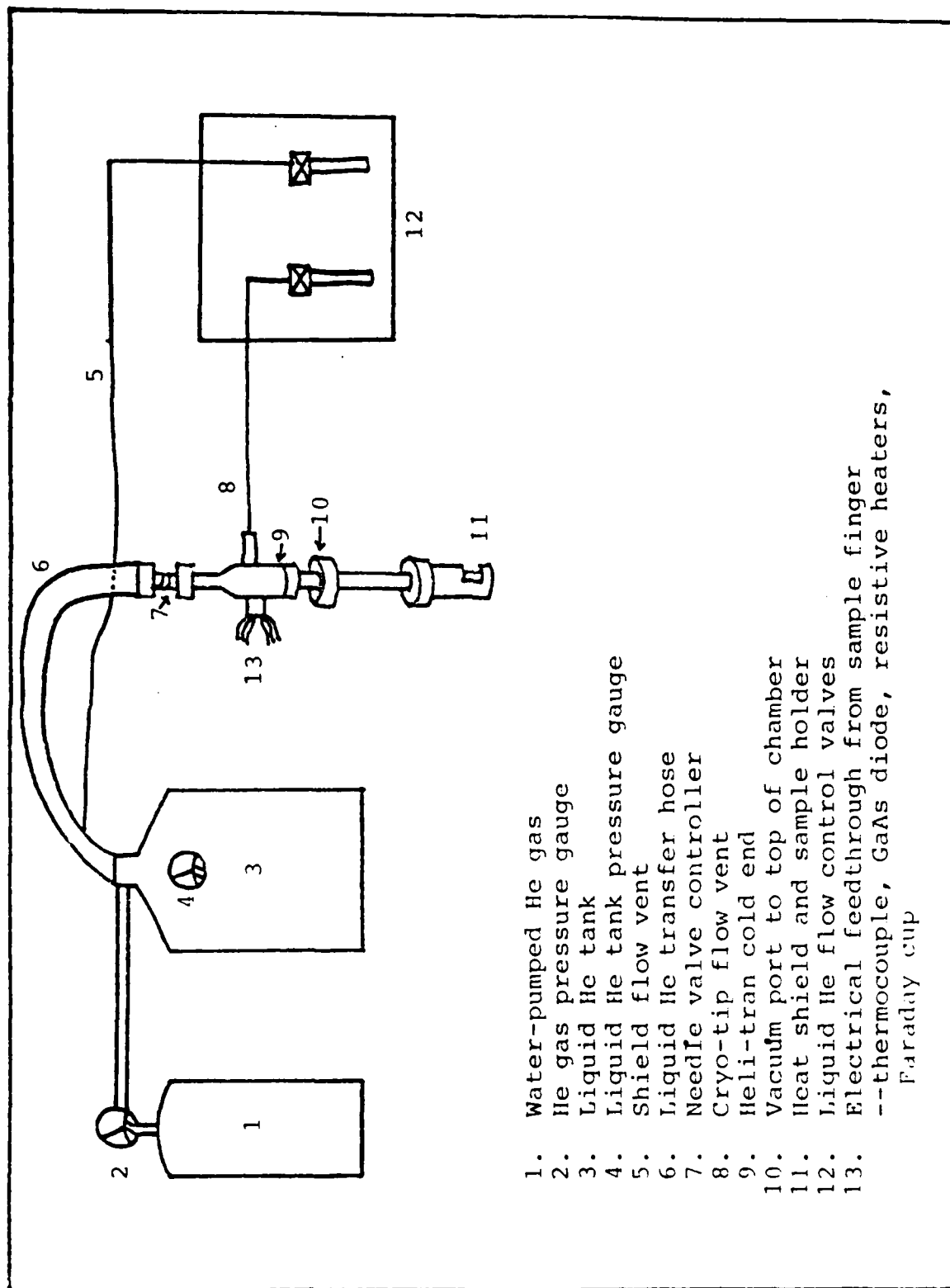


Fig. 21. The cryogenic transfer system.

cup on a retractible arm was mounted at 45° to the left of the exit window in another of the 2.75-inch ports. The Helitran transfer tube was mounted in the top of the vacuum chamber so that the samples were suspended at the level of the exit window.

The vacuum chamber was pumped down to 0.5-0.7 microns with two 10 liter Varian Vacsorb sorption pumps to maintain an oil-free sample environment. A bottom-mounted 110 liter/sec Varian Model 92/0041 vac-ion pump was then used to bring the pressure down to a typical operating level of 5×10^{-9} torr. On several occasions, it was necessary to operate a titanium sublimation pump located 0.3 m below the sample level for as much as one hour to start the vac-ion pump.

Cryogenic Transfer System. The sample was cooled by an Air Products Model LT 3-110 Helitran System (Figure 21). A central cryo-tip line served to transfer liquid helium directly from a 60 liter dewar to the end of the sample finger. The cryo-tip line was surrounded by two inter-connected tubes used to pre-cool and insulate the cryo-tip line. Liquid helium flowed through the inner of the tubes toward the sample finger and then returned to the dewar through the outer tube. The cryo-tip and insulating tubes were surrounded by a vacuum sheath. Exhaust gasses from the cryo-tip and insulating tubes were routed to control valves used to control the rate of flow of liquid helium through the system. The maximum cooling rate

achieved by this system provided a temperature at the sample finger of 9.0 K.

Temperature Control System. After the Helitran transfer lines were purged of air and moisture with dry helium gas, the transfer line was inserted through a valve a short distance into the liquid helium dewar with the cryo-control valves fully open. The liquid helium dewar was maintained at a pressure of about 5 psi with a bottle of dry helium gas. After allowing the cold helium gas to flow through the transfer system for at least 5 minutes, the transfer line was slowly lowered into the dewar until it was below the liquid helium level. It took between 30 and 45 minutes from insertion to cool the sample finger down to 10 K by this method. When the temperature of the sample finger approached 200 K from the high side, a heater jacket was activated to prevent freeze-up of the cryo-tip exhaust line.

The sample finger (Figure 22) was formed from copper with several holes to hold the Helitran cryo-tip cooling line, three resistive heaters, a GaAs temperature sensing diode (on the back of the holder), a Faraday cup, and a Au-Chromel thermocouple (also on the back). The front and back of the sample finger were cut flat. The temperature of the sample finger was actively controlled with a Lakeshore Cryotronics temperature controller linked to the GaAs diode and the three resistive heaters. The Au-Chromel thermocouple linked to a digital Instrulab 5000 indicator

provided an additional check on the temperature of the sample finger. This system served to control the temperature to better than 0.1 K.

Sample handling. The experimental samples were kept sealed in individual plastic containers lined with lens tissue. The samples were held lightly to the flat front of the sample finger with a thin, flexible copper mask (Figure 22). The mask was held to the surface of the sample finger with four brass screws. As many as four samples could be mounted at one time behind four round holes, each 4 mm in diameter. The sample finger was surrounded with a chrome-plated brass cylinder to prevent black-body radiation from the walls of the vacuum chamber from reaching the surfaces of the samples (and therefore reducing a source of noise in the detection system). Samples were handled only with clean, metal tweezers. Sample surfaces were never cleaned, but debris was occasionally blown off the samples with a slow jet of dry helium gas.

The actual temperature of the sample was not directly determined since the temperature sensing diodes were attached to the back and side of the sample finger and not to the sample itself. Additionally, localized heating of the samples due to the electron beam must also have occurred (the electron gun produced between 0.01 and 0.2 watts). A comparison of the temperature shift in energy position of several of the cubic phase emission peaks with

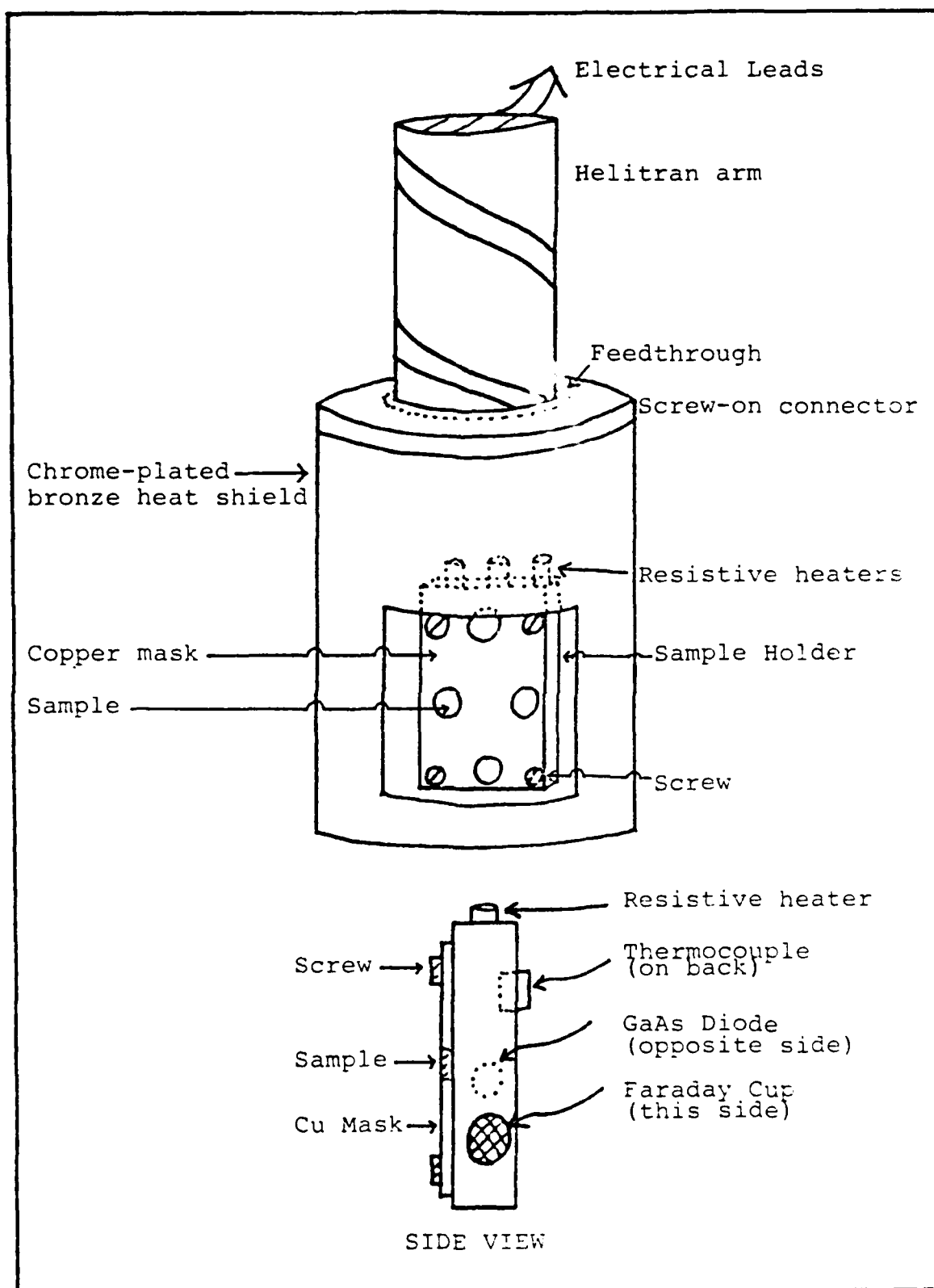


Fig. 22. The sample finger.

similar data published by Yacobi showed so close an agreement at all points from 10 K to room temperature that the sample temperature was probably no more than 2 K hotter than the sample finger (146). This result is probably attributable to the high liquid helium flow rates maintained during the investigation and the short distance between the sample and the two temperature sensors.

Electron gun. A diagram of the Superior Electronics electron gun is included in Figure 23. The cathode of the electron gun was an indirectly-heated barium oxide coated aluminum cap. The cathode was replaced four times during the course of the investigation. Each cathode was aged and activated according to the manufacturer's specifications (Table IV).

TABLE IV
Aging schedule for BaO cathode

Time (min)	Filament Voltage (Volts,DC)	Grid Voltage (Volts,DC)	Anode Voltage (Volts,DC)
1	6.3	0	0
1.5	12.5	0	0
10	9.0	5	150
5	6.3	0	0

The grid, cathode, and filament of the electron gun were floated at about -2000 V by a Keithley 246 power supply. The electron beam was moved electrostatically by a

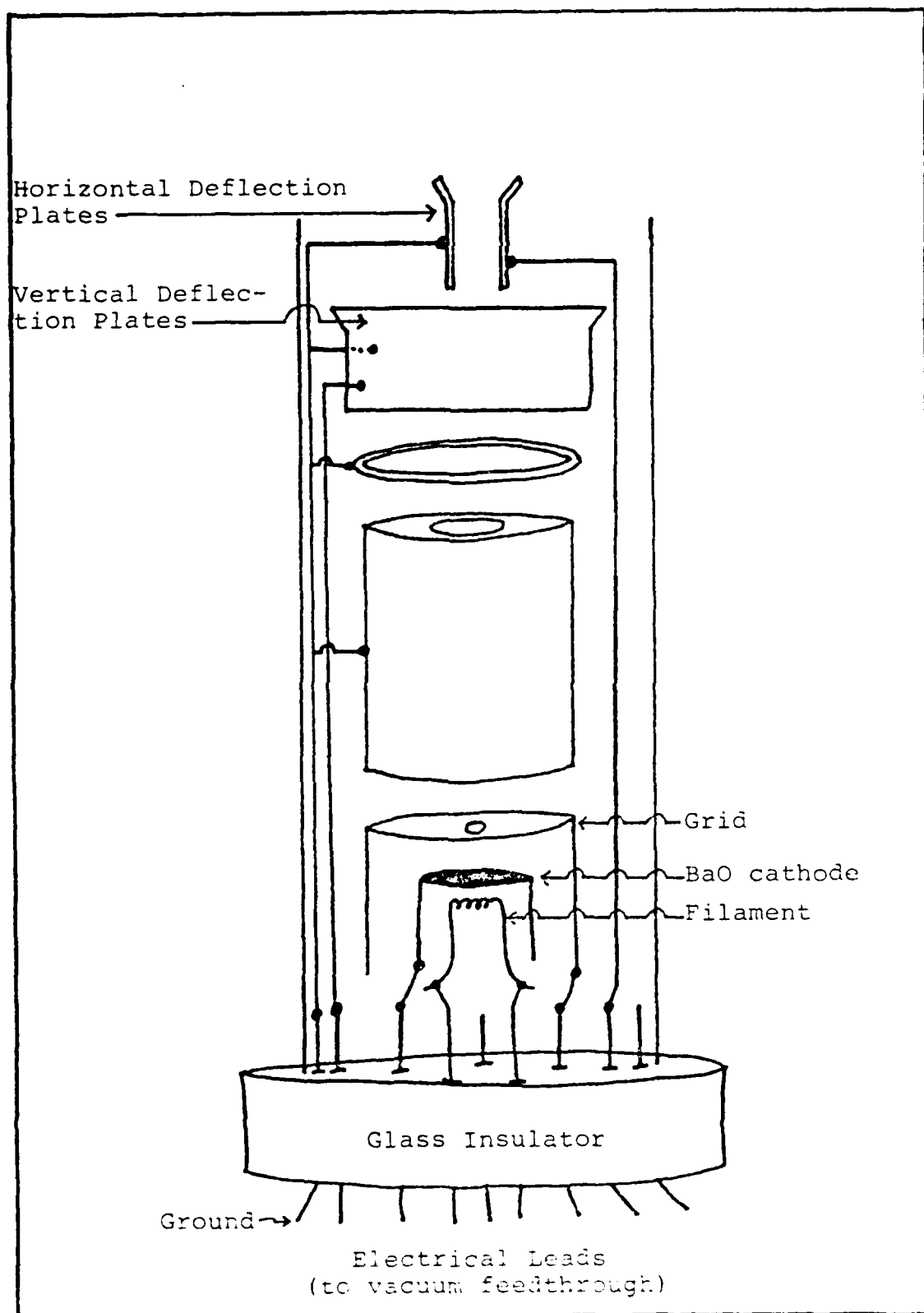


Fig. 23. The Superior Electronics nude electron gun.

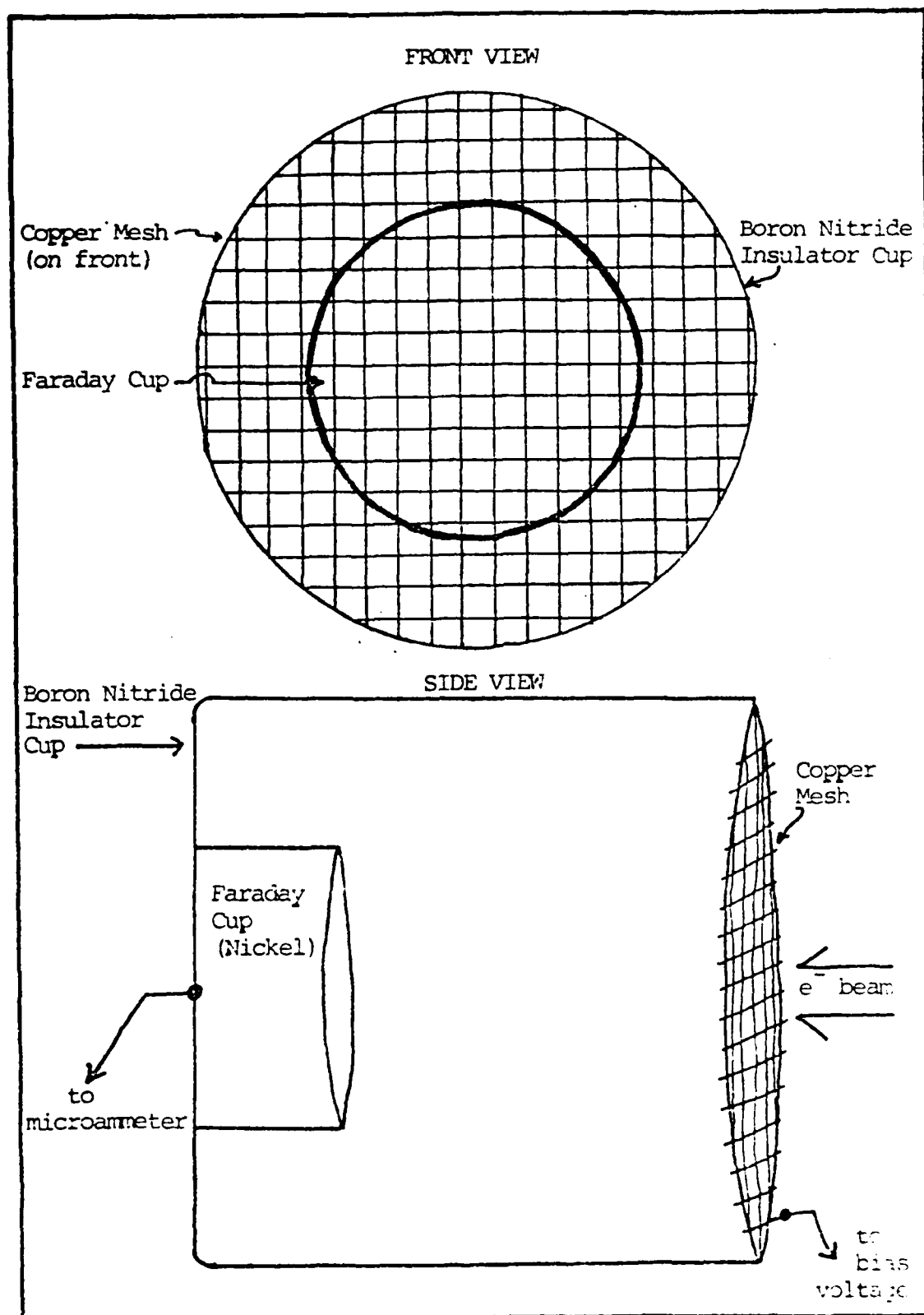


Fig. 24. The Faraday cup.

pair of horizontal and vertical deflection plates attached to a set of high amp-hour batteries. The beam current was primarily measured with a Faraday cup made of nickel and boron nitride (Figure 24). The front of the Faraday cup was covered with a copper screen kept at a bias of -45 V to improve the measurement by reducing the loss of back-scattered electrons. The beam current was varied from 0.5 μ A to 100 μ A by varying the grid voltage and the current through the heating filament. The spot size of the electron beam on the sample was varied from 2 mm to 0.4 mm radius by controlling the voltage at the focussing ring.

The electron gun voltage was at first varied between 1.5 kV and 3.0 kV, but as there was never any discernable difference in the sample luminescence the bulk of the spectra were taken with an electron gun voltage of 2 kV. Applying the model of Kanaya and Okayama (equation 2) to our samples and a 2 keV beam energy, the likely penetration range for the electron beam during the bulk of this work was 65 nm.

Optical System. The sample luminescence was collected and focussed onto the entrance slit of a 3/4 m monochromator by an optical system consisting of two 1.5-inch diameter quartz lenses. The focal lengths of the lenses were chosen to slightly (10%) overfill the monochromator grating and reduce the alignment sensitivity of the monochromator. A 2 mW HeNe laser beam was sent through a 0.1 mm aperture and co-aligned with the electron

beam spot on the sample surface. The system was then pre-aligned by focussing the scattered HeNe light on the straight entrance slit of the monochromator. This alignment was fine-tuned by observing the detector count rate when the monochromator was set to pass a strong sample line (such as the Cu-blue line).

Signal detection and processing system. Two distinct detection systems were used during the course of this project. Each detection system required a different set of processing electronics.

The heart of the first detection system was a Tracor Northern TN-6122 Intensified Diode-Array Rapid Scan Spectrometer. The primary component of the TN-6122 is a cooled linear, self-scanned array of 1024 silicon photodiodes at 0.025 mm spacing fronted with a 25 mm image-inverting micro-channel plate intensifier coupled to the diode array with fiber optics. A coating of sodium salicylate was sprayed on the protective quartz window of the detector array. Sodium salicylate is a phosphorescent compound capable of converting ultraviolet photons into more easily detected visible photons with a quantum efficiency near 1. When placed in the Spex 1702 3/4 m monochromator equipped with a 1200 line/mm grating, the detector spacing corresponds to 0.0270 nm/channel or 0.307 meV/channel at 330 nm. The manufacturer specifies a resolution of 4-5 diodes (full width at half maximum); a number validated by measurements of narrow gas lines in the

laboratory. Each silicon photodiode has the S-20 Extended Red response when removed from the array (see Figure 25).

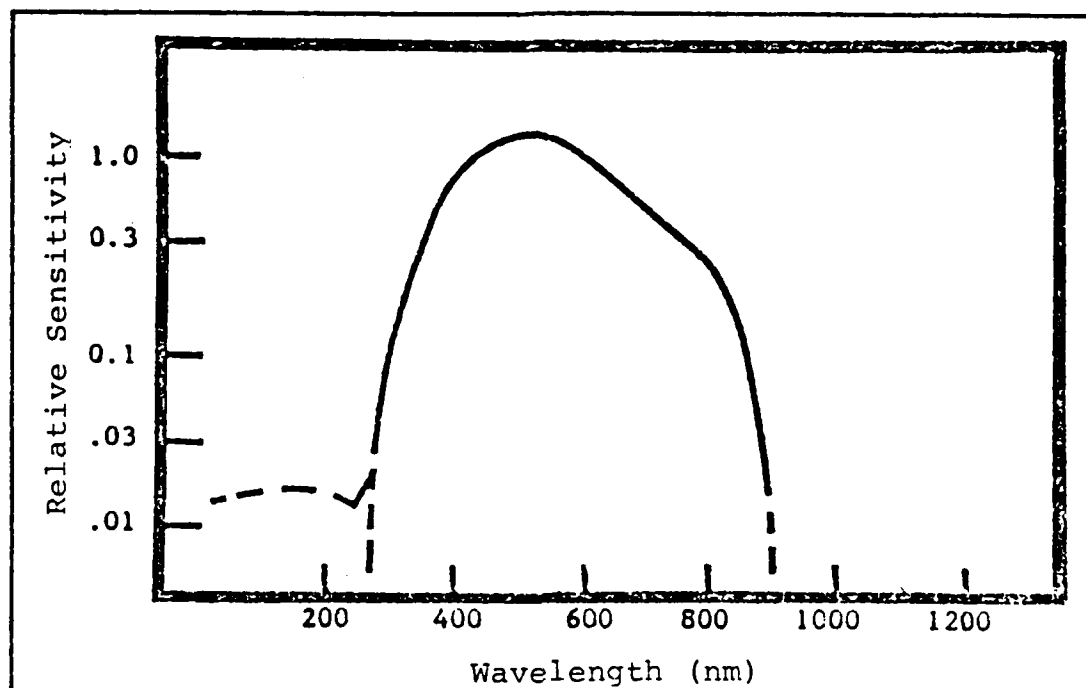


Fig. 25. Spectral response of TN-6122 photodiode.

The multiplexed signals produced by the detector array were captured and processed with a Tracor Northern TN-1710A Acquisition System configured as an optical multichannel analyzer (OMA). The OMA had front-panel controls for selecting the exposure time of the array, the number of scans per run, and the gain of the intensifier. Intensifier gain could be set as low as 10 and as high as 6000. A memory subgroup module provided four separate sections of memory, each of which was capable of recording an entire 1024-point spectrum. This made it possible to record a background spectrum for subtraction of such noise sources as light leakage, dark-current, and video pedestal from the raw data. Once the background noise was

subtracted from the data, the spectra were archived on 8-inch floppy disks.

The main component of the second detection system was an RCA 8850 photomultiplier tube cooled to -50°C in a Products for Research TE-114 housing. The output of the photomultiplier tube was routed to a PAR Model 1121 Amplifier/Discriminator set to remove low frequency noise. The signal was then sent to either a PAR Model 1112 Photon Counter/Processor (and immediately plotted on a Hewlett Packard Model 7045 XY plotter) or a Canberra Model 8100 OMA. In order to condition the discriminator's output for the OMA, the pulses from the discriminator were conditioned by a home-made interface. The spectrum stored in the Canberra's memory was either archived on cassette tape with a Techtran Datacassette Drive or on 5.25-inch floppy disks. The spectra were stored on floppy disks by transferring the Canberra's memory through its built-in RS-232C serial interface to a Zenith Model 100 microcomputer. The software necessary to perform this task is discussed in the Appendix.

All sample spectra were corrected for instrument response by direct comparison of the response of each detection system to an EG G Model 597 lamp system equipped with a calibrated FEL 1000 W tungsten halogen lamp. The lamp standard was obtained by transfer measurement from National Bureau of Standards calibration lamps. The software necessary to compare the system response to the

lamp standard and produce corrected data is discussed in the Appendix.

The corrected spectra were plotted by importing the data into Lotus123's spreadsheet and graphics packages with Lotus's own translation routines. The graphs prepared by Lotus123 were then transferred to paper by an Epson FX80 dot matrix printer run by the Lotus123 quad-density printer driver. The figures included in this thesis are either the direct output of the printer, a graphics artist's rendition of XY plots produced by the Hewlett Packard plotter, or a graphics artist's rendition of a part of one of the printer plots.

IV. Results and Discussion

Sequence of Presentation

The cathodoluminescence of each form of ZnS investigated will be discussed in the following order: cubic single crystal ZnS grown by Eagle-Picher Co., crystal platelets grown by D. C. Reynolds, polycrystalline cvd ZnS grown by Raytheon, polycrystalline cvd ZnS grown by CVD Inc., and finally Cleartran. In each section, the variation of the cathodoluminescence from spot to spot on a single sample and from sample to sample of the same form of ZnS will be discussed. The temperature dependence of the cathodoluminescence will also be described in the range of 10-300 K. Following these individual treatments, the various cathodoluminescent responses of the different forms of ZnS will be compared to one another. Chapter IV will close with a discussion of the temperature dependence of the band gap in cubic single crystal ZnS and Cleartran.

Single Crystal ZnS (Eagle-Picher)

The Eagle-Picher single crystal material was as transparent to the eye as the Cleartran material. The cathodoluminescence from the cleaved surface of the Eagle-Picher samples was more intense both in the near band-edge region and in the visible or SA regions than any other form of ZnS. This high efficiency emission is undoubtedly associated with the relative perfection of the

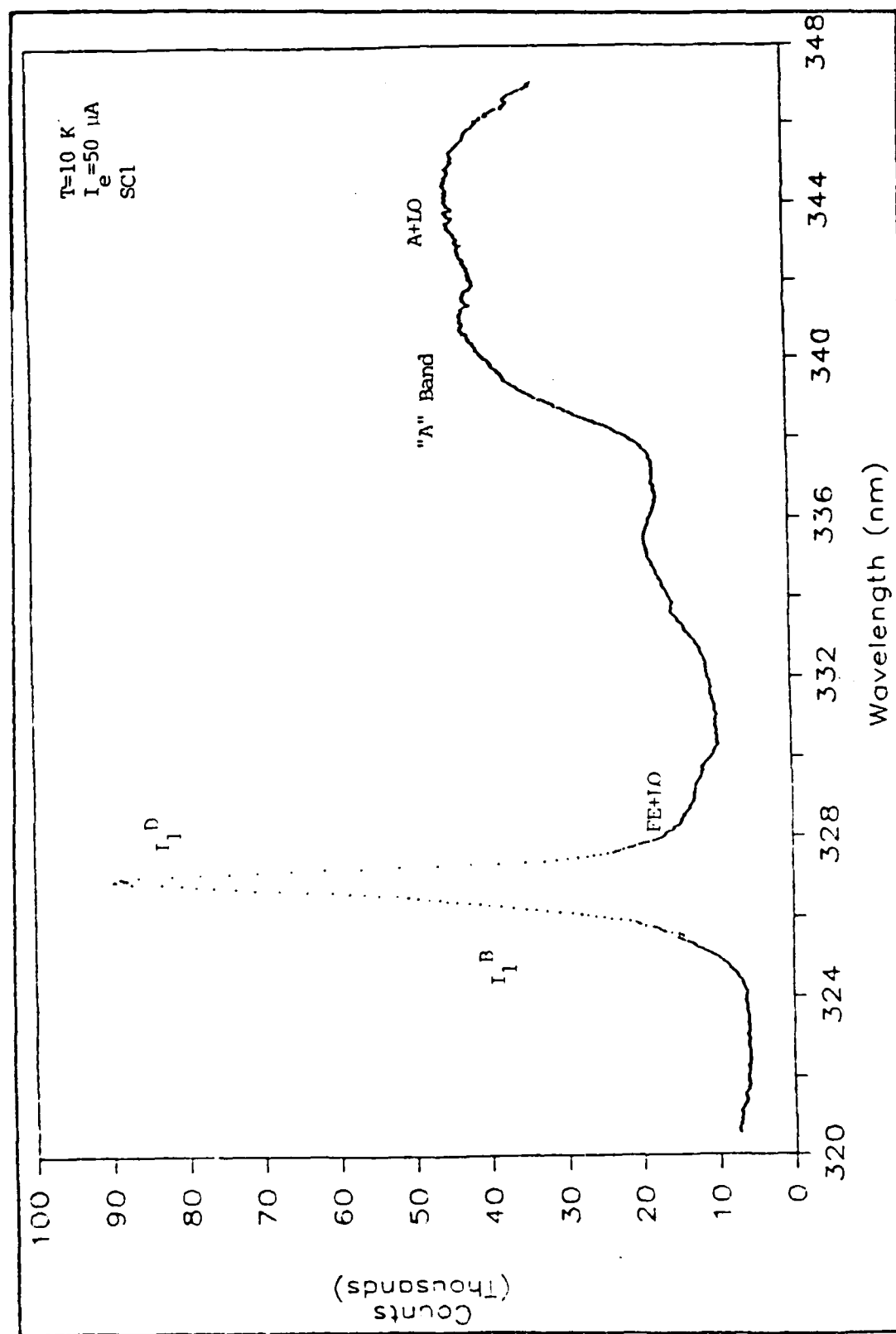


Fig. 26. The 10 K cathodoluminescence of a sample of Eagle-Picher single crystal ZnS.

cleaved surface.

The cathodoluminescence of this form of ZnS was characteristic of pure cubic phase ZnS. Although these crystals were originally grown as hexagonal phase ZnS crystals ten years ago, they apparently lapsed into the cubic phase after extended storage at room temperature. This lapsing is a consequence of the room temperature thermodynamic instability of the hexagonal phase noted by a number of authors including U. Flesch who also measured the cathodoluminescence of hexagonal crystals that had converted into the cubic phase during storage (48:137). A representative cathodoluminescence spectrum in the near band-edge region is shown in Figure 26.

The low temperature cathodoluminescence was dominated by the Cu-blue and SAL bands. The luminescence from these peaks was so strong that the sample was difficult to view with the naked eye even at current densities as low as 0.1 A/m^2 . As the temperature of the sample rose above 50 K, the Cu-blue band became the dominant visible emission, persisting strongly even at room temperature.

The low temperature near band-edge luminescence consisted of a pair of DBE lines at 326.4 nm (I_1^B) and 327.0 nm (I_1^D) with the latter line generally dominant; the LO phonon-assisted replica of the $n=1 \Gamma_6 - \Gamma_8$ free exciton at 329.6 nm; two broad, low intensity emission bands at 334 nm and 335.3 nm; and a strongly broadened 340.0 nm DA band with at least one phonon replica. The DA band has been

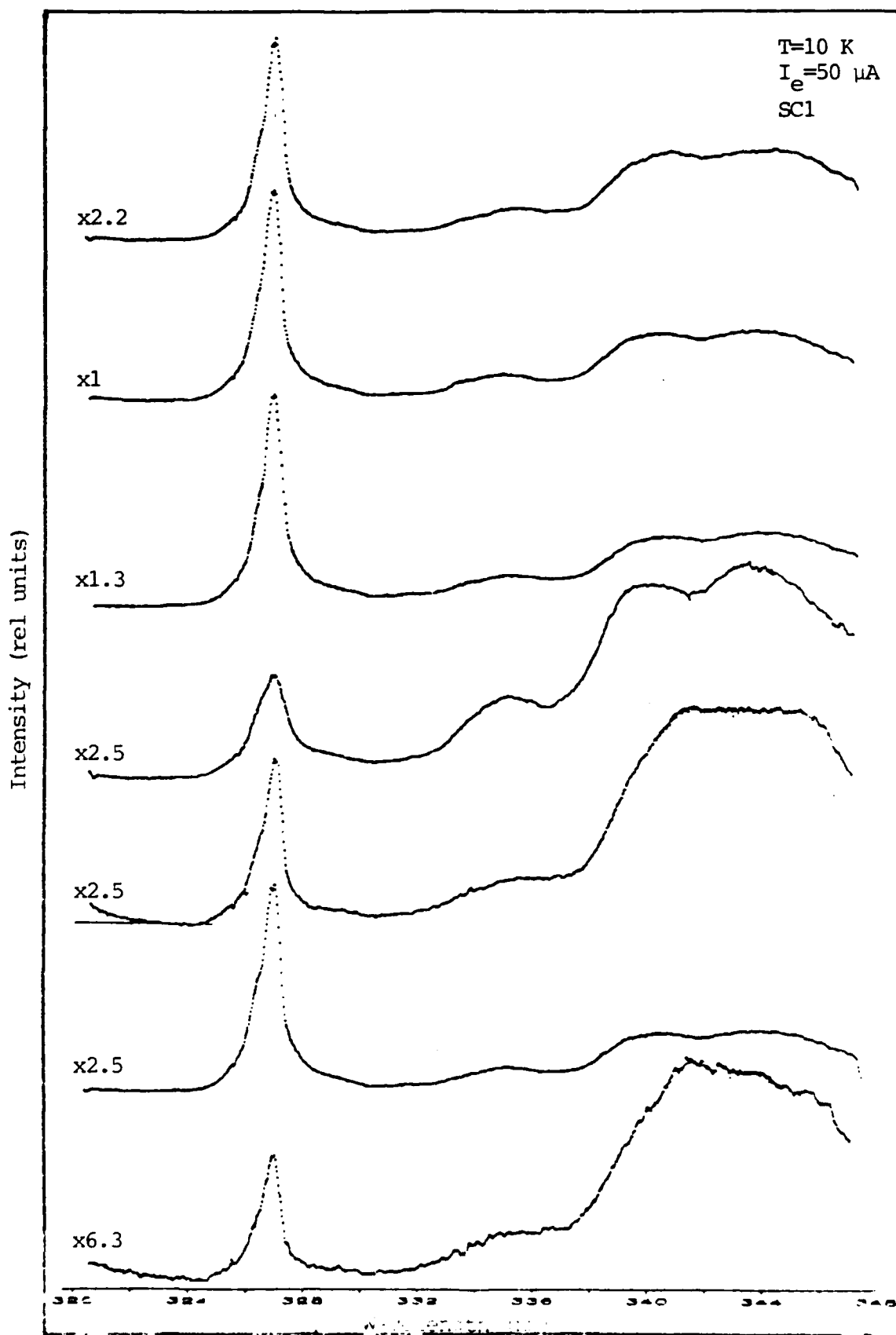


Fig. 27. The variation of cathodoluminescence with position on the surface of a sample of Eagle-Picher single crystal ZnS (SC1).

labelled "A" in Figure 26. The LO phonon replica of the A band is separated from the parent by 43.5 meV---a number that agrees very well with previous theoretical predictions and actual measurements of the LO phonon energy in cubic ZnS (18, 43). The full width at half maximum of the joint $I_1^B - I_1^D$ peak was variously measured as 7-10 meV. The low end of this range of widths refers to cases where the I_1^D line was strongly dominant over the other line

Spot to spot variations. The changes in sample cathodoluminescence at different locations on the surface of a single sample of this material are illustrated in Figure 27. As the electron beam scanned the surface of the sample, the relative importance of the A band and its phonon satellite fluctuated sometimes significantly. In most locations on the sample surface, the DBE emission lines were greatly dominant (Figure 27 a-d) and there were only slight changes in the importance of the A band with respect to the DBE lines. The only significant change in the cathodoluminescence between these locations was in the absolute intensity of the emission. The intensity of the DBE lines displayed in Figure 27 d) increased three-fold in Figure 27 b) (these two spots were physically very close). There were also locations near the edge of the sample surface where the intensity of the DBE emission dropped by nearly a factor of 10 from that shown in Figure 27 d).

There were locations on the surface of the sample where the DA emission band labelled A was the dominant emission

in the near band-edge region (Figure 27 e-g). These spots were relatively rare and may well be associated with a greater concentration of the impurities responsible for the A band. The A band was usually broadened into its phonon replica at these spots (Figure 27 f-g), although the associated DBE lines were not appreciably broadened.

Sample to sample variations. The samples of Eagle-Picher single crystal ZnS were all cut from the center of the same boule. The variation in cathodoluminescence from sample to sample mirrored the spot to spot variations. This indicates that the Eagle-Picher material is very homogeneous, as one would expect for a single crystal.

Temperature variation. As the temperature of the sample rose, the DBE lines broadened according to kT . Above 110 K, the broadened DBE lines began to merge into the remains of the A band. At room temperature, a severely broadened but still distinct and intense emission at 336.5 nm was the only remaining feature of the near band-edge cathodoluminescence. These changes are illustrated in Figures 28 and 29, a sequence of cathodoluminescence spectra taken at the indicated temperatures.

ZnS Platelets

The platelets studied here were transparent spears and thin plates no longer than 0.5 cm and no thicker than 100 μ m. The cathodoluminescence from these platelets was very

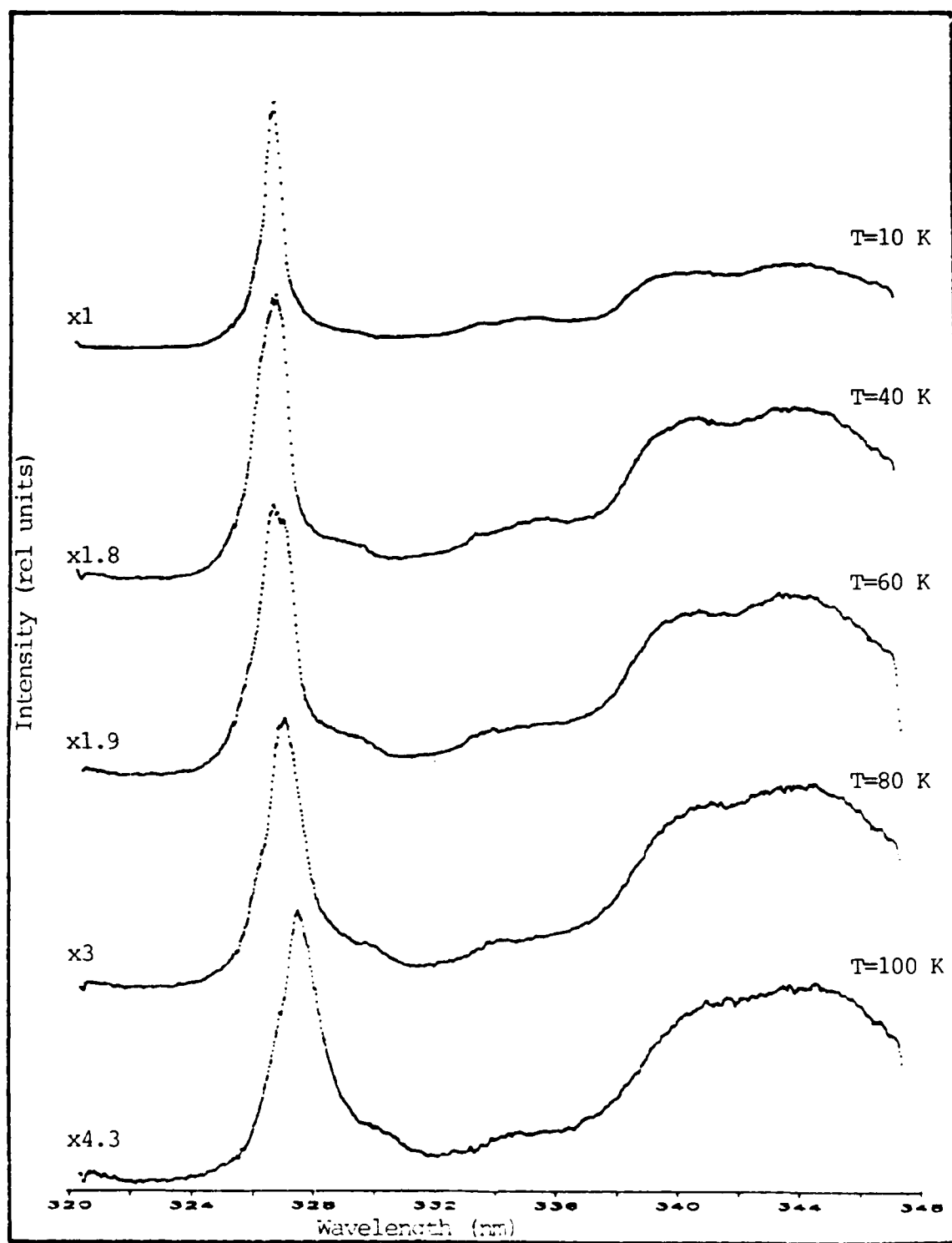


Fig. 28. The variation of cathodoluminescence with temperature for 10 K \leq T \leq 100 K on a sample of Lead-Picher single crystal ZnS (SC1).

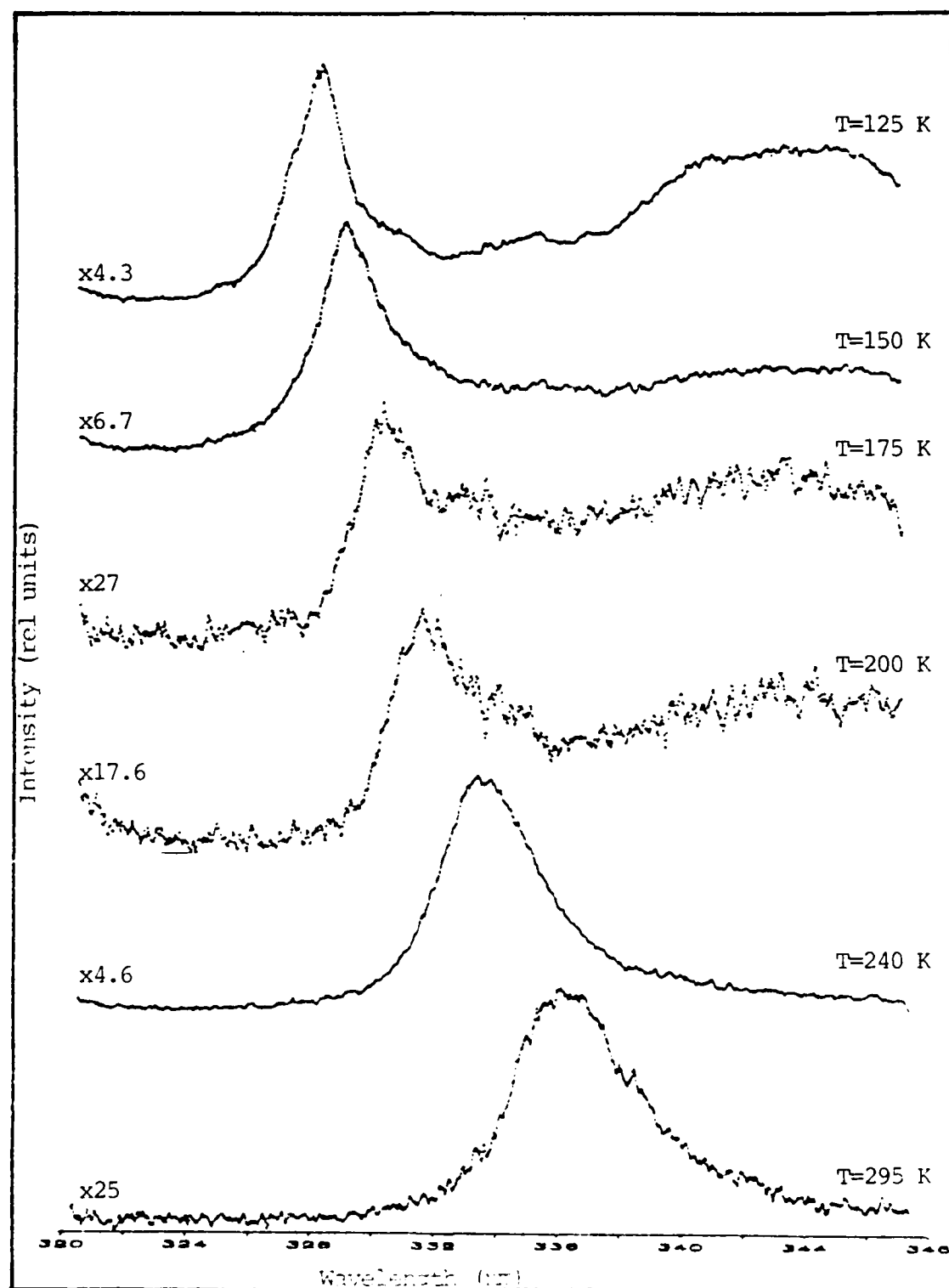
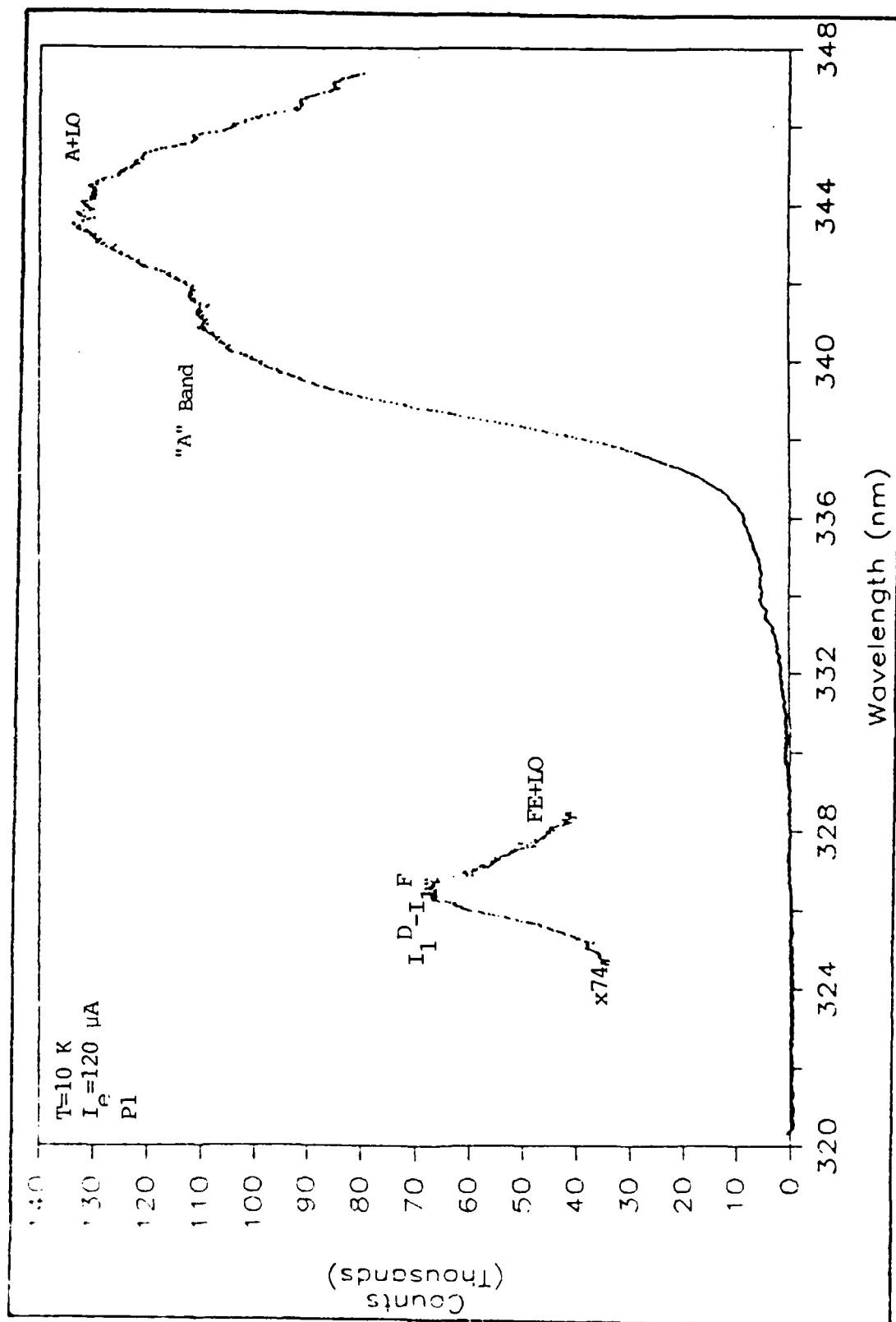


Fig. 29. The variation of cathodoluminescence with temperature for 125 K \leq T \leq 300 K on a sample of Eagle-Picher single crystal ZnS (ST1).



The 10 K cathodoluminescence of a crystal platelet (P1).

poor. Under a polarizing microscope, the platelets revealed distinct bands of differing birefringence with dimensions ranging from 5 μm up to about 40 μm . It has already been shown that the degree of birefringence of a ZnS crystal varies linearly with the crystal's degree of hexagonality (22, 147) where the cubic phase has zero birefringence and the hexagonal phase has the greatest birefringence. It is therefore expected that each of these small-scale bands within the platelets corresponds to a different polytype of ZnS. This phenomenon of polytype banding in platelets has been seen and investigated before with low resolution SEM-CL devices (32, 61, 142, 144). A cathodoluminescence spectrum from one of the platelets is illustrated in Figure 30.

The spectrum of Figure 30 is primarily cubic. The dominant feature of the spectrum is an extremely bright A band with a single LO phonon duplicate. There is a very weak, broad emission band near 327-330 nm attributable to DBE recombination, but there are no other significant features in the spectrum. The visible emission from this spot consisted of a very broad, featureless Cu-green band; an almost vanishingly small Cu-blue band; and very occasionally a tiny, broad red band near 690-720 nm.

Spot to spot variations. Most spots on the platelets produced cathodoluminescence similar to Figure 30, although at some locations there were faint indications of emission in hexagonal ZnS. There were also a great number of

locations where all near band-edge luminescence was completely quenched. These regions were not associated with any structure, defect, or inclusion visible at a magnification of 250 under a polarizing microscope.

The character of the visible luminescence changed dramatically from spot to spot. Usually, the Cu-green band was dominant, but the Cu-blue band and a red band attributable to the presence of tin or (possibly) of copper were often seen as well.

Sample to sample variations. As was true for the Eagle-Picher material, the sample to sample variation of cathodoluminescence did not differ from the spot to spot variations already described.

Temperature variation. The cathodoluminescence of the platelets in the near band-edge region began to quench rapidly above 50 K. As the sample temperature rose to 100 K, only the visible emission bands could be detected. At room temperature, the platelets produced only a very weak green luminescence band.

Raytheon cvd ZnS

The cvd material grown by Raytheon was an opaque brownish-yellow color. High current densities on the order of $100-200 \text{ A/m}^2$ were necessary to excite a measureable amount of luminescence. A representative cathodoluminescence spectrum is shown in Figure 31.

The visible cathodoluminescence was dominated by either

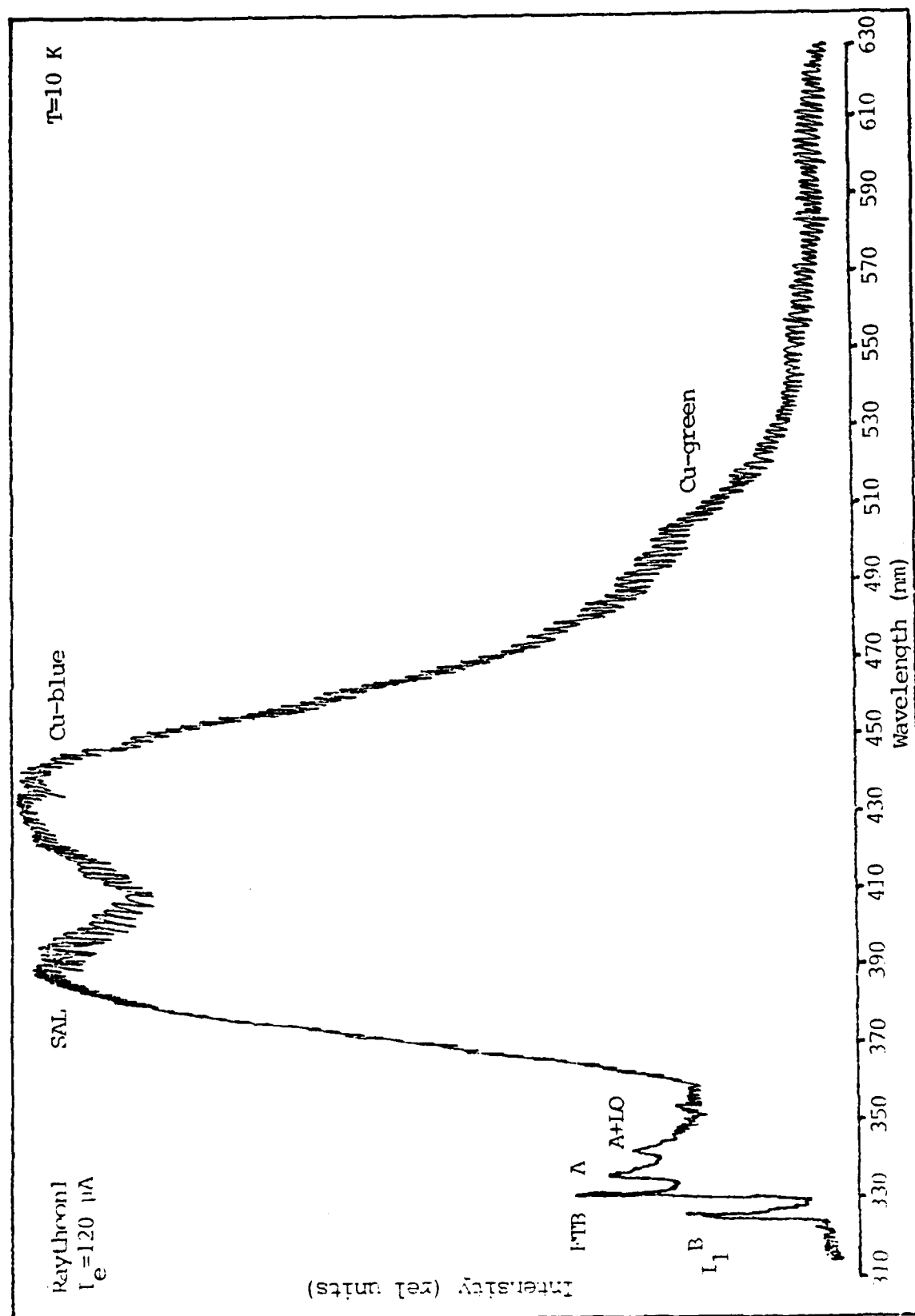


Fig. 31. The 10 K cathodoluminescence of a sample of Raytheon cvd ZnS (Raytheon1).

the SAL or Cu-blue bands at temperatures below 50 K. The well-known Cu-green band was also generally present as a long wavelength shoulder to the Cu-blue band. The near band-edge cathodoluminescence consisted of three main centers: the I_1^A or I_1^B lines at 326.2 nm or 326.4 nm; a FTB recombination band at either 331.3 nm or 331.7 nm; and a DA band labelled "B" at about 337.5 nm with one or more LO phonon replicas. All of the near band-edge and visible luminescence was extremely weak---the spectrum of Figure 31 was taken over the space of several hours. The emission bands were also unusually broad; the width of the DBE lines varied from 18 to 22 meV.

Spot to spot variations. The character of the emissions from this form of ZnS changed very little with position on the samples. There were, however, regions on the sample surfaces where all luminescence was strongly quenched even at 10 K. Despite careful viewing at a magnification of 250 to 500, these regions did not appear to be associated with any imperfections or inclusions visible under white light.

Sample to sample variations. There were no discernable variations from sample to sample. All Raytheon samples were cut from a single large piece of Raytheon ZnS, and the intensity and character of the cathodoluminescence attested to this fact.

Temperature variation. As with the single crystal ZnS, the intensity of the cathodoluminescence dropped off

rapidly above about 50 K. First, the band-edge luminescence became undetectable, then the SAL band vanished into the high energy side of the Cu-blue peak. Finally, at temperatures slightly in excess of 100 K, even the Cu-blue band became difficult to detect. At room temperature, the Raytheon material had virtually no detectable cathodoluminescence.

CVD Inc. cvd ZnS

The cvd material grown by CVD Inc. was a translucent yellow color. The two parent blocks examined during this effort were composed of larger, better oriented crystals than the Raytheon material. The cathodoluminescence from the cvd ZnS grown by CVD Inc. was more intense than that from the Raytheon cvd ZnS.

The first block of this material was composed of relatively large (3-10 μm) crystals. These crystals were oriented so as to present a side view of the crystal growth direction at the surface of the samples. Samples cut from this block produced the strongest cathodoluminescence of any of the polycrystalline samples except Cleartran. The near band-edge peaks dominated the cathodoluminescence. A representative low temperature spectrum is shown in Figure 32. The cathodoluminescence produced by samples from this block consisted of a single identifiable DBE line, usually the I_1^F line at 327.6 nm; a weak DA band centered at 337-338 nm (the B band) with a single LO phonon replica; a

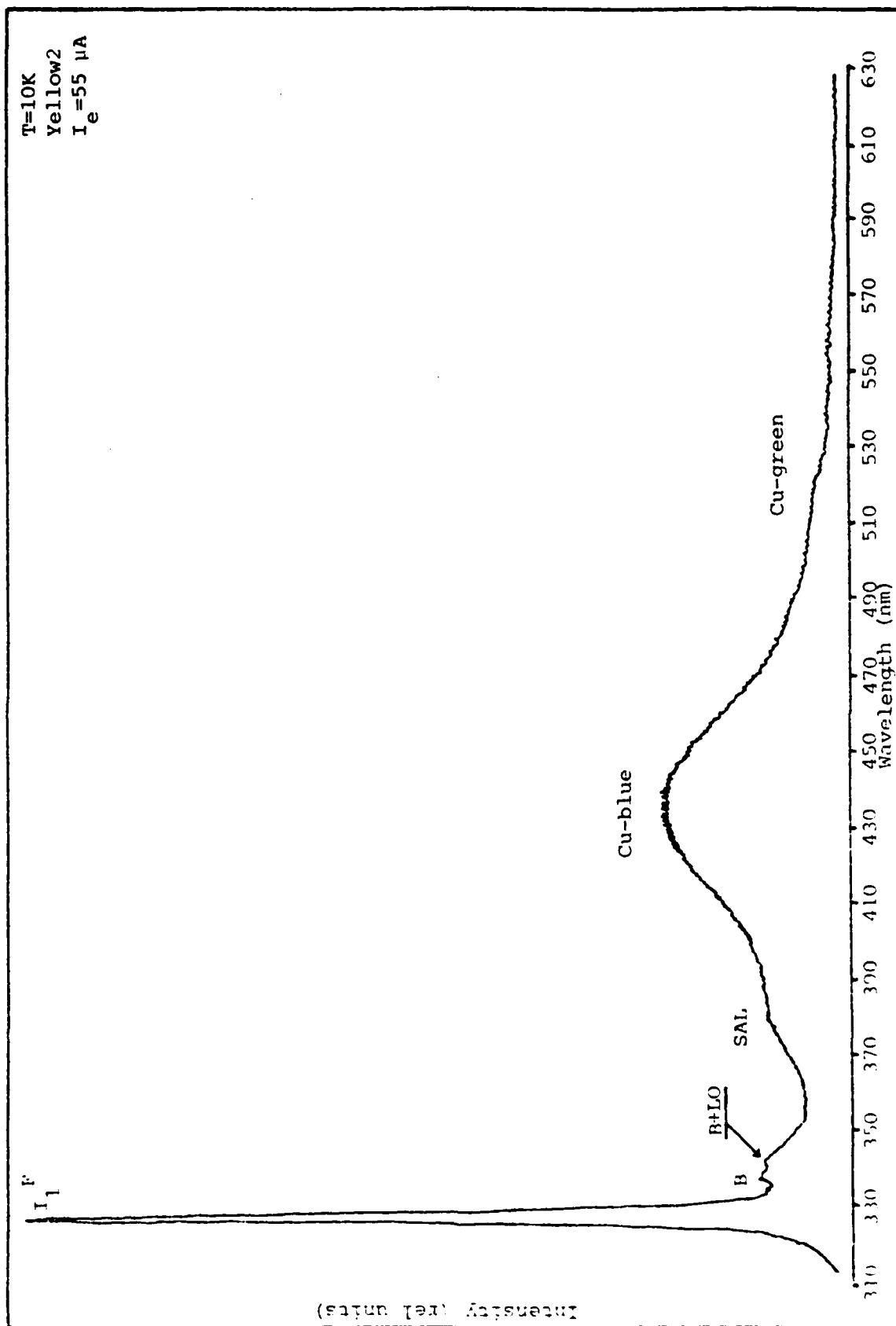


Fig. 32. The 10 K cathodoluminescence of a sample from the first block of CVD Inc. cvd ZnS.

broad, asymmetric Cu-blue emission band; and weak SAL and Cu-green bands. The width of the DBE line was typically 16-20 meV, indicating considerable broadening and/or the presence of other, less intense DBE lines.

The second block of this material was composed of smaller crystals (2-4 μm) which were oriented in a mixture of the side (30%) and end (70%) views at the surface of the block. Samples cut from this block had relatively weak cathodoluminescence dominated by the Cu-blue band at low temperatures. A cathodoluminescence spectrum from a surface location yielding comparatively strong near band-edge luminescence is displayed in Figure 33. The near band-edge luminescence consisted of a very broad (18-30 meV) composite DBE line centered at either 326.4 nm (I_1^B) or 326.6 nm (I_1^C); an occasionally intense FTB line near 331.4 nm; and the B band centered at 337-338 nm with one or two phonon replicas. The SAL band was often seen as a high energy shoulder to the Cu-blue band at temperatures below 50 K. The Cu-green band was also a persistent feature.

Spot to spot variations. As the electron beam scanned across the surface of these samples, the overall intensity of the cathodoluminescence varied greatly. At some locations, only the Cu-blue and SAL peaks could be detected at low temperatures. At other locations, all cathodoluminescence was so strongly quenched that nothing could be seen. There were also small, isolated regions where the Cu-green or Cu-blue bands were very intense and

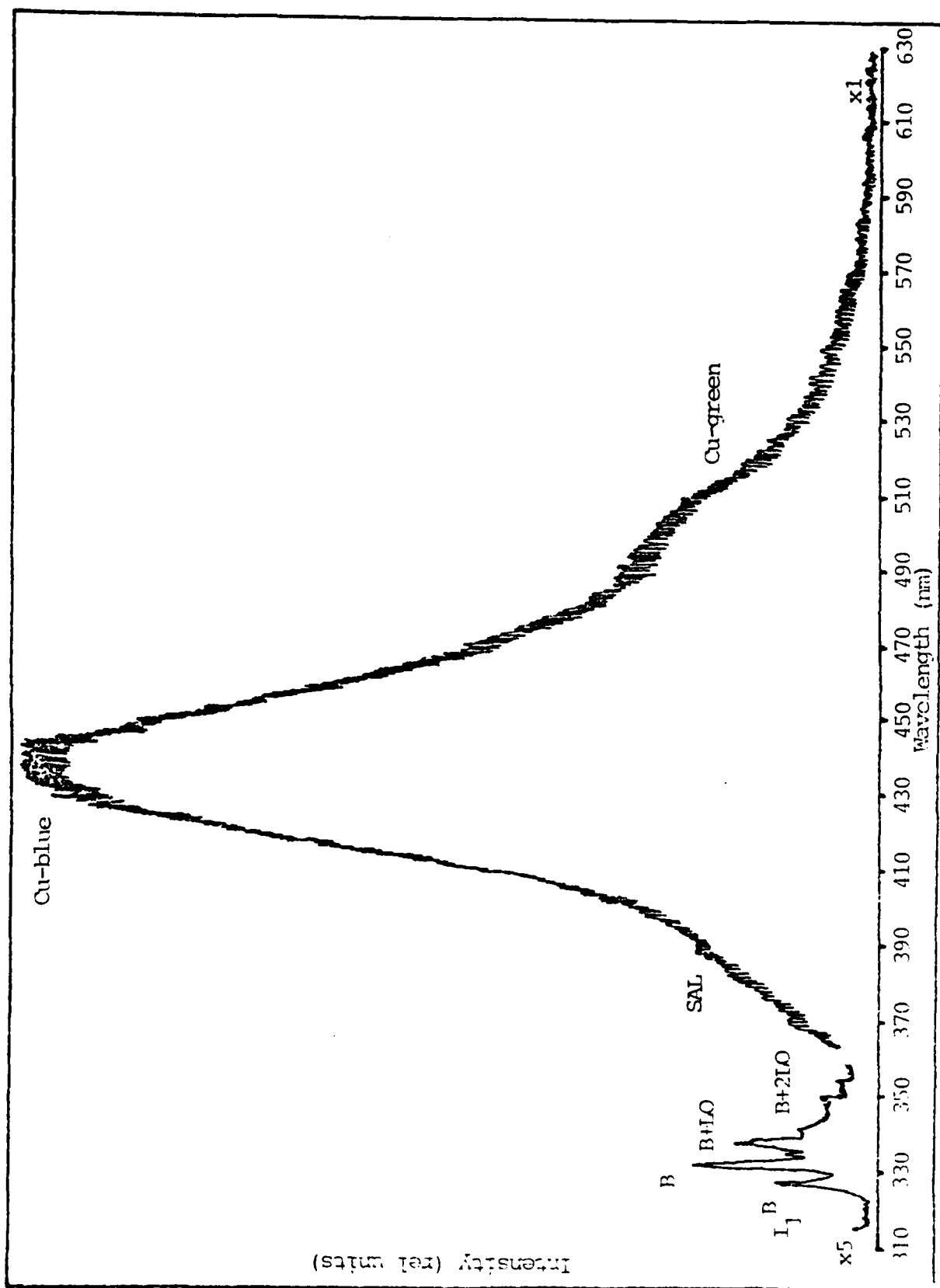


Fig. 23. The 10 K cathodoluminescence of a sample from the second block of CVD Inc. cvd ZnS.

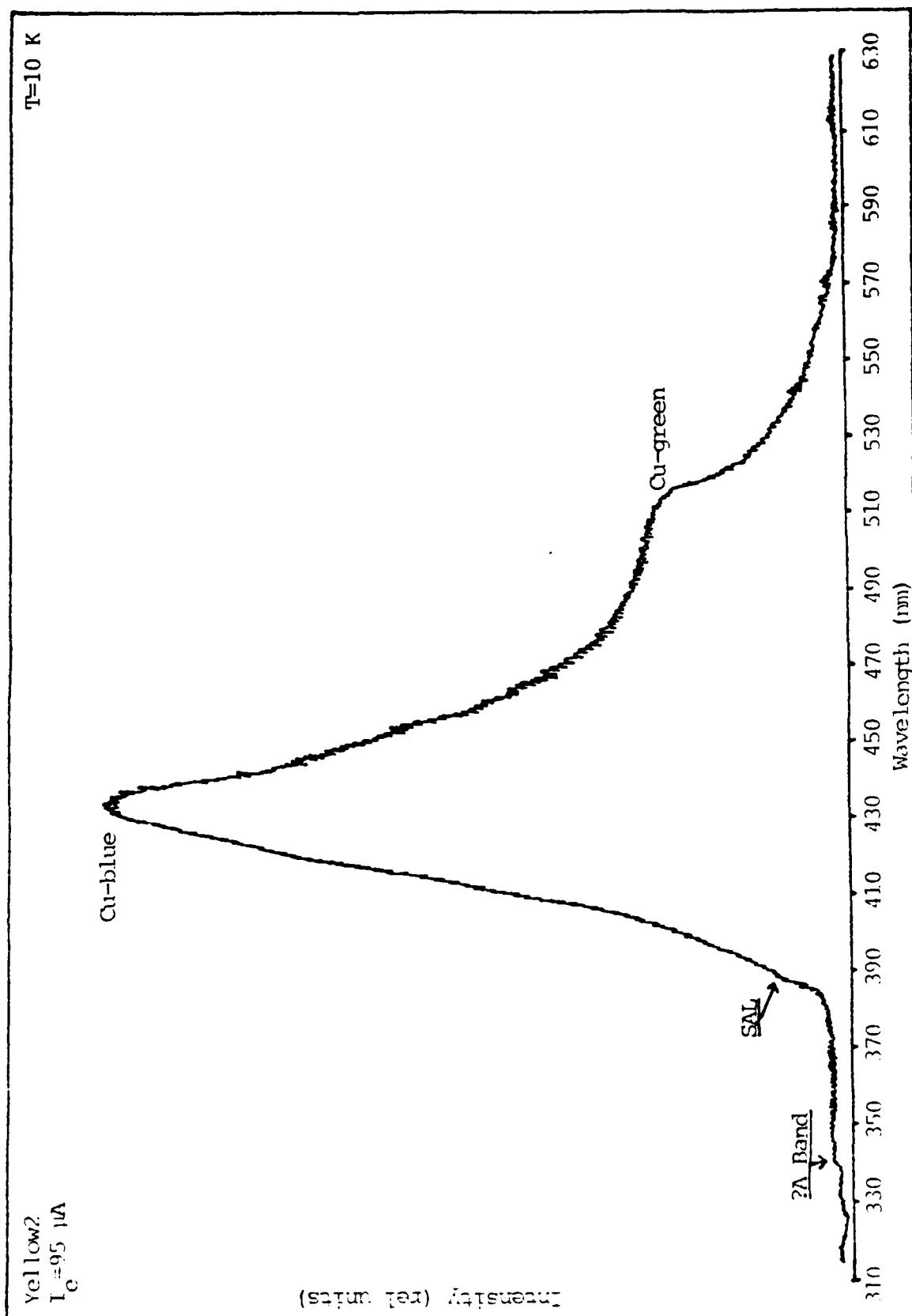


Fig. 34. Cathodoluminescence from a region where the visible bands were intense and the near band-edge luminescence was very weak.

the near band-edge luminescence was strongly broadened and nearly undetectable (Figure 34). These regions were not associated with any inclusion or surface imperfection visible under white light at a magnification of 250-500.

The maximum of the Cu-blue band shifted between 430 nm and 450 nm with the position of the electron beam on the sample surface (Figure 35). Weak emission bands at 330 nm, 332-4 nm, and 335 nm appeared and vanished as the electron beam scanned across the surface. Despite careful searching, the A band was never detected.

Sample to sample variations. The cathodoluminescence from different samples cut from the same parent block of cvd ZnS was very similar. There were indeed variations, but these variations were no greater than those already discussed under the topic of spot to spot variations. The single exception to this rule was sample Yellow1, which gave little or no radiative response to the electron beam. Careful examination of this sample under the microscope revealed that its surface preparation was very poor and that it may not have been etched.

Temperature variation. The cathodoluminescence from all samples of this cvd ZnS quenched rapidly as the temperature rose above 50 K, but not as severely as had the Raytheon cvd ZnS. The luminescence from block two samples (mixture of side and end views) always quenched much faster than block one samples. The strong I_1^F line detected in block one samples often persisted beyond 120 K. The

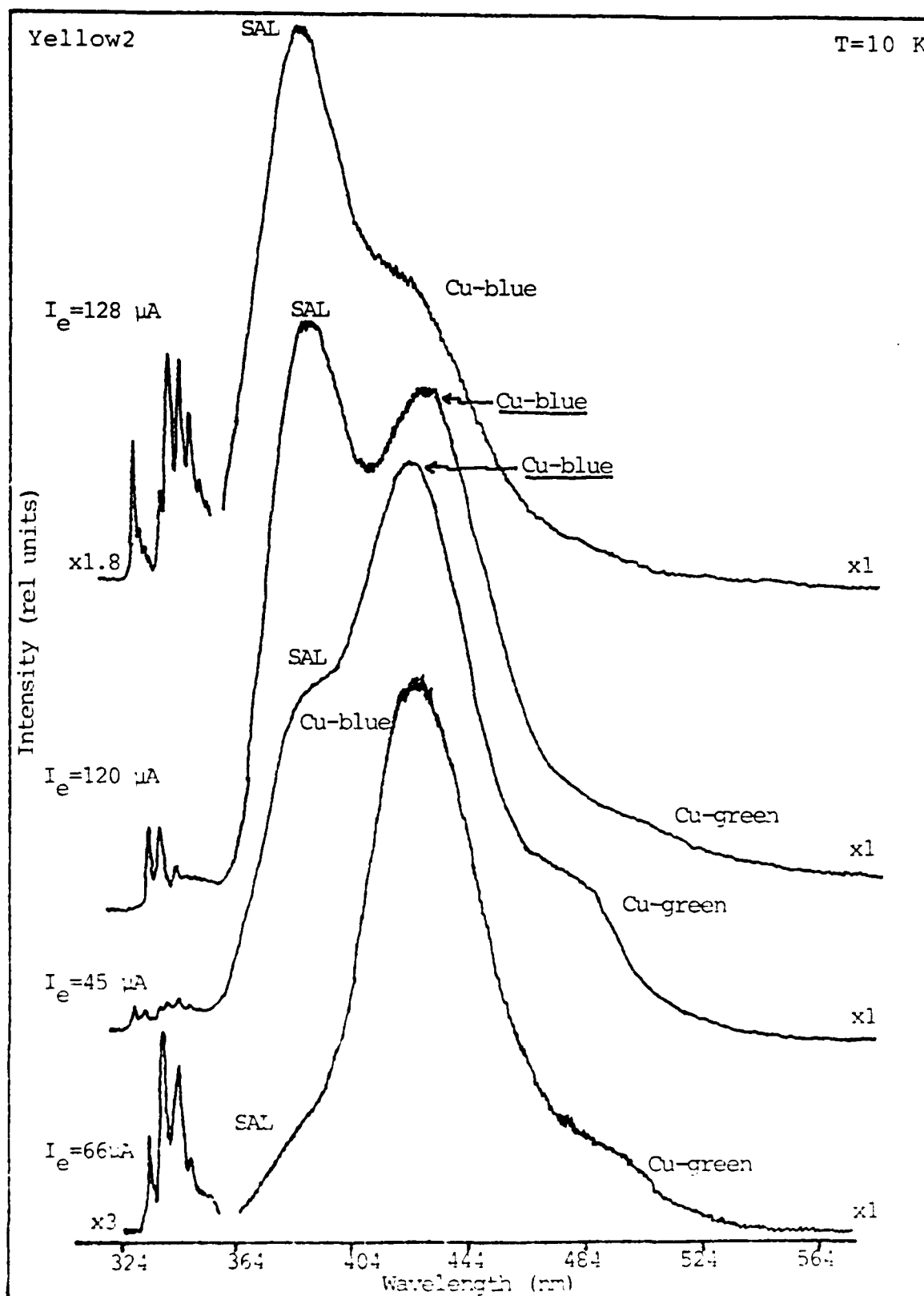


Fig. 35. The shift in energy position of the Cu-blue peak with position on the surface of a sample of CdTe and ZnS.

Cu-blue band was undetectable even in block one samples by 200 K. No room temperature cathodoluminescence was ever detected in any of these samples.

Cleartran

Only the cleaved surfaces of Eagle-Picher single crystal ZnS exhibited stronger cathodoluminescence than the Cleartran samples. The cathodoluminescence spectra of the Cleartran material proved far more detailed and less broadened than any other cubic phase material reported in the literature (32, 34, 48, 51, 94, 104, 108, 113, 114, 115, 116, 126). Regardless of the relative shape of the cathodoluminescence spectra shown in this section of the thesis, it must be remembered that the intensity of the near band-edge emission was extremely high.

Eleven samples of Cleartran were studied during this effort. Four of the samples were cut so that the side view of the crystal growth direction was present in the surface, and seven were cut so that the end view was present (Table II). After over 300 separate cathodoluminescence spectra were processed and analyzed, it was discovered that the same spectral details were present in all samples, but end view samples generally had a lower cathodoluminescence intensity than side view samples. It was also generally true that end view samples had relatively low near band-edge luminescence intensity compared to side view samples---end view cathodoluminescence spectra always

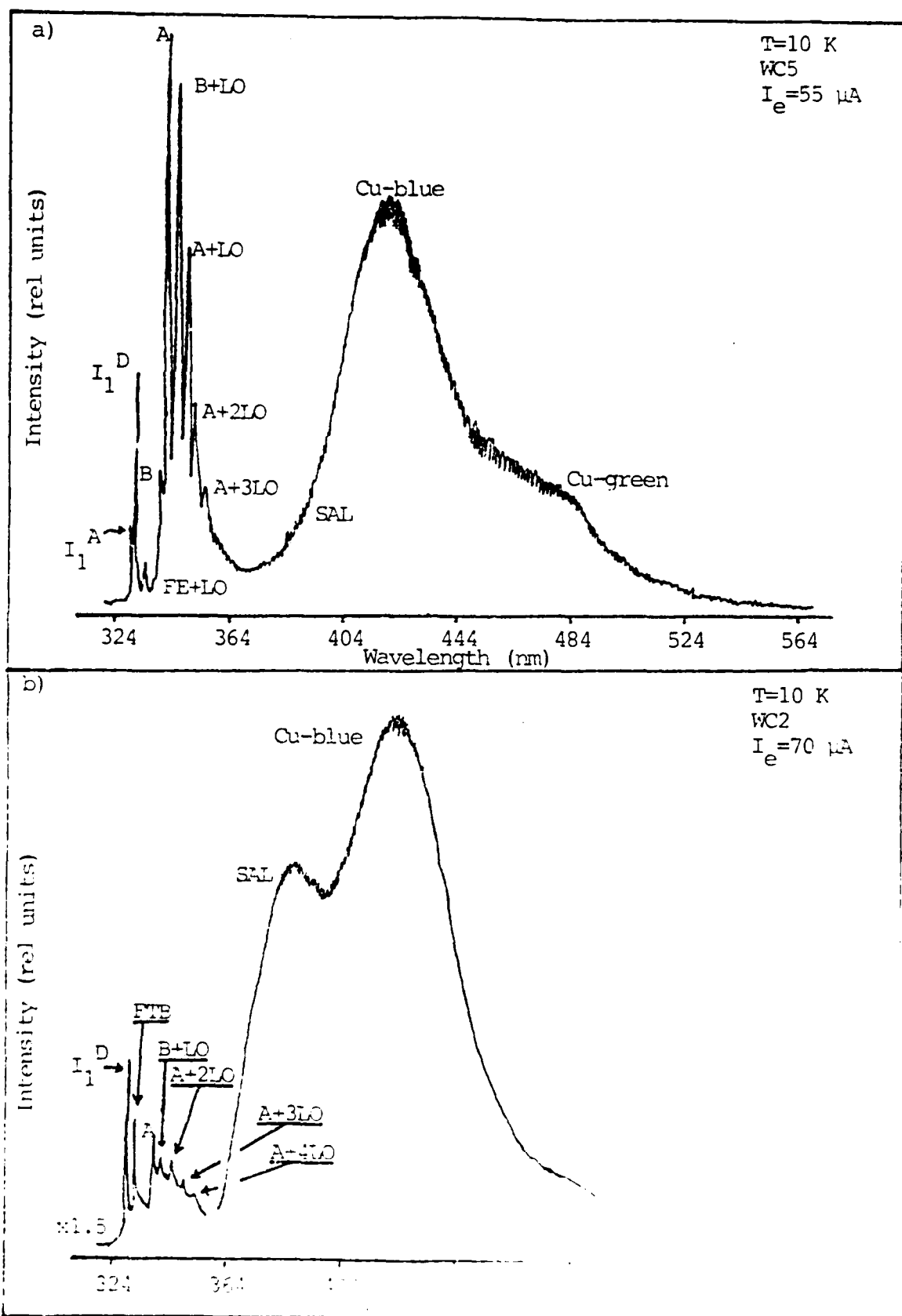


Fig. 36. The 10 K photoluminescence spectra of the Cleartran (997) diodes.

AD-A179 211

THE CATHODOLUMINESCENCE OF CLEARTRAN: A NOVEL FORM OF
POLYCRYSTALLINE ZNS(U) AIR FORCE INST OF TECH
WRIGHT-PATTERSON AFB OH SCHOOL OF ENGINEERING

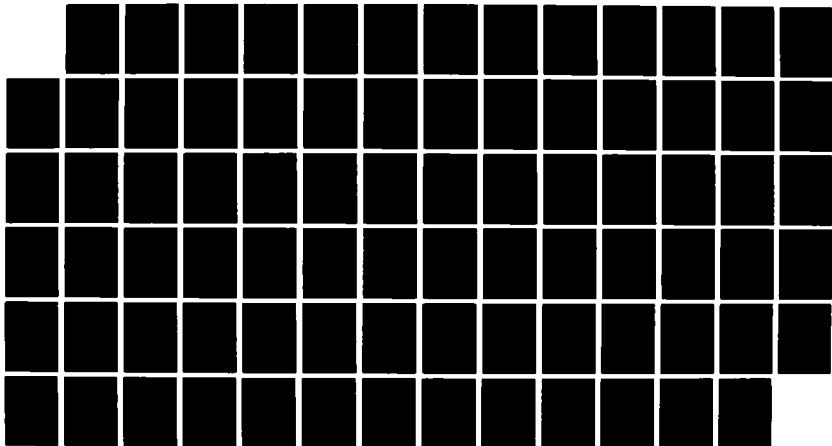
2/2

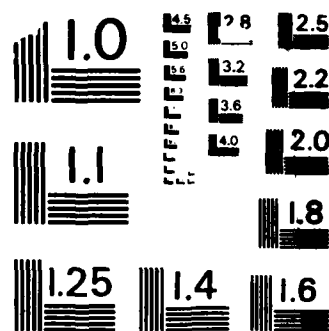
UNCLASSIFIED

J G VARNI DEC 86 AFIT/DS/ENP/86-2

F/O 20/12

NL





MICROCOPY RESOLUTION TEST CHART
NATIONAL BUREAU OF STANDARDS - 1963 - A

displayed stronger visible emission than near band-edge emission. The cathodoluminescence of side view samples showed very intense near band-edge emissions which were comparable to or stronger than the Cu-blue band. Characteristic side and end view cathodoluminescence spectra are shown in Figure 36; the spectra displayed there came from sample WC5 (side view) and WC2 (end view). Weak emission peaks at 322.6 nm and 324.0 nm were occasionally seen in the cathodoluminescence of end view samples only. These emission peaks have been attributed to packing defects (113).

Some of the cathodoluminescence spectra of Cleartran plotted and discussed in this thesis were originally taken by D. Blessinger (18). Before inclusion in this thesis, Blessinger's spectra were first corrected for instrument response and then re-analyzed and collated with the larger body of my work.

In the near band-edge region, the sample cathodoluminescence included two or more of the following DBE lines: 326.2 nm, 326.4 nm, 326.6-7 nm, 327.0 nm, 327.2 nm, and 327.6 nm. These DBE lines were designated I_1^A - I_1^F . Since a single DBE line was never seen alone, it was difficult to determine the width of these peaks. By examination of spectra where one DBE was strongly dominant over all others, the width of the DBE lines in Cleartran was determined to be 3-6 meV. An example of a spectrum where this measurement could be made is given in Figure 37.

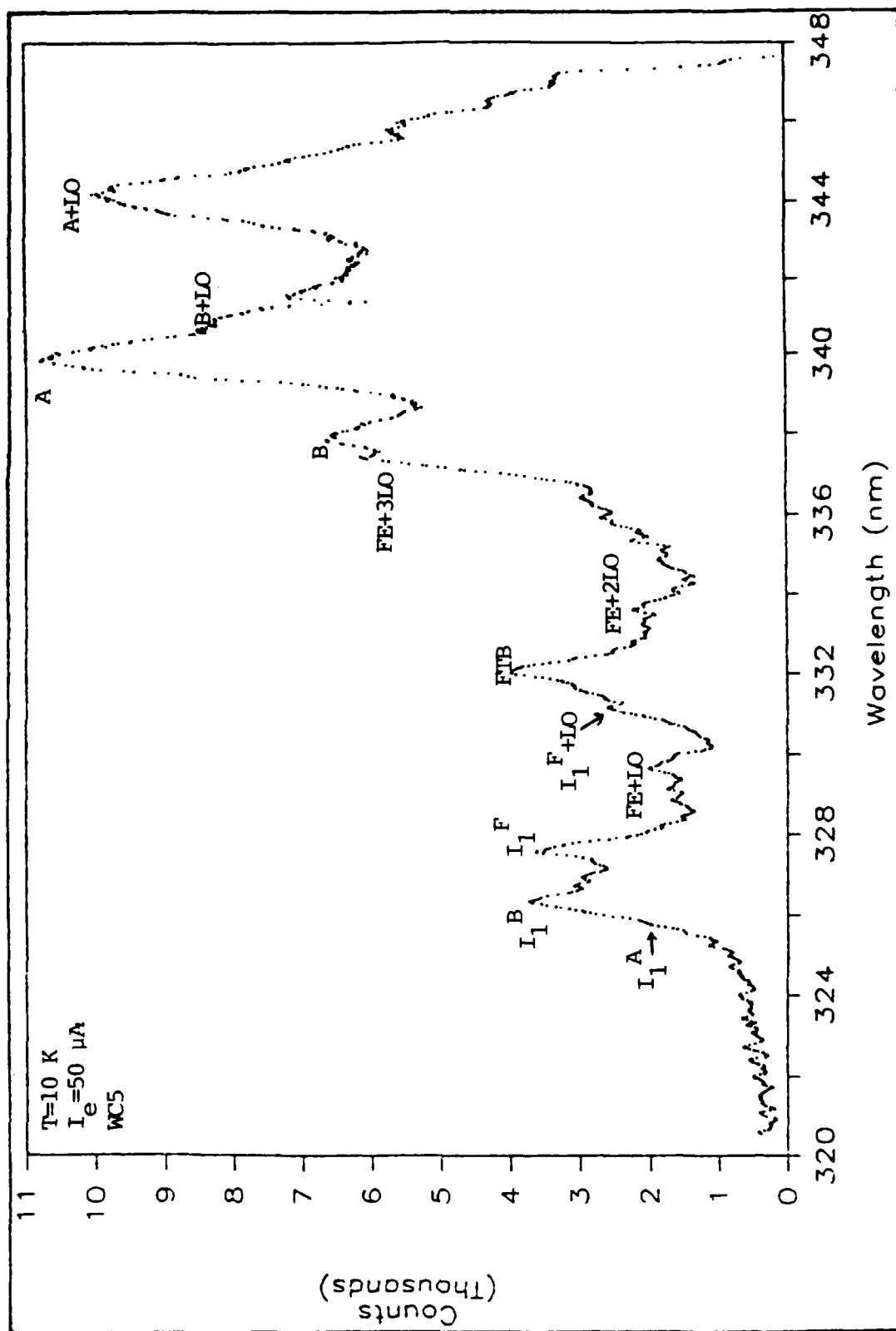


Fig. 37. The 10 K cathodoluminescence of a sample of Cleartran showing the apparent dominance of a single donor bound-exciton line.

The free exciton recombination band (FE) for the $n=1$ $\Gamma_6 - \Gamma_8$ exciton was occasionally seen as a high energy shoulder to the composite DBE band, but usually only in the spectra of side view samples. These observations permit a tentative assignment of 325.8-325.9 nm for the FE. D. Blessinger reported the first reliable sighting of FE recombination (18:55-56), but his uncorrected data resulted in an incorrect assignment of 325.9 nm for the FE. Small but persistent emission peaks probably due to acceptor bound-exciton (ABE) recombination included 328.2 nm, 328.7-8 nm, 329.2 nm, 330.0 nm, and 330.3-6 nm. These ABE lines were designated $I_2^A - I_2^E$. No emission peaks attributable to two-electron transitions or to recombination resulting in an excited donor or acceptor impurity were ever detected. The near band-edge region was difficult to analyze due to the presence of LO and TO (transverse optical) phonon replicas of the many DBE and ABE lines. The FE-LO (329.6 nm) and FE-2LO (333.6 nm) were particularly persistent spectral features.

Emission peaks attributable to FTB recombination were seen in the region of 331.0 - 331.7 nm and near 332.1 nm. The assignment of these peaks to FTB recombination was made difficult by the presence of strongly-coupled LO replicas of the I_1^E , I_1^F , and I_2^A lines at 331.0 nm, 331.4 nm, and 332.0 nm. The lack of a shift in energy position with a large change in excitation intensity indicated that the peaks in this region could not be attributed to DA

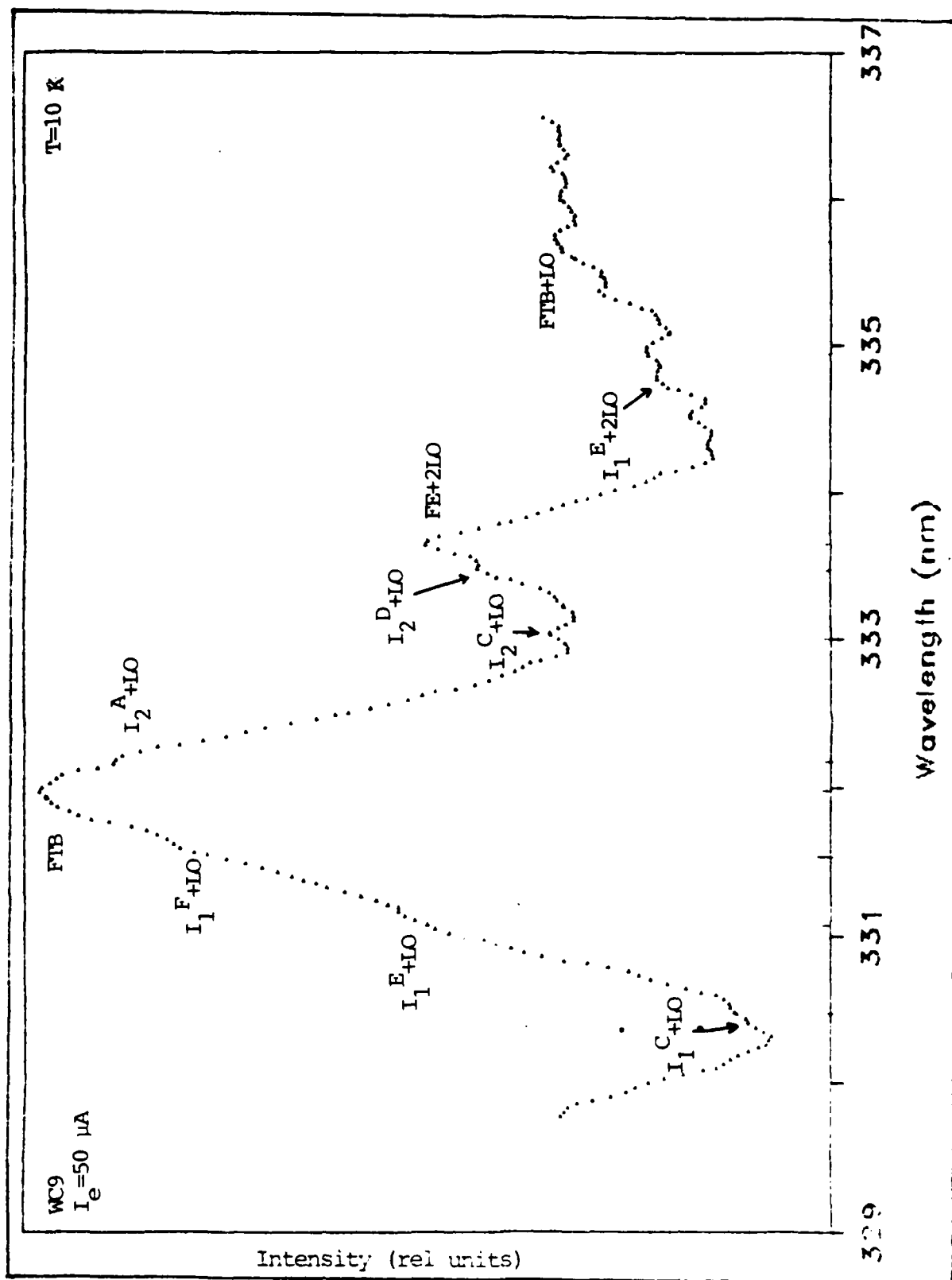


Fig. 38. A typical 10 K cathodoluminescence spectrum of a sample of Cleartran (WC9) showing the level of detail in the region from 329 nm to 335 nm.

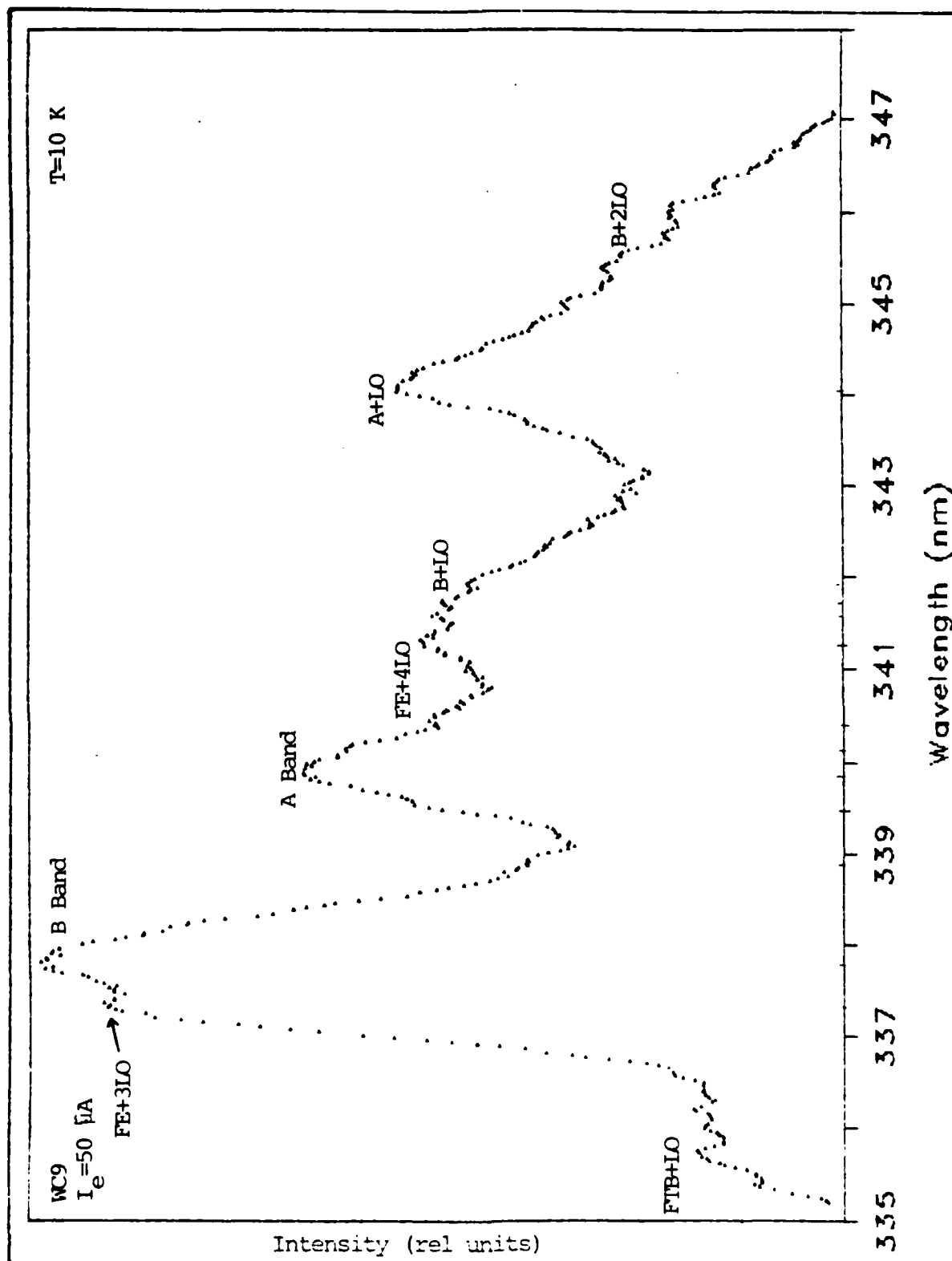


Fig. 39. A typical 10 K cathodoluminescence spectrum of a sample of Cleartran (WC9) showing the level of detail in the region from 335 nm to 340 nm.

emission. Discriminating between the I_2^A -LO line and a line at 332.1 nm is near the limit of accuracy for the primary detection system, but spectra such as Figure 38 argued for the existence of an independent FTB emission line at 332.1 nm. A FTB recombination peak at 332.1 nm would indicate an impurity center at a depth of 107 meV---a number consistent with previous estimates of donor depths in cubic ZnS (12:20).

Two emission bands at 337.4-7 nm and 338.2-5 nm were persistent features of the cathodoluminescence, particularly in side view samples such as WC9. These two peaks were usually broadened into one another (Figure 39). The first peak is probably the FE-3LO line. The 338.2-5 nm band behaves as a DA emission band and is probably identical to the DA band seen in the parent cvd ZnS (the B band). Several phonon replicas of the 338.2-5 nm band were present whenever the band was detected. The DA band labelled "A" at 340.0 nm was usually also present in the cathodoluminescence. The A band was always accompanied by LO replicas, sometimes as many as six (Figure 40).

The SAL, Cu-blue, and Cu-green bands were ubiquitous features of the low temperature cathodoluminescence. The self-activated blue (SA-blue) band, which has been confirmed by OPMR to be a DA emission band associated with a zinc vacancy-chlorine atom A-center (64, 148), was sometimes seen as a change in slope on the long wavelength side of the Cu-blue band. The strongest peak in the

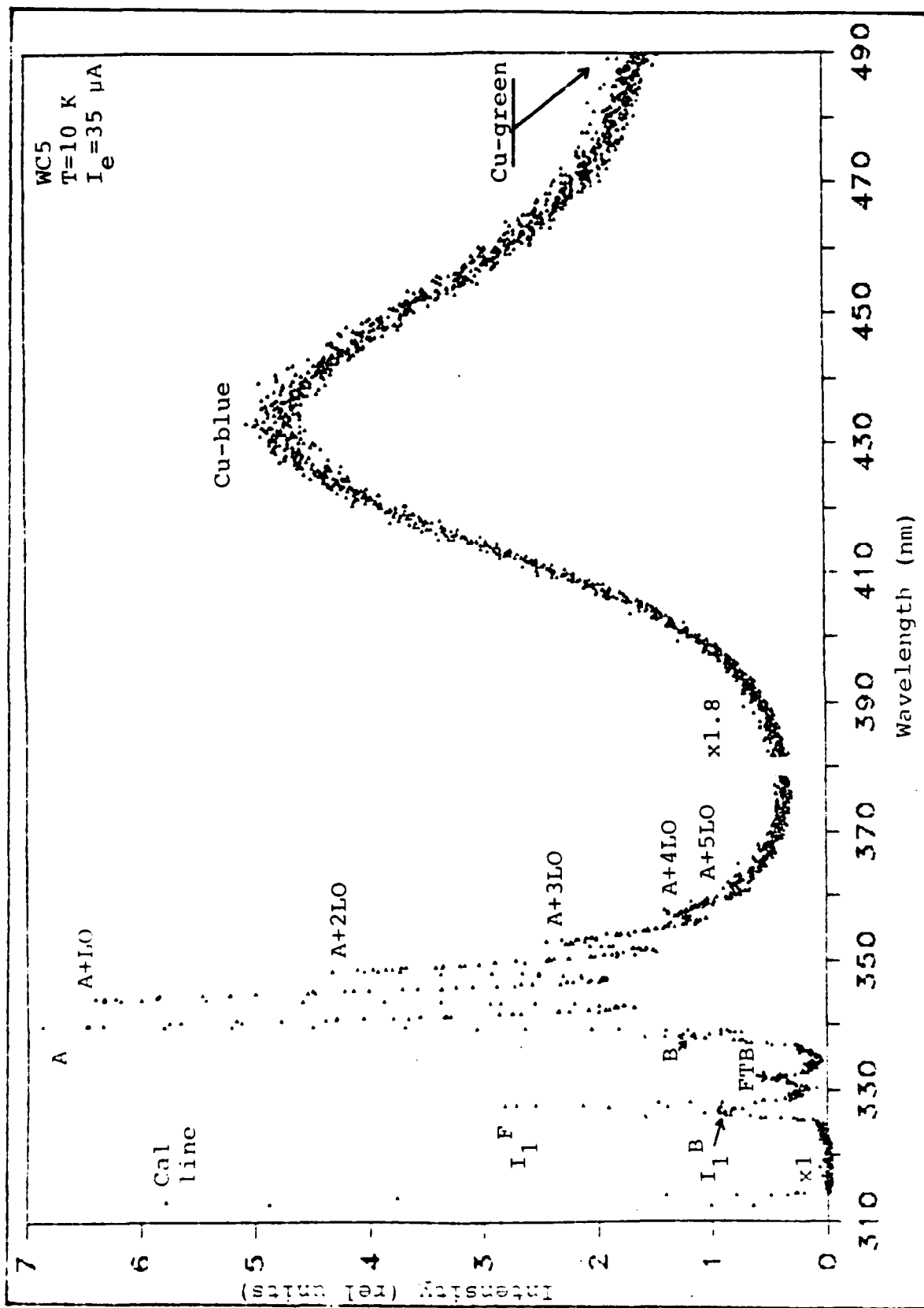


Fig. 40. The donor-acceptor pair band labelled "A" at 10 K in sample WC5.

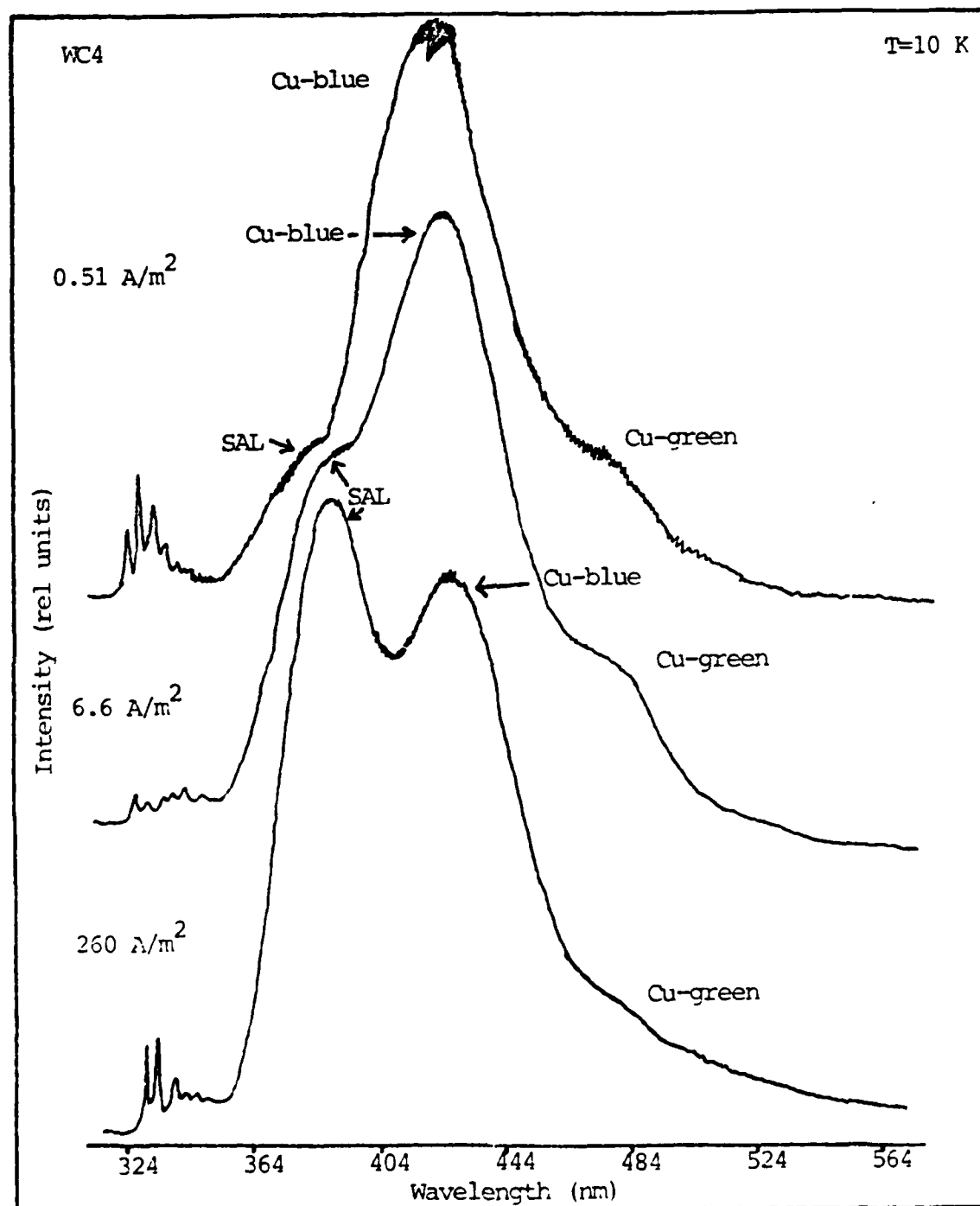


Fig. 41. The behavior of the SAL band under differing levels of excitation (18:73-75).

visible region was the Cu-blue band at low electron beam current densities ($\sim 0.5 \text{ A/m}^2$). As the current density increased to 10 A/m^2 , the SAL band became nearly as large as the Cu-blue band. When the current density was greater than 20 A/m^2 , the SAL peak dominated the visible low temperature luminescence. This behavior was first noticed by Blessinger, and is reproduced in Figure 41 as a convenience to the reader. The behavior of the SAL band would indicate that the SAL recombination channel is strongly coupled to the presence of excitons and/or free electrons and that the SAL band is probably not due to DA recombination. A weak emission band was seen several times in end view samples at 574-8 nm. This band has been seen previously in Mn-doped samples of cubic phase ZnS and has therefore been attributed to manganese (1, 43, 58, 81).

The band gap energy of cubic phase ZnS is 3.84 eV at 4.2 K (100). The observation of a highest energy near band-edge emission at 325.85 nm fixes the free exciton binding energy at about 35 meV. This figure agrees well with previous measurements (13, 64, 100). The corresponding exciton binding energies and donor ionization energies for lines $I_1^A - I_1^F$ and for line I_2^A (under the assumption that it may actually be a DBE line) are listed in Table V. The donor ionization energies for Table V were calculated following Sharma and Rodriguez (117):

Table V

Exciton Binding Energies and Donor Ionization
Energies for Seven Unknown Donors in Cleartran

Line	Exciton Binding Energy (meV)	Donor Ionization Energy (meV)
I_1^A	4 \pm 1	41 \pm 12
I_1^B	6 \pm 1	64 \pm 12
I_1^C	9.5 \pm 1.5	95 \pm 18
I_1^D	13 \pm 1	134 \pm 12
I_1^E	16 \pm 1	157 \pm 12
I_1^F	20 \pm 1	203 \pm 12
I_2^{A*}	27 \pm 1	273 \pm 12

*Although designated an acceptor bound-exciton, this line may well be due to donor bound-exciton recombination.

$$E_D = \frac{E_G - E_{ex} - (D^0, X)}{0.1} \quad (8)$$

where E_D is the donor ionization energy, E_G is the band gap energy, E_{ex} is the free exciton binding energy, and (D^0, X) is the neutral donor bound-exciton recombination energy.

This relationship (equation 8) agrees with an early observation by J. R. Haynes (149:362) that the dissociation energies of donor complexes in silicon were equal to approximately one tenth of the ionization energy of the donor impurity. The simple linear relationship expressed by Haynes' rule is known to fit II-VI compounds such as ZnSe and CdS (150:553) and it is unsurprising that it should hold for ZnS as well.

Spot to spot variations. As with the other forms of polycrystalline ZnS, the cathodoluminescence was not constant in intensity or in the level of detail at different locations on the sample surfaces. The visible luminescence in the SA region was always intense, but the near band-edge luminescence changed sometimes drastically with position. A set of cathodoluminescence spectra taken at different locations on the surface of a side view sample (WC9) are displayed in Figure 42. A similar set of cathodoluminescence spectra from an end view sample (WC6) are shown in Figure 43. In regions of intense near band-edge luminescence, the cathodoluminescence was always

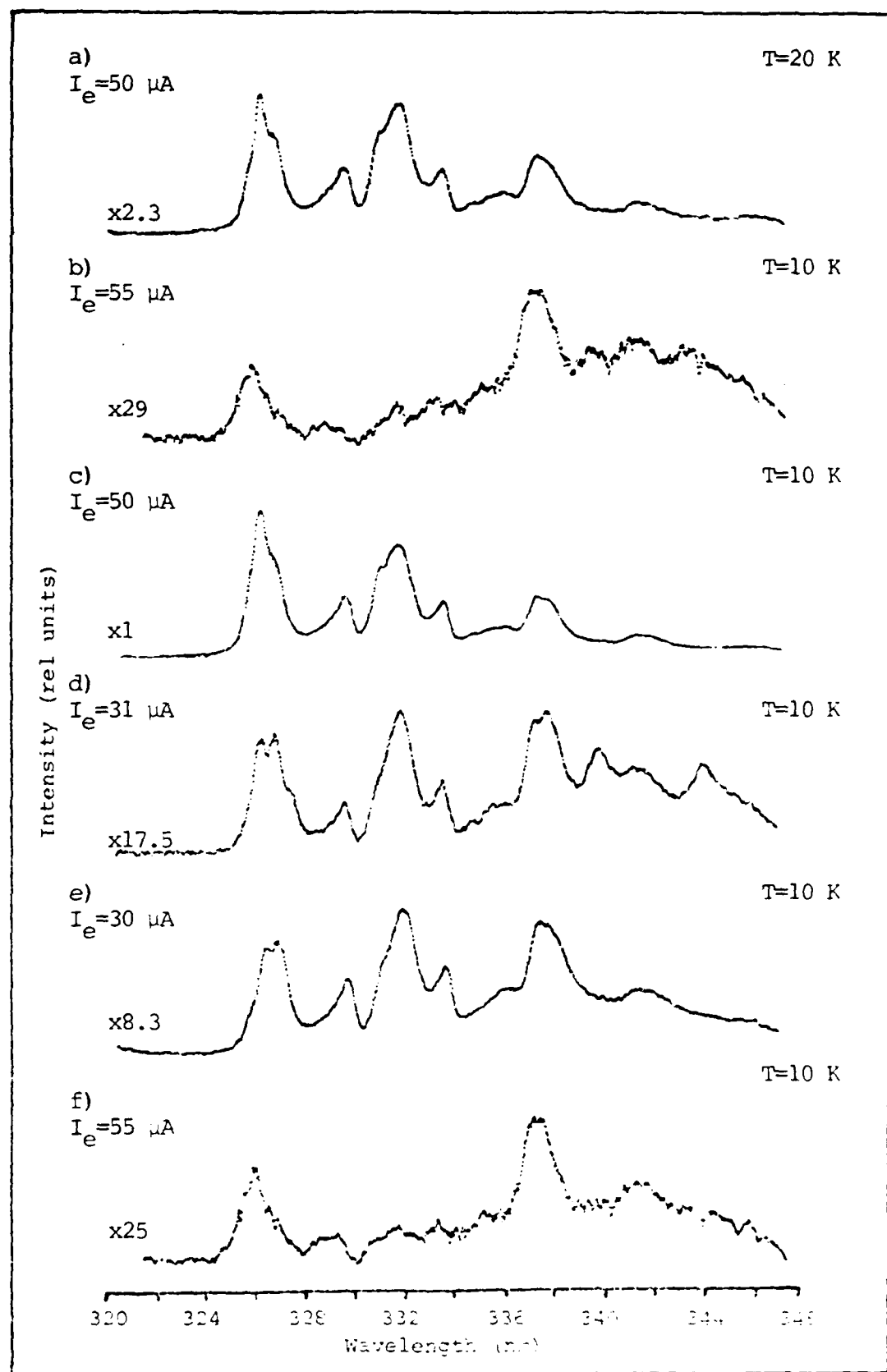


Fig. 42. The variation in the cathodoluminescence of a side-view Cleartran sample (WC9) with position on the surface of the sample.

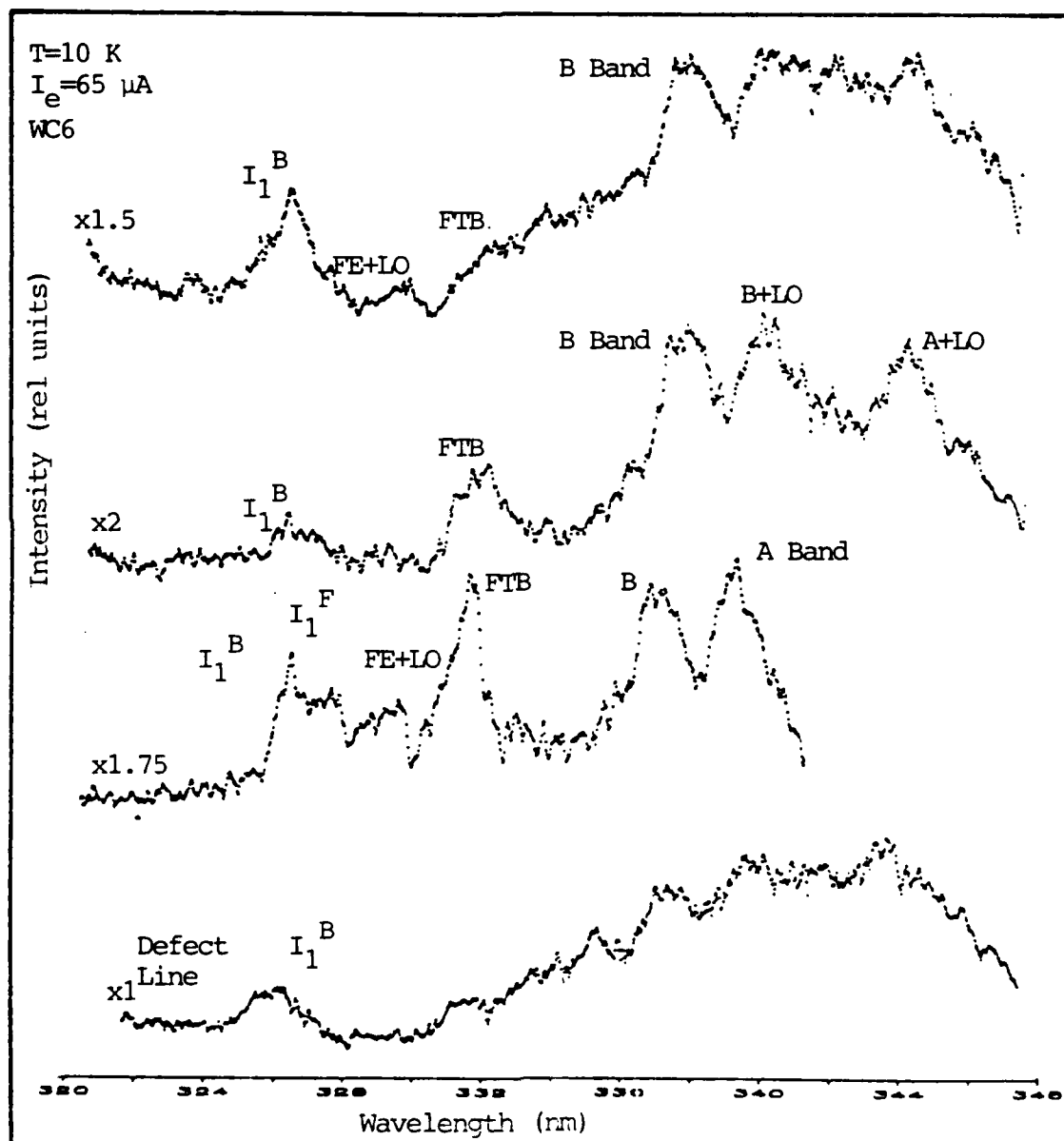


Fig. 43. The variation in the cathodoluminescence of an end view Cleartran sample (WC6) with position on the surface of the sample.

detailed, but the dominant DBE line frequently changed and the A and B bands appeared and vanished at random. In the side view samples, the I_1^F , I_1^E , and I_1^A lines were always present. In the end view samples, the I_1^E , I_1^D , I_1^C , and I_1^B lines were usually more significant. The B band was most easily seen and best resolved in the cathodoluminescence spectra from side view samples. There were also isolated regions on sample surfaces where the near band-edge cathodoluminescence was either strongly quenched or entirely absent (Figure 44). These regions were usually associated with an increase in the intensity of the Cu-blue or Cu-green bands, and in one case with a visible, subsurface inclusion. All emission peaks in the near band-edge region were broadened as the luminescence quenched, especially the A and B bands.

Sample to sample variations. Despite the variation in the cathodoluminescence with position on a sample's surface, the spectra from an individual sample bore a "family resemblance" to one another. This "family resemblance" was often influenced by the condition of the surface of a sample---it appeared that some of the samples were not as well prepared as others and, in addition, a carbonaceous film related to the presence of hydrocarbons in the sample chamber damaged the surface of some samples.

In Figures 45 and 46, we gather representative spectra from every sample that had a "good" luminescent response---side view samples in Figure 45 and end view

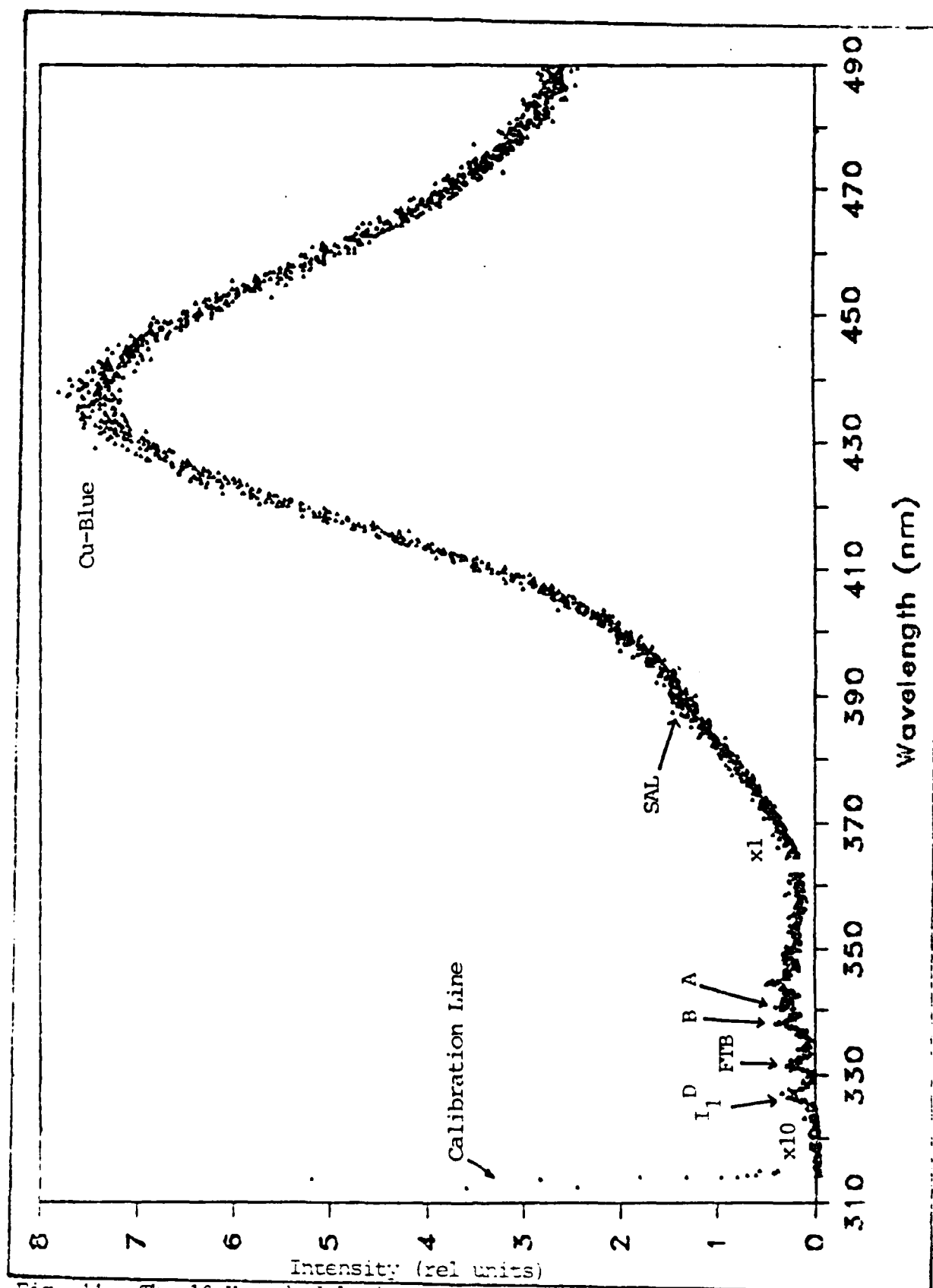


Fig. 44. The 10 K cathodoluminescence of a quenching region on the surface of Cleartran sample WC4.

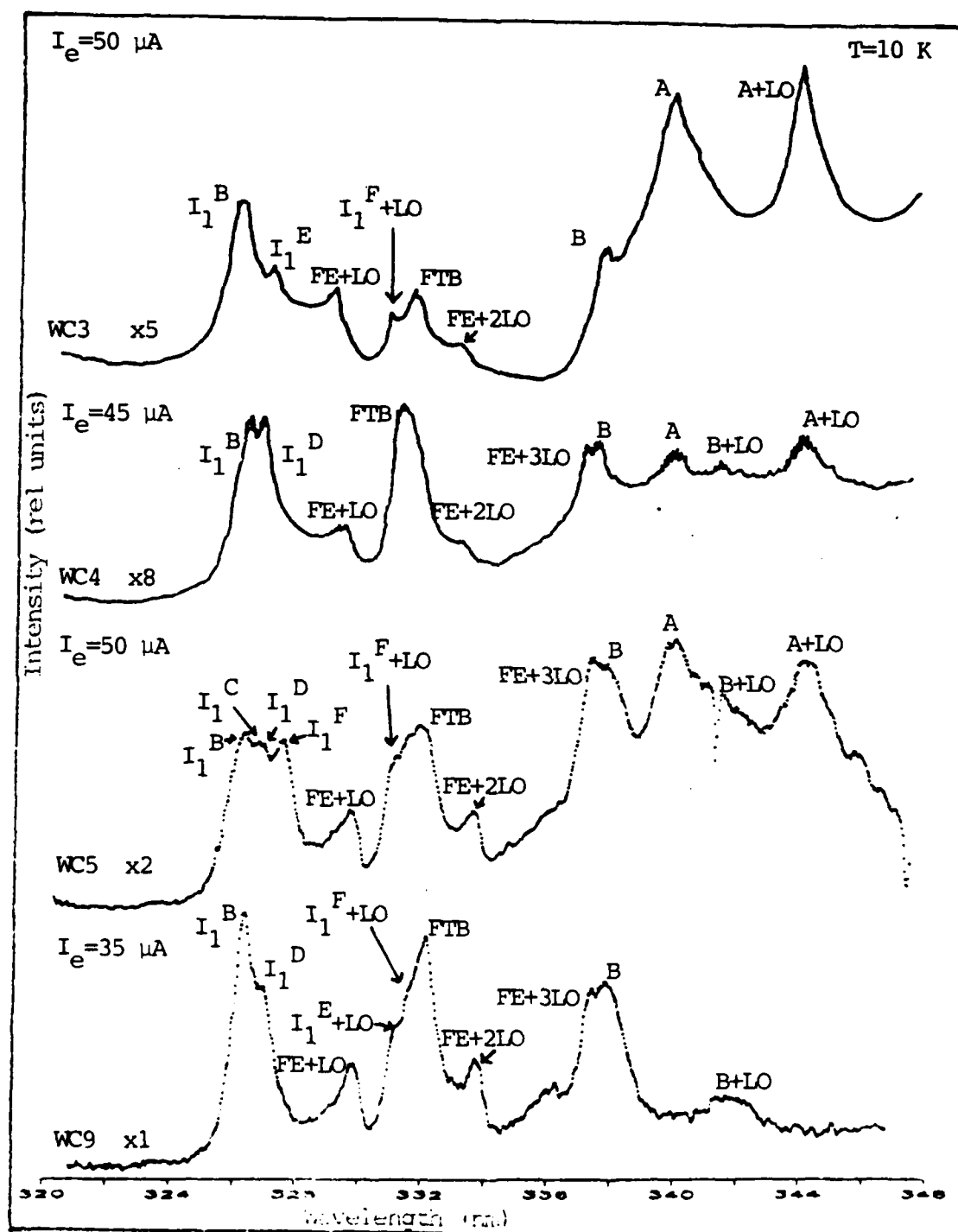


Fig. 45. The representative cathodoluminescence from high quality side view samples of Cleartran.

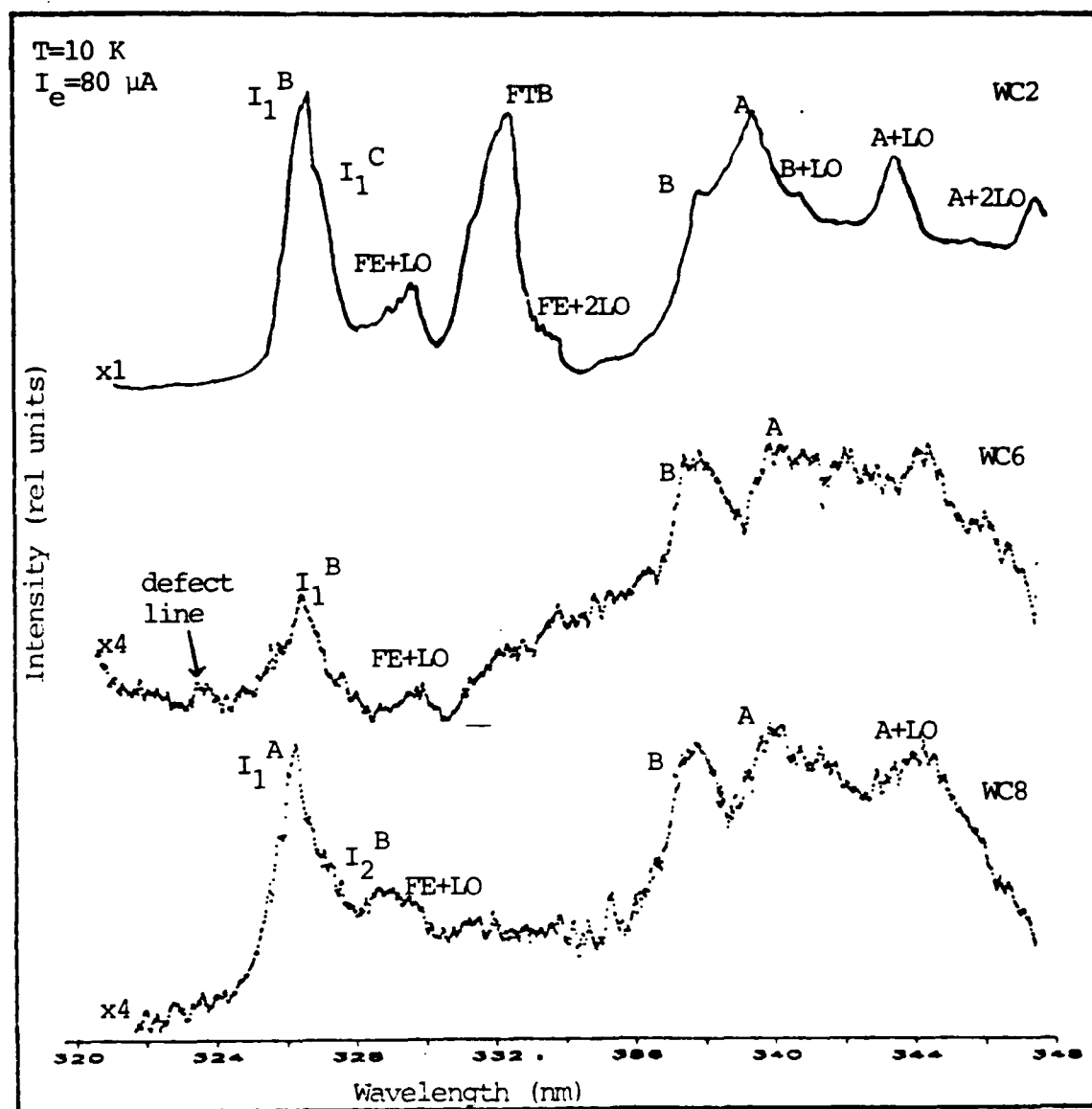


Fig. 46. The representative cathodoluminescence from high quality end view samples of Cleartran.

samples in Figure 46. The absence of spectra from samples WC7, WC10, and WC11 from these figures is due to the poor surface preparation of these samples and their correspondingly poor luminescent response. While individual details might change slightly (the dominant DBE might change or a DA emission band might increase or decrease in relative intensity), all the spectra from a given sample looked very similar to the spectra plotted in Figures 45 and 46.

In every case, the "best" spectra came from samples whose surfaces appeared smooth and shiny under the microscope. Samples with this appearance included WC2, WC3, WC5, WC6, and WC9. Samples WC1, WC4, and WC8 appeared slightly pitted or pocked and produced less detailed, lower intensity cathodoluminescence. In addition, samples which were frequently examined with the electron beam eventually built up a dark, oily surface film. This film seriously degraded the sample cathodoluminescence. The film eventually formed on samples WC2, WC3, and WC4. Figure 47 contains several spectra taken from these samples after the advent of the dark film. The cathodoluminescent response from samples covered with this oily film was very similar to the response of samples with poor surface preparation. Near the end of this effort, it was discovered that extensive cleaning (as much as 4 hours worth) of the interior of the vacuum chamber and the surface of the electron gun with alcohols and other reagents minimized the

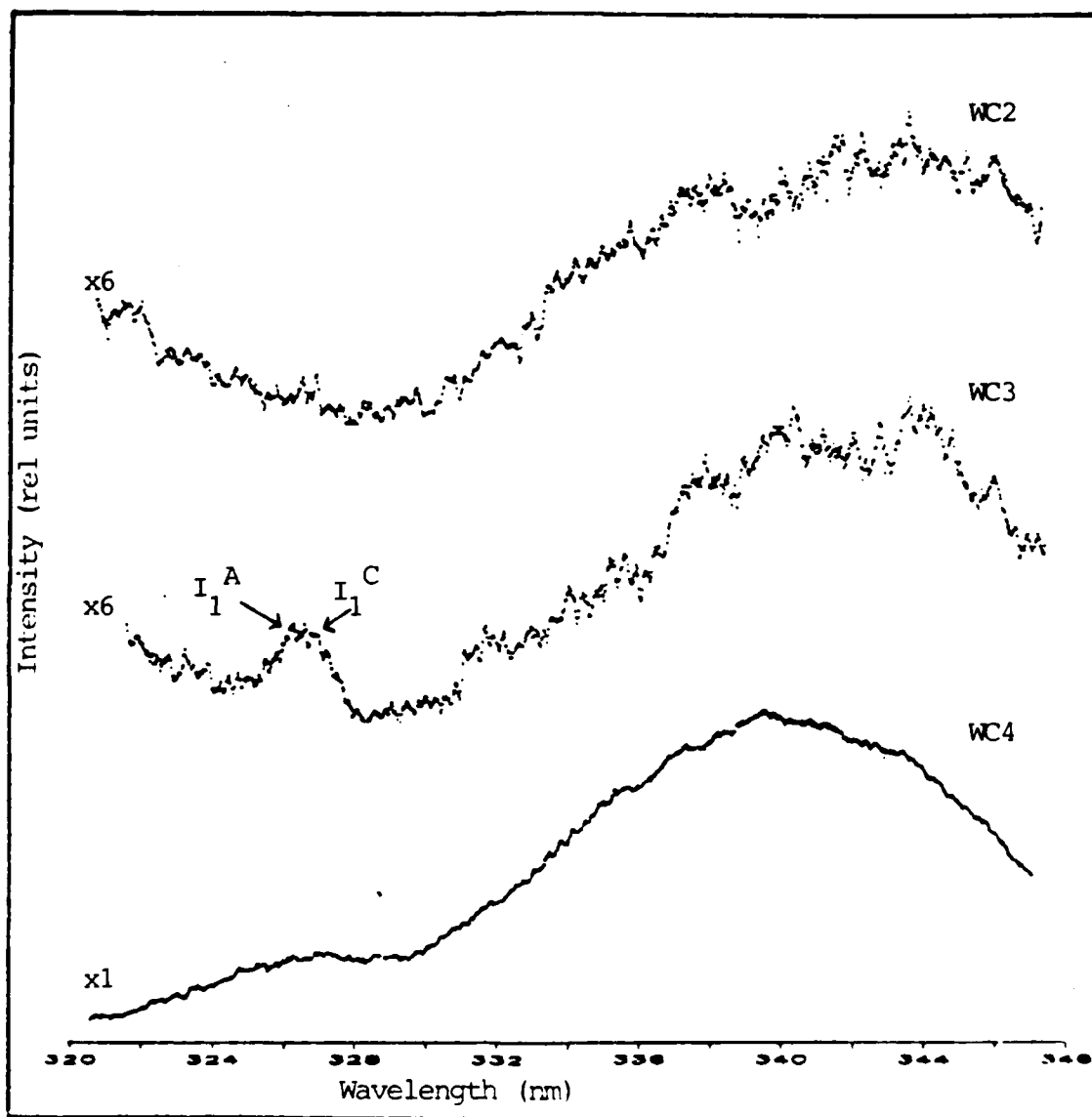


Fig. 47. The 10 K cathodoluminescence of samples WC2, WC3, and WC4 after an oily film was deposited on these samples.

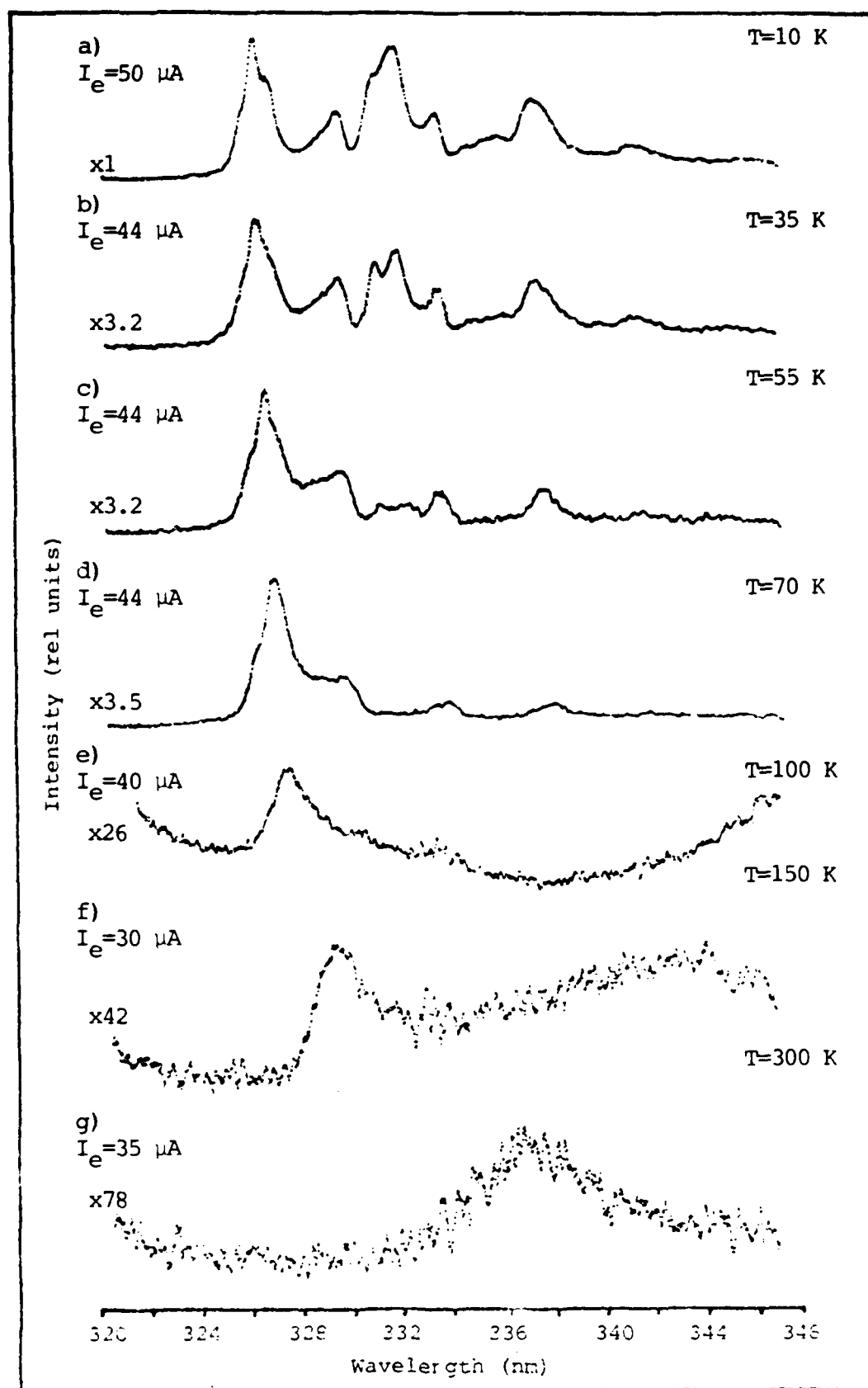


Fig. 48. The variation in the cathodoluminescence of a Cleartran sample (WC9) with temperature.

build-up of the oily film.

Temperature variation. The evolution of the near band-edge cathodoluminescence with temperature is illustrated by a series of cathodoluminescence spectra taken at two different locations on the surface of a single side view sample (Figure 48). The B band broadens and decays as the temperature rises toward 100 K. The peaks at 331.4 nm and 332.1 nm diminish more rapidly than the B band, vanishing from the spectrum at 80 K. Past 50 K, the FE-LO peak also begins to diminish, revealing details of the ABE lines at 329.2 nm, 330.0 nm, and 330.4 nm. Once the sample temperature has reached 100 K, the only clear features of the cathodoluminescence are a broadened, composite DBE line with a long wavelength shoulder due to residual ABE or FE-LO recombination and a severely broadened, low intensity band between 340 nm and 350 nm. At room temperature, the cathodoluminescence consists of a weak band 540 meV wide at 336.8 nm and a similarly broadened but more intense Cu-blue band at 460 nm. The cathodoluminescence of the end view samples evolves in an exactly similar fashion, but quenches more rapidly. Near band-edge luminescence from end view samples was nearly undetectable above 150 K.

The width (full width at half maximum) of the DBE lines in Cleartran was difficult to track because there were always several present in a given sample. Figure 49 shows the shift in width of a particularly narrow DBE line with

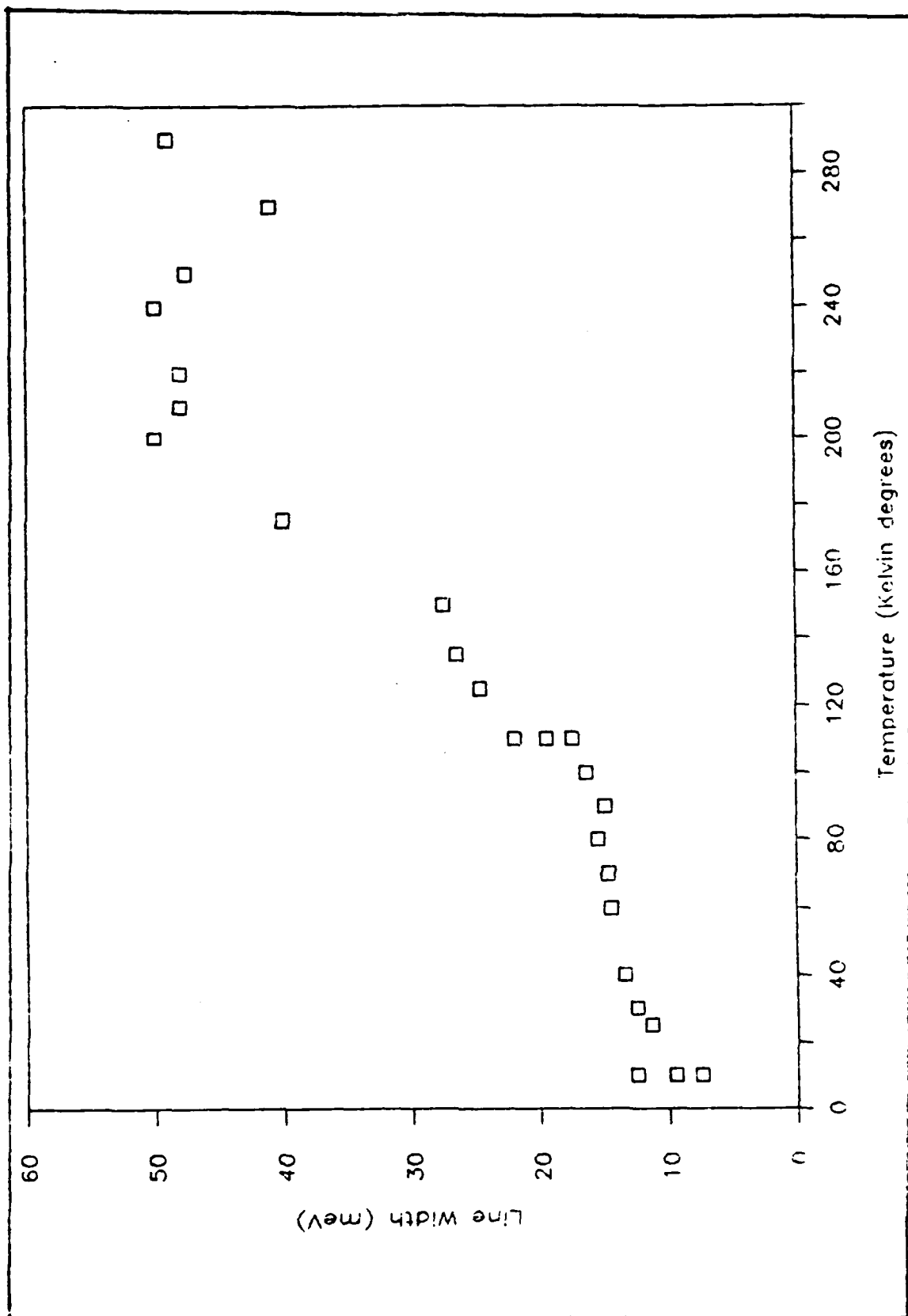


Fig. 49. The full-width-at-half-maximum of a donor bound-exciton line in sample WC9 as a function of temperature.

temperature for a particularly "good" sample, WC9 (side view). From 10 K to 100 K, the width follows the expected kT dependency. Near 110 K, there is a sudden jump in the width of the composite DBE line (which may be entirely due to sampling noise in my data), followed by renewed kT dependence until about 160 K. After 160 K, there is another and larger jump in the width. The width of the peak stays roughly constant from 200 K to 300 K. This anomalous behavior is probably due to the presence of more than one DBE line and to the fact that the room temperature peak is unlikely to be due to simple donor bound-exciton recombination.

Comparison of the Luminescent Response of the Forms of ZnS

Certain locations on the surface of the ZnS platelets produced a small amount of hexagonal phase cathodoluminescence. With this single exception, the cathodoluminescence of the single crystal and cvd polycrystalline ZnS materials examined during this effort was characteristic of the cubic or 3C phase of ZnS.

The Raytheon cvd ZnS and the crystal platelets had the poorest cathodoluminescent response. These materials produced a very low intensity, strongly broadened cathodoluminescence that quenched rapidly between 50 K and 100 K. The cvd ZnS grown by CVD Inc. had a stronger cathodoluminescent response that revealed more details of the radiant response of the cubic phase, but the

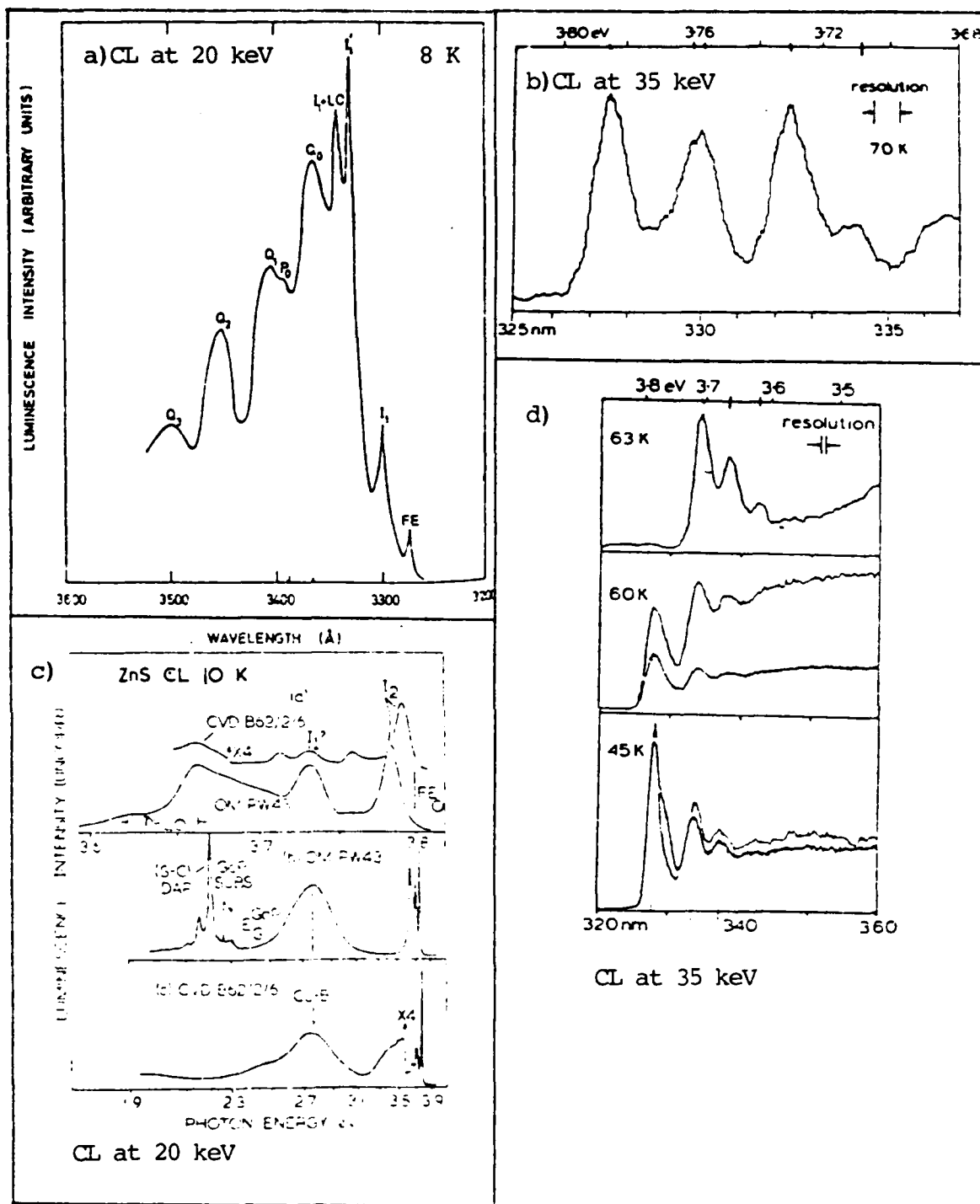


Fig. 50a. A comparison of the cathodoluminescence of Clear-tran sample WC9 with previous reports of cubic ZnS in the literature. a) single crystal (51:1366), b) cvd (104:314), c) cvd and organometallic cvd (34:306), d) single crystal (104:314).

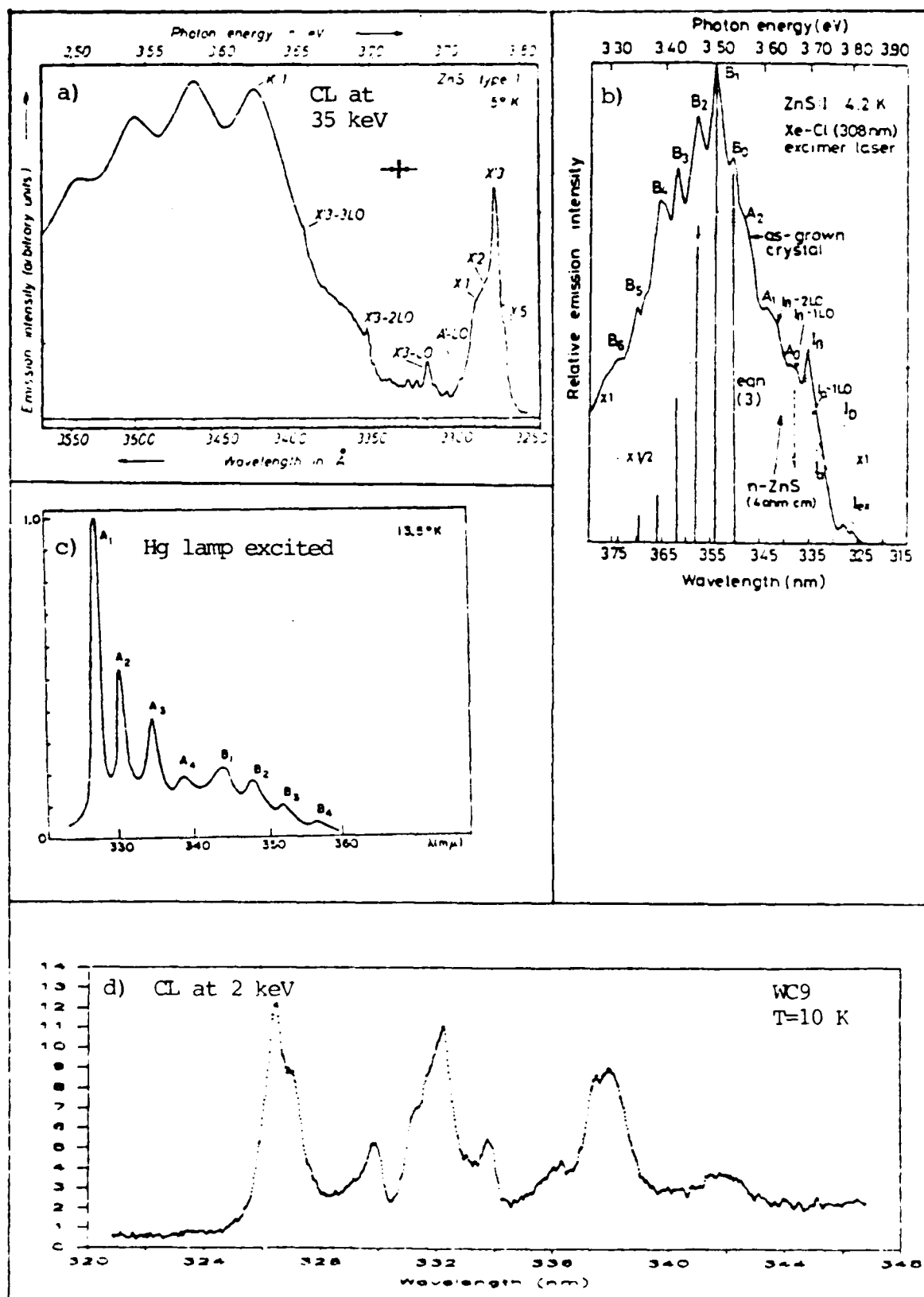


Fig. 5b. A comparison of the cathodoluminescence of Cleartran sample WC9 with previous reports of cubic ZnS in the literature. a) single crystal (48:139), b) single crystal (126:552), c) single crystal (108:904), d) sample WC9.

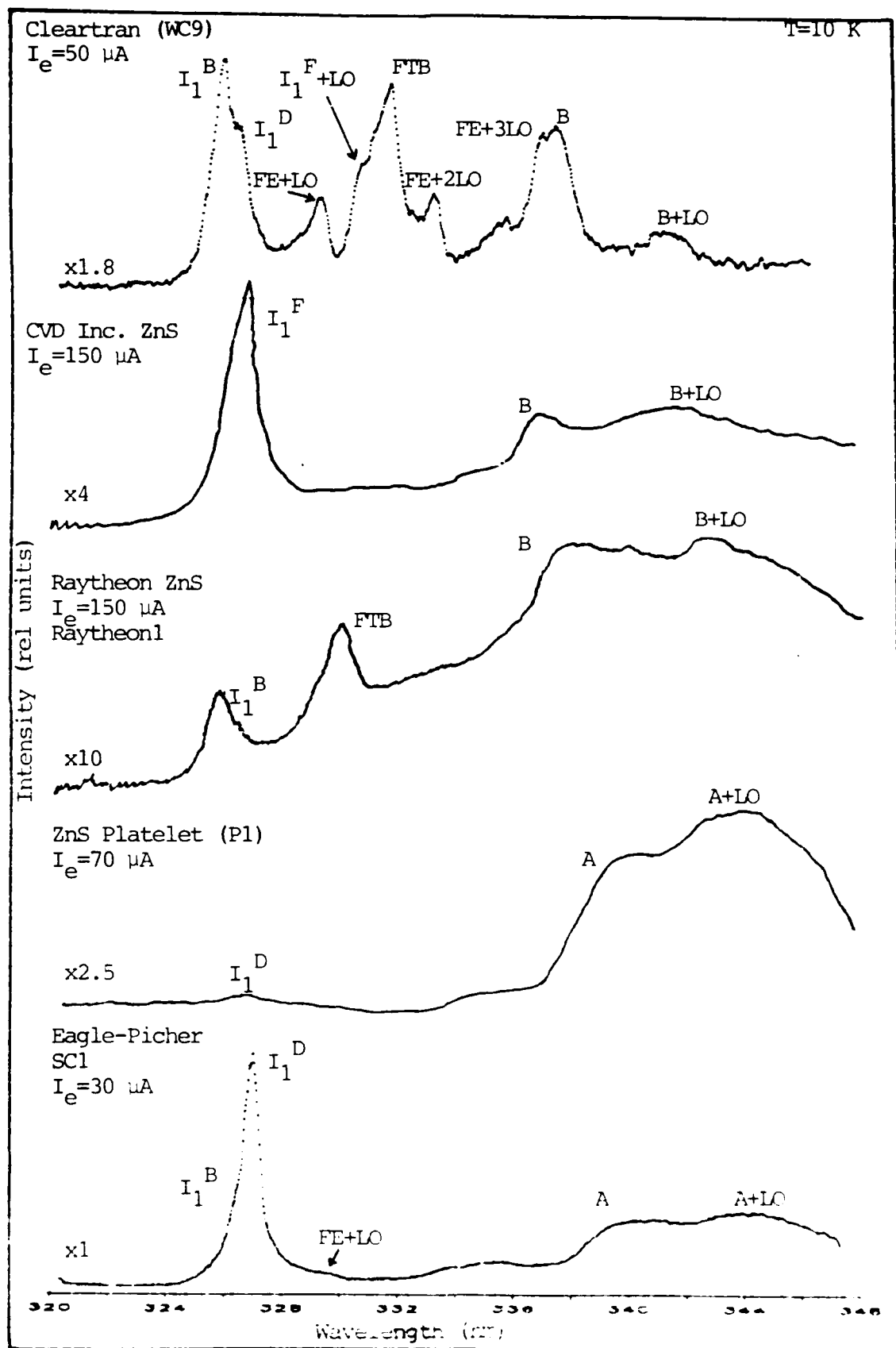


Fig. 51. The average low temperature cathodoluminescence of each of the forms of ZnS examined during this effort.

cathodoluminescence still quenched rapidly with increasing temperature and the emission peaks were very broad. The Eagle-Picher single crystal and Cleartran samples produced extremely strong cathodoluminescence in both the visible and near band-edge regions. The composite DBE band from the Eagle-Picher single crystal samples was still very broad (7-10 meV), while the DBE lines from the Cleartran samples were very narrow (3-6 meV) as compared to reports in the literature. Perhaps the most significant finding was that the cathodoluminescent response from Cleartran lacked the strong broadening and large background seen at 340-370 nm in previous samples (48, 51, 104, 108, 126) of cubic phase ZnS reported in the literature (Figure 50). A comparison of the average cathodoluminescent response from each of the forms of ZnS studied during this effort is presented in Figure 51.

In general, the strongest and sharpest cathodoluminescent response was produced by samples composed of large crystals strongly oriented along the primary crystal growth direction. Given the 65 nm range of the electrons used to excite the samples, the condition of the surface of the samples was also a crucial factor in the quality of the cathodoluminescence.

Observed Emissions Between 300 nm and 800 nm

This section summarizes the emissions I observed from each of the forms of ZnS between 300 nm and 800 nm, the

sensitivity range of my detection systems. I also comment on the probable nature of impurities responsible for the observed emissions.

Single Crystal ZnS (Eagle-Picher). The emissions of this form of ZnS are listed in Table VI. The Eagle-Picher ZnS was the only form I studied that had a measurable concentration of impurities---aluminum, in this case. It is logical to assume that either the I_1^B or I_1^D bound exciton emission must be associated with the aluminum donor. Although the I_1^D line is generally the stronger of the two emissions, recent work by Taguchi (126) would seem to indicate that the I_1^D bound-exciton line is associated with iodine. For this reason, I have assigned aluminum as the likely donor for the I_1^B line.

A broad, indistinct emission band at 335.3 nm is probably an LO phonon replica of a FTB emission seen clearly in Cleartran samples. The parent FTB peak is seen at 332.1 nm in Cleartran samples---this indicates an impurity depth of approximately 110 meV.

The DA emission band labelled "A" is also clearly seen in Eagle-Picher ZnS. This band is undoubtedly the band labelled " B_0 " by Samelson and Lempicki (108) and " P_0 " by Gezci and Woods (51). A similar band was also seen by Flesch (48) at 340.7 nm (band " K'_2 "). I attribute the A band to chlorine, primarily due to Samelson and Lempicki's pioneering work with chlorine-doped cubic ZnS.

The familiar Cu-blue band is always present in the

cathodoluminescence. This band does not arise from DA emission since it displays neither the characteristic DA time or intensity shift (118:964). There is general agreement in the literature that the Cu-blue peak is associated with copper substituted at zinc sites and interstitial copper ions (54).

A violet SAL band is clearly seen in all Eagle-Picher samples at 390-400 nm for temperatures below 50 K. This is one of three distinct violet emissions seen in ZnS at approximately 390 nm, 410 nm, and 425 nm respectively (54:250). These emission bands have been variously attributed to zinc vacancies (52), chlorine substituted at sulfur sites (108), and oxygen vacancies in ZnSO precipitates within the ZnS lattice (90). Given the confusion in the literature, it is not possible at present to definitely assign an emission center to this band.

ZnS Platelets. The emissions of this form of ZnS are listed in Table VII.

The low luminescent efficiency of the crystal platelets makes impurity identification a difficult task. The presence of the A band indicates that chlorine is present in the platelets, while the Cu-blue and Cu-red bands signal the presence of copper (2, 118-120). Early work by Mita and Sugibuchi indicates that a red band due to tin (Sn-red) may also be present in the platelets.

The well-known Cu-green band is also present in the emission spectra of the platelets. This band is

unambiguously known to be DA emission from substitutional copper (probably on a zinc site) and either chlorine (54) or possibly aluminum (118).

Finally, very weak lines between 320 and 322 nm at certain locations on the platelets reveal the presence of the hexagonal or 2H phase of ZnS.

Raytheon cvd ZnS. The emissions of Raytheon cvd ZnS are listed in Table VIII.

The low temperature cathodoluminescence of Raytheon cvd ZnS is very weak and is dominated by the SAL band. That copper and either aluminum or chlorine are present in the Raytheon samples is proven by the appearance of strong Cu-blue and weak Cu-green emission bands.

Weak donor bound-exciton lines are frequently present in the emission spectrum---particularly the I_1^B line attributed to aluminum. These lines are very strongly broadened due to high impurity content and/or disorder.

A broad emission band usually centered at 337.5 nm and designated "B" in Table VIII has been tentatively attributed to DA emission, although the characteristic intensity shift is in this case very small. The poor signal to noise ratio in Raytheon emission spectra made it difficult to assign a wavelength to the B peak---the value of 337.5 nm is only accurate to 0.5 nm. The B band is probably the band seen by Taguchi (and labelled " A_0 ") in his iodine-doped cubic crystals (127).

CVD Inc. cvd ZnS. The emissions produced from block 1

samples of CVD Inc. ZnS are listed in Table IX. The block 2 sample emissions are listed in Table X.

The main differences in cathodoluminescence between the two types of CVD Inc. samples are that different bound excitons were dominant, the block 1 samples produced much stronger bound-exciton luminescence, and that block 2 samples often displayed a strong (but broad) line at 331.4 nm attributable to FTB recombination from a center at a depth of approximately 100 meV (probably a donor). Samples from both blocks betray the presence of copper and either aluminum or chlorine (the Cu-green and -blue bands again) as well as the ubiquitous SAL band at 390 nm to 400 nm.

The I_1^E donor bound-exciton appears at 327.2 nm in block 1 samples. This bound-exciton is probably associated with chlorine as it was a prominent line in Samelson and Lempicki's (108) chlorine-doped crystals. A strong donor bound-exciton line labelled I_1^F appears at 327.6 nm in all block 1 samples. Block 2 samples often emit a bound-exciton line at 326.6 nm (I_1^C). This line was seen in the excitation spectroscopy of Mn-doped cubic ZnS phosphors by Kawai and Hoshina (70).

Cleartran. The cathodoluminescent emission lines of all the Cleartran samples are gathered in Table XI.

As one might expect, given the superior optical properties of Cleartran, the emission lines of Cleartran include all those mentioned previously in this section. Thus, Cleartran does contain copper, aluminum, chlorine;

and (to a lesser degree of confidence) manganese, and iodine. Emissions in the bound-exciton region still display the characteristic asymmetry due to Stark broadening from high impurity concentrations (118:23-25), but the broadening is much less than in all the other forms of cubic ZnS.

Weak lines near 367.5 nm reveal the presence of ZnO precipitates within the ZnS lattice (18). The SA or SA-blue band is sometimes seen in Cleartran samples. This longer wavelength blue band is due to DA recombination between an acceptor composed of a Zn^{2+} vacancy and an adjacent coactivator ion (probably chlorine) and a donor consisting of an isolated coactivator ion (54, 64:971). Additional weak emission lines between 573.5 and 577 nm confirm the presence of manganese in Cleartran. Strong FTB lines at 331.4 nm and 332.1 nm due to centers at depths of approximately 100 meV and 110 meV, respectively, cannot be fully identified without further studies involving doping with likely impurities (aluminum and chlorine). Faint indications on the high energy side of the SAL peak (not mentioned in Table XI) may be due to transitions in ZnSO precipitates within the ZnS lattice according to Morozova (90, 91). The great majority of emission lines in Cleartran are simply attributable to phonon-assisted recombination.

Table VI

The Emissions of Single Crystal ZnS (Eagle-Picher)

Wavelength (nm)	Energy (eV)	Symbol	Nature	Ref
326.4	3.799	I_1^B	DBE	51,113
327.0	3.792	I_1^D	DBE	
330	3.757	FE+LO	Phonon	
330.8	3.748	I_1^D +LO	Phonon	48
334	3.71	FE+2LO	Phonon	48,51,108
335.3	3.698	FTB+LO*	Phonon	
340	3.647	A	DA	
344.1	3.603	A+LO	Phonon	52,54,108
390-	3.18-	SAL	Various**	
400	3.10			54,98,118
430-	2.88-	Cu-blue	Cu _S +	
440	2.82		interstitial Cu	

*The FTB referred to here was seen at 332.1 nm in Cleartran samples.

**See the text for elucidation.

Table VII

The Emissions of ZnS Platelets

Wavelength (nm)	Energy (eV)	Symbol	Nature	Ref
320-	3.872	HEX	Transitions in the	73,142
322	3.85		hexagonal phase	
327-	3.79-	---	Various DBEs	48
330	3.76		plus FE+LO	
340	3.647	A	DA	48,108
344.4	3.600	A+LO	Phonon	
440-	2.82-	Cu-blue	Cu _s +	98,118
450	2.76		interstitial Cu	
510	2.43	Cu-green	DA due to Cu ₂ Zn	64,119
			and Cl or Al	
690-	1.8-	Cu-red/	Unknown	89,120
720	1.72	Sn-red		

Table VIII

The Emissions of Raytheon cvd ZnS

Wavelength (nm)	Energy (eV)	Symbol	Nature	Ref
326.2	3.800	I_1^A	DBE	18,48
326.4	3.799	I_1^B	DBE	
331.3	3.742	FTB or $I_1^F + LO$	Probable FTB	
331.7	3.738	FTB	Probable FTB	
337.5	3.674	B	Probable DA	48,127
390-	3.18-	SAL	Various*	52,54,108
395	3.14			
430-	2.88-	Cu-blue	$Cu_S +$	54,98,118
440	2.82		interstitial Cu	
505-	2.46-	Cu-green	DA due to Cu_{Zn}	89,120
510	2.43		and Cl or Al	

*See the text for elucidation.

Table IX

The Emissions of CVD Inc. cvd ZnS (Block 1 samples)

Wavelength (nm)	Energy (eV)	Symbol	Nature	Ref
326.2	3.800	I_1^A	DBE	18,48
327.2	3.788	I_1^E	DBE	48,108
327.6	3.785	I_1^F	DBE	48
330	3.76	FE+LO	Probably a phonon replica of the FE	48
335	3.70	I_1^F +LO	Phonon	
337- 338	3.68- 3.67	B	Probable DA	48,127
343	3.62	B+LO	Phonon	
347	3.57	B+2LO	Phonon	
390- 400	3.18- 3.10	SAL	Various*	52,108
430- 450	2.88- 2.76	Cu-blue	Cu _s + interstitial Cu	98,118
505- 515	2.46- 2.41	Cu-green	DA due to Cu _{Zn} and Cl or Al	89,120

*See the text for elucidation.

Table X

The Emissions of CVD Inc. cvd ZnS (Block 2 samples)

Wavelength (nm)	Energy (eV)	Symbol	Nature	Ref
326.4	3.799	I_1^B	DBE	48,70
326.6	3.794	I_1^C	DBE	
330	3.76	FE+LO	Probably a phonon replica of the FE	48
331.4	3.741	FTB or $I_1^F + LO$	Probable FTB or Phonon	
337-	3.68-	B	Probable FTB	48,127
338	3.67			
343	3.62	B+LO	Phonon	52,108
347	3.57	B+2LO	Phonon	
390-	3.18-	SAL	Various*	98,118
400	3.10			
430-	2.88-	Cu-blue	$Cu_s +$	89,120
450	2.76		interstitial Cu	
505-	2.46-	Cu-green	DA due to Cu_{Zn}	89,120
515	2.41		and Cl or Al	

*See text for elucidation.

Table XI

The Emissions of Cleartran

Wavelength (nm)	Energy (eV)	Symbol	Nature	Ref
322.6- 322.9	3.843- 3.839	---	Packing defect	115
323.8- 324.0	3.829- 3.827	---	Packing defect	115
325.85	3.805	FE _A	Free exciton	18
326.2	3.800	I ₁	DBE	18,48
326.4	3.799	I ₁ ^B	DBE	
326.6- 326.7	3.794	I ₁ ^C	DBE	48,70
327.0	3.792	I ₁ ^D	DBE	51,113
327.2	3.788	I ₁ ^E	DBE	48,108
327.6	3.785	I ₁ ^F	DBE	
328.2	3.777	I ₂ ^A	Probable ABE	18
328.7- 328.8	3.771	I ₂ ^B	ABE	18,48
329.2	3.766	I ₂ ^C	ABE	
329.7	3.760	FE+LO	Phonon	48
330.0	3.757	I ₂ ^D	ABE	
330.2	3.755	I ₁ ^B +LO	Phonon	
330.3- 330.6	3.754 3.750	I ₂ ^E	ABE	108
331.0	3.746	I ₁ ^E +LO	Phonon	
331.4	3.741	FTB or I ₁ ^F +LO	Probable FTB or Phonon	
331.5	3.740	FTB	Probable FTB	
332.0	3.735	I ₂ ^A +LO	Phonon	
332.1	3.733	FTB	Probable FTB	18

Table XI Continued

The Emissions of Cleartran

Wavelength (nm)	Energy (eV)	Symbol	Nature	Ref
332.6	3.728	$I_2^B + LO$	Phonon	18
333.1	3.723	$I_2^C + LO$ of FTB+TO**	Phonon	
333.5	3.718	FE+2LO	Phonon	
333.8- 333.9	3.714- 3.713	$I_{1D}^A + 2LO$ $I_2^D + LO$	Phonon	
334.3	3.709	$I_1^C + 2LO$	Phonon	
334.7	3.704	$I_1^D + 2LO$	Phonon	
334.9	3.702	$I_1^E + 2LO$	Phonon	
335.3	3.798	FTB+LO*	Phonon	
336.0	3.690	FTB+LO**	Phonon	
337.0	3.679	$I_2^C + 2LO$	Phonon	
337.4	3.675	FE+3LO	Phonon	48,127
337.8	3.760	$I_{2A}^D + 2LO$ $I_1^A + 3LO$	Phonon	
338.2- 338.5	3.666 3.663	B $I_{1E}^C + 3LO$ $I_2^E + 2LO$	Probable DA	
338.9	3.659	$I_1^E + 3LO$	Phonon	
339.3	3.654	$I_1^F + 3LO$	Phonon	
340.0	3.647	A	DA	
341.5	3.631	FE+4LO	Phonon	
342.4	3.621	B+LO	Phonon	
344.2	3.601	A+LO	Phonon	
346.6	3.578	B+2LO	Phonon	
348.4	3.559	A+2LO	Phonon	48,51,108
350.8	3.534	B+3LO	Phonon	
352.7	3.515	A+3LO	Phonon	

Table XI Continued

The Emissions of Cleartran

Wavelength (nm)	Energy (eV)	Symbol	Nature	Ref
355.2	3.491	B+4LO	Phonon	
357.1	3.472	A+4LO	Phonon	
361.7	3.428	A+5LO	Phonon	
366.3	3.385	A+6LO	Phonon	
367.5	3.373	ZnO	ZnO transition from precipitates	91
392-	3.162	SAL	Various***	54
396	3.130			
430-	2.883	Cu-blue	Cu _s + interstitial Cu	54
449	2.761			
460-	2.70-	SA	DA due to Zn vacancy + 64	
470	2.64		Cl A-center	
504-	2.460-	Cu-green	DA due to Cu _{Zn} and Cl or Al ^{Zn}	119
515	2.407			
573.5-	2.162	Mn	---	81
577	2.149			

All energies were calculated via
 $E(\text{eV}) = 12398.541 / \text{Wavelength}(\text{Angstrom})$

*The FTB referred to here lies at 331.5 nm.

**The FTB referred to here lies at 332.1 nm.

***See the text for elucidation.

Temperature Dependence of the Emission Edge

By tracking the energy position of the highest energy edge emission band with temperature, one can obtain a good approximation of the band gap shift with temperature. Since the binding energy of the free exciton in Cleartran is about 35 meV, it is theoretically possible to detect FE recombination even at 300 K. This is difficult in practice because the near band-edge cathodoluminescence quenches rapidly in polycrystalline materials above 100 K. I was only able to follow the evolution of the highest energy edge emission with temperature for the side view Cleartran and Eagle-Picher single crystal samples. The experimental data is plotted in Figure 52.

At 10 K, the highest energy edge emission band is easily identified as one of the six well-resolved DBE lines of cubic ZnS. This identification is difficult to maintain as relative peak intensities shift with rising sample temperature. Given the exciton binding energies of the donor impurities, it is reasonable to assume that the density of donor bound-excitons at the shallowest donor impurities begins to decline at temperatures as low as 50 K. Even the strong I_1^F line is unlikely to persist at temperatures in excess of 210 K. Since there is no abrupt shift in the data plotted in Figure 52, the 300 K near band-edge luminescence cannot be due to band-to-band recombination, as has been previously suggested (32). It is much more likely that this luminescence can be explained

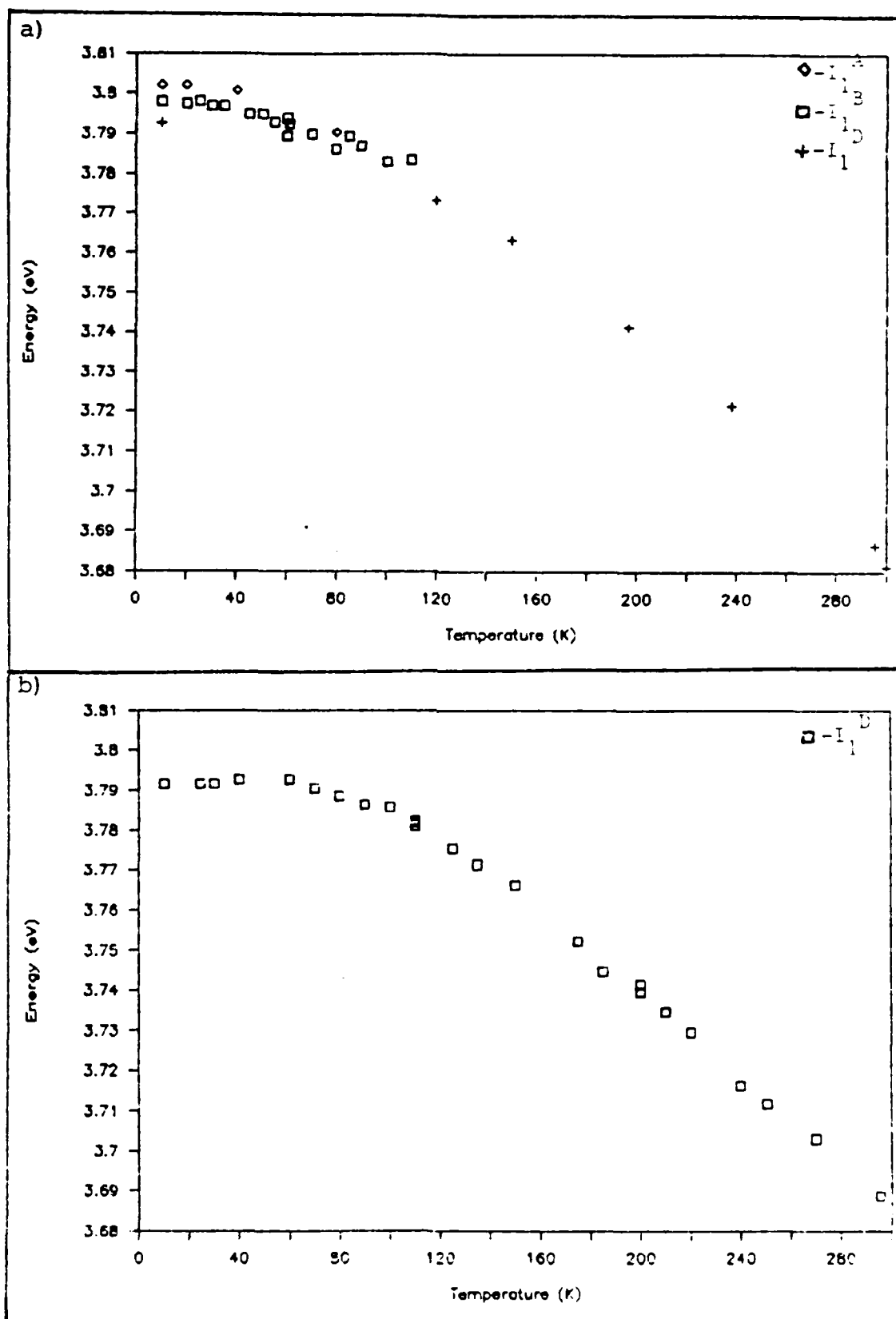


Fig. 52. The temperature shift of the highest energy edge emission band for a) Cleartran and b) Eagle-Picher single crystal ZnS.

with the FE-electron interaction model of Era and Langer (44) and Fan and Woods (46), which has served so well to explain similar luminescence in ZnSe.

The position of a single DBE line in Cleartran and another DBE line in our Eagle-Picher single crystal samples is plotted vs $\coth \frac{\hbar\omega_{LO}}{2kT}$ in Figure 53. The straight line obtained for $T > 100$ K supports the dependence postulated in Equation 7. In Figure 54, we plot E_p vs $\coth \frac{\hbar\omega_{LA}}{2kT}$, demonstrating that for $50 \text{ K} < T < 100 \text{ K}$, the LA phonon is responsible for the temperature shift. From these plots, we obtain the values $S'_{LO} = -0.22 \text{ eV}$ and $S'_{LA} = -0.02 \text{ eV}$. Our value for S'_{LO} is only slightly different from the value of $S'_{LO} = -0.20 \text{ eV}$ obtained by Yacobi (145). This discrepancy may be attributed to either a change in the Franz-Keldysh coefficient γ' for the DBE lines in Cleartran or to a different applicable polaron cutoff wave vector q_c .

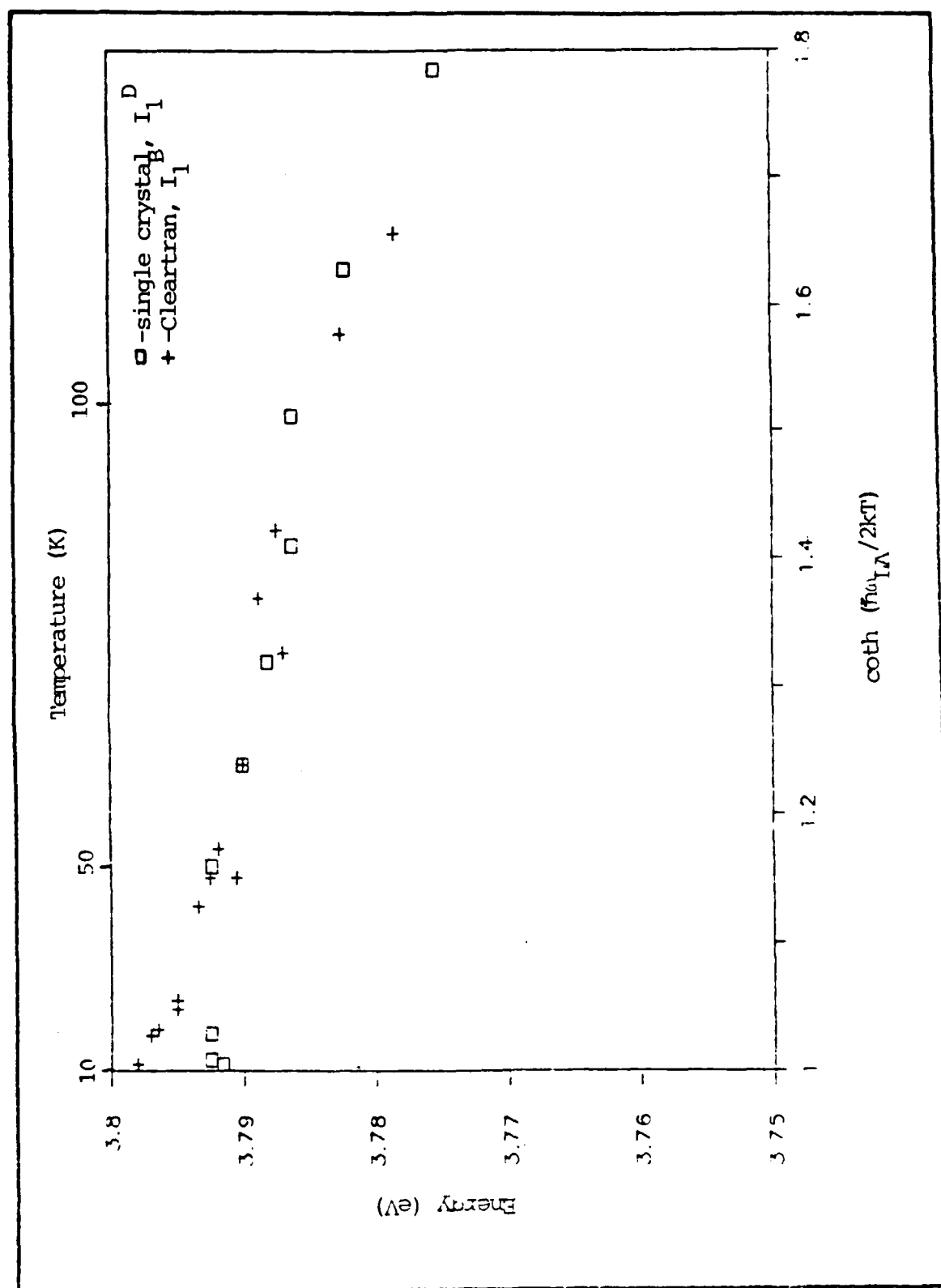


Fig. 54. The energy position of a single bound-exciton line in Cleartran (+) and Eagle-Picher single crystal ZnS (\square) vs $\coth (\hbar\nu_{LA}/2kT)$.

V. Conclusions and Recommendations

X-ray diffraction and spark-source mass spectrometry of Cleartran show it to be a well-ordered, high purity ($<10^{16}$ impurities/cm³) form of polycrystalline cubic ZnS. The post-deposition processing technique used to create Cleartran from cvd ZnS not only increases the size of individual crystals, it also increases the degree of orientation of the crystals. There is no indication of the intergrowth of any polytype phase material within the cubic phase lattice.

The cathodoluminescence of Cleartran is characteristic of pure cubic phase material. The low temperature cathodoluminescence of Cleartran is sharper, more detailed, and more intense than that of the parent cvd ZnS or the fine-grained Raytheon cvd ZnS. The intensity of the near band-edge luminescence from cleaved surfaces of cubic single crystal ZnS is more intense than for the Cleartran material, but far fewer details are present in the low temperature cathodoluminescence and the near band-edge emission peaks are broader than those in Cleartran. Phonon coupling is much stronger in Cleartran than in any of the other forms of cubic ZnS we investigated.

Comparison of the Cleartran spectra with the literature indicates that the relative intensity of the near band-edge luminescence is unusually high. The degree of detail in the cathodoluminescence of Cleartran is greater and the

emission peaks are sharper than previous reports on cubic phase samples of cvd, single crystal, thin film, and organometallically grown cvd ZnS (32, 34, 48, 51, 94, 104, 108, 113, 114, 115, 116, 126). The shallow BE lines are very sensitive to strain and interimpurity interactions. The limiting BE linewidth of 3-6 meV in the Cleartran samples; while unremarkable for such extensively studied semiconductors as Si, Ge, and GaAs; is yet another indicator of the high purity and crystalline quality of the Cleartran crystals.

The cathodoluminescence of Cleartran varies sometimes dramatically with location on a sample. We believe this is due to spot-to-spot variations in the segregation of impurities during HIP processing, a change in the amount of local lattice strain and the concentration of lattice defects, and the fact that even the smallest electron beam spot available to us simultaneously excites luminescence from 100+ crystals.

The relatively poor luminescence of the end view samples versus the side view samples of Cleartran is also related to the HIP processing. The cracks and crevices visible in microphotographs of end view samples suggest that growth-induced strain and defects along the principal growth direction are responsible for the observed reduction in near band-edge luminescence.

The temperature dependence of the highest energy luminescence band in Cleartran and cubic single crystal ZnS

was measured in the range of 10 to 300 K. The observed shift was explained by Yacobi's synthesis of the Dow-Redfield theory of phonon-generated microfields and the Franz-Keldysh field-induced shift of the absorption edge (146). The small difference between Yacobi's value for the slope constant ($S'_{LO} = -0.20$ eV) and our higher value ($S'_{LO} = -0.22$ eV) can be attributed to a difference in the Franz-Keldysh coefficient or the polaron cutoff wave vector q_c . We also obtained the first value for the slope constant due to LA phonon-generated microfields, $S'_{LA} = -0.02$ eV.

Due to the poor crystalline quality of previous samples of cubic ZnS, it has been very difficult to assign impurities to emission bands. This makes the determination of the nature of Cleartran's impurities a chancy proposition. Nevertheless, we may say with some confidence that Cleartran retains a significant concentration of copper, chlorine, aluminum, manganese, and oxygen; and that iodine and Zn vacancies are probably also present. Other impurities are doubtless also present in Cleartran, but determining the nature of these impurities will require further work.

Much work may still be done with Cleartran samples. Since Cleartran appears to have a very high (if not uniquely high) crystalline quality, it should be possible to begin good doping studies to search for candidates for creating high mobility p-type cubic ZnS or for formulating

white, violet, and blue ZnS LEDs. It is also desirable to study the response of individual cubic crystals within the Cleartran matrix by employing a SEM-CL device. Careful searching might well locate very low-strain crystals with even smaller BE linewidths. To this end, Cleartran samples created at higher temperatures with larger grain sizes would be desirable. The reduction in impurity concentration claimed for Cleartran by CVD Inc. is probably the result of venting of impurities along grain boundaries (131). Selective excitation of likely impurities (O_2 , ZnO, Al, SO_2 , etc) at the grain boundaries could help settle this question. It is also possible to create large populations of excitons bound to excited impurity states with a high energy dye laser and thereby study the quantum mechanics of excited states of impurity atoms within the large direct band gap of cubic ZnS (6, 7, 36, 37). The cathodoluminescence of these same samples at higher electron beam energies (~35 keV) could be used to check the response and environment of more deeply buried crystals (95, 143).

Appendix: Data Manipulation Programs

After the spectral information was collected from the diode array or the photomultiplier tube, there were still two tasks yet to accomplish. The data stored by the Tracor Northern and Canberra optical multichannel analyzer (OMA) systems was stored in odd formats on 8 inch floppy disks and datacassettes, respectively. These storage modes were inconvenient for manipulating and plotting the data. The first task was therefore to convert the data into a more universal format. Each of the detection systems introduced error into the data. The second task was to remove from the data at least the systematic error due to deviations of the instrument response from the ideal.

Both the Tracor Northern and Canberra optical multichannel analyzers were equipped with a "standard" RS-232C serial communications port. The data was converted to a standard format by connecting a Zenith Z100 microcomputer to the optical multichannel analyzers through this serial port. Although this communication could theoretically occur at very high BAUD rates, it proved most practical to operate at 1200 BAUD to prevent overflow of the computer's input buffer. A Basic routine titled TNCOMM was written to handle this communication task. The program initialized the input buffer and saved the incoming data to Zenith Z100 5.25 inch floppy disk files, preserving the unique Tracor Northern and Canberra data formats. Program

TNCOMM is listed in Figure A1.

At the user's leisure the data files, now resident on standard Zenith 5.25 inch floppies, could be converted into a more useful format. A simple Zenith Basic routine was used to strip the channel number and photon count information out of the non-standard OMA formats and save this information as two columns of ASCII numbers on 2100 5.25 inch floppy disks. Since each of the detection systems used unique formats to record detector information, two Basic routines were written to perform this necessary conversion: CANBCONV (to convert Canberra 8100 data) and TNCONV (to convert Tracor Northern data). Program listings for these two routines are the subject of Figures A2 and A3.

A standard file-naming scheme was employed to help keep all of this information straight. The Tracor Northern OMA saved data on disk files named WTAG##---the two numbers indicated by the "#" sign ranged from "00" to "75" before a single 8 inch floppy disk was full. During the course of the investigation, four 8 inch floppy disks were written full of data. Therefore, data read off 8 inch Tracor Northern disks by program TNCOMM was always saved in files named D#WTAG##.DAT. The first "#" symbol was labelled with a number ranging from 0 to 3 corresponding to the number of the 8 inch floppy disk on which the original data was stored. The second set of "#" symbols was labelled with the same two numbers as the original data file. In this

way, it was always possible to cross-check 5.25 inch data files against the original 8 inch data files. Files read from Canberra datacassettes were labelled RUN##.DAT, where the two "#" symbols were labelled with numbers corresponding to the order in which the data was originally taken (as listed in the laboratory notebooks). Once the data files had been converted into the standard format (two columns of numbers: the first being the channel number and the second the photon count), the converted files were labelled P#WTAG##.DAT (for Tracor Northern data) or PRUN##.DAT (for Canberra data). The P designator was meant to suggest that these files were easily plottable.

No instrument or set of instruments ever records information (in this case photon count) with perfect fidelity. The method chosen to determine the deviation of my detection systems from perfect fidelity employed a standard lamp system and an NBS-calibrated tungsten halogen bulb driven by a very high precision power supply and current shunt. First, I recorded the response of each detection system to the lamp in all of the wavelength ranges used during the course of the investigation. I then designed a Fortran program to compare this response to the ideal black-body emittance for the lamp's measured color temperature of 3143 K. From this comparison, the program computed a response filter labelled IRF##.DAT which was saved to 5.25 inch floppy disk. The response filter was a 1 by 1024 point vector which, when multiplied by a vector

representing the raw photon count, returned another 1 by 1024 point vector freed of instrument response problems. The "cleansed" vector representing the corrected photon count was then saved to 5.25 inch floppy disk as a column of ASCII numbers paired with a counter which labelled the instrument channel. These corrected data files were always called I#WTAG##.DAT or IRUN##.DAT, where the "#" symbols were labelled with the same numbers described in the previous paragraph.

This process of removing instrument response from the data has two distinct parts to it. First, a raw measurement of the system's response to the calibrated source must be compared to the ideal black-body emittance of the source and a computed instrument response filter saved to disk (Task 1). Second, raw data newly converted to the standard two-column format must be multiplied by the appropriate instrument response filter and the "cleansed" or "corrected" data saved to disk (Task 2). To accomplish these tasks, I wrote two Fortran subroutines called NORMAL (Figure A4) and CALCDAT (Figure A5) designed to run under a shell program called DATARED (Figure A6). Subroutine NORMAL accomplished the first task, and subroutine CALCDAT accomplished the second task. The shell, DATARED, determined which task the user wished to perform, called raw data into computer memory if the second task was selected, and then called the appropriate subroutine. These routines were fully prompted for ease of use by the

operator and carefully commented so that future workers would find them easy to maintain. This system of routines was written under MSFORTRAN: a standard microcomputer language which is a subset of ANSI-standard FORTRAN 77 written by Microsoft Corporation, and which will run on either the Zenith 2100 or IBM Personal computers. The routines were compiled with MSFORTRAN Version 3.10.

These routines were designed to work with 1024 point data files, the standard file size on the Tracor Northern TN1710A OMA. The Canberra 8100 OMA was a 4096 point device. When converting and correcting Canberra files, I worked with one quarter of a file at a time---a process made simple by the fact that the Canberra could be easily set to read out its data memory in quarters. When I was finished processing the Canberra data, I combined the quarters into two halves generally labelled PRUN##A.DAT and PRUN##B.DAT for plotting. If it is considered desirable to re-write the computer codes to deal with whole Canberra files, it should be remembered that MSFORTRAN does not allow data arrays larger than 64K.

The corrected data files were plotted by importing them into the LOTUS123 spreadsheet via the proprietary LOTUS "import" function. Once the data was in the LOTUS spreadsheet, it was a trivial task to plot the data with LOTUS's integral GRAPHICS package. Data files from the Canberra OMA were plotted as two halves due to the inherent 2048 cell column limitation in the LOTUS spreadsheet.

Authorship of the computer codes described in this appendix is shared between myself and Captain Jeffrey R. Cavins.

```

10 DIM D$(6000)
20 KEY OFF:CLS:C=1:J=0:N=1:L=0
30 LOCATE 1,1:PRINT"COMMUNICATIONS PROGRAM FOR TRACHOR
  NORTHERN 1710"
40 LOCATE 2,1:PRINT"THE COMMUNICATIONS PARAMETERS ARE:
50 LOCATE 3,10:PRINT"1200 BAUD, 7 BITS, ODD PARITY, AND
  ONE STOP BIT"
60 LOCATE 6,1:INPUT "WHAT DO YOU WANT TO CALL THE DATA
  FILE?",A$
70 A$=A$+".DAT"
80 CLOSE
90 REM OPEN THE COMMUNICATIONS FILE
100 OPEN"COM1:1200,O,7,1" AS 1
110 OPEN A$ FOR OUTPUT AS 2
120 REM OPEN A$ AS THE DATAFILE
130 PRINT"PRESS ANY KEY TO CONTINUE"
150 IF INKEY$="" GOTO 150
160 PRINT"START THE DATA"
170 L=L+1
180 IF LOC(1)=0 THEN GOSUB 430 'THE SUBROUTINE WAITS
190 IF LOC(1)=0 THEN GOTO 230
220 D$(L)=INPUT$(LOC(1),1)
230 IF C=1 THEN GOTO 170
240 FOR I=1 TO L
250 PRINT #2,D$(I)
260 NEXT I
265 REM PUT NAME OF DATAFILE IN NAME.FIL FOR LATER USE
270 OPEN"NAME.FIL"FOR OUTPUT AS #3
280 PRINT #3,A$
290 CLOSE
300 SYSTEM
360 END
430 FOR X=1 to 1000
440 IF LOC(1)=0 GOTO 460
450 C=1:X=1000:GOTO 470
460 C=0
470 NEXT X
480 RETURN

```

Fig. A1. Program TNCOMM.

```

10 DIM D$(200),E$(2000),G$(2000),W(2000,2)
20 CLOSE
25 W(1,1)=1
30 J=0
40 REM TRANSLATION OF DATA
50 INPUT"WHAT IS THE NAME OF THE FILE TO TRANSLATE";A$
80 Z$="Z"+A$
85 Z$="B:"+Z$
90 OPEN Z$ FOR OUTPUT AS #4
95 C$="B:"+A$
100 OPEN C$ FOR INPUT AS #1
110 M$="M"+A$
115 M$="B:"+M$
120 OPEN M$ FOR OUTPUT AS #2
130 J=J+1
140 C=1
150 R=((J-1) MOD 20)+1
160 IF EOF(1) THEN 190
170 INPUT #1, D$(R)
180 IF (NOT EOF(1)) AND (J MOD 20 <> 0) THEN GOTO 130
190 IF EOF(1) THEN C=0
200 IF EOF(1) THEN PRINT "END OF FILE"
210 N=1
220 FOR K=1 TO R
230 SN=INSTR(1,D$(K),"??") 'FINDS THE CHANNEL MARKERS
240 H=INSTR(1,D$(K),"?")
250 IF (H=0) AND (SN=0) THEN 370
260 IF SN<5 GOTO 300
265 IF SN>H THEN GOSUB 1000
270 IF SN>5 THEN 370
280 Y=SN-4:E$(N)=MID$(D$(K),Y,4)
290 GOTO 370
300 G$(N)=LEFT$(D$(K),6)
310 N=N+1
320 H=INSTR(1,D$(K),"?")
330 IF H=0 THEN 370
340 MID$(D$(K),H,1)="0"
350 G$(N)=MID$(D$(K),H,7)
360 GOTO 310
370 NEXT K
380 FOR L=1 TO (N-1)
390 IF E$(L)="" THEN E$(L)="0"
400 IF G$(L)="" THEN G$(L)="0"
410 PRINT #2,G$(L)
420 NEXT L
430 CLOSE 2,3

```

Fig. A2. Program CANBCONV. Continued on next page.

```

440 OPEN M$ FOR INPUT AS #2
450 I=0
460 WHILE NOT EOF(2)
470 I=I+1
480 INPUT #2,W(I,2)
490 WEND
500 FOR J=1 to I
510 W(J,1)=W(J-1,1)+1 'COUNTER FOR THE DATA
520 NEXT J
530 FOR K=1 TO I
540 PRINT #4,W(K,1),W(K,2)
550 NEXT K
560 CLOSE #2
565 W(1,1)=W(I,1)+1
570 IF C=1 THEN GOTO 120
580 PRINT"DATA IS TAKEN AND CONVERTED"
590 CLOSE
600 END
1000 G$(N)=LEFT$(D$(K),6)
1010 IF SN=H THEN 1100
1020 N=N+1
1030 H=INSTR(1,D$(K),"?")
1040 MID$(D$(K),H,1)="0"
1050 G$(N)=MID$(D$(K),H,7)
1060 GOTO 1010
1100 RETURN

```

Fig. A2. Program CANBCONV.

```

10 DIM C$(1024)
20 CLS:PRINT"REMOVE THE PROGRAM DISK."
30 PRINT"PUT THE DISK CONTAINING DATA INTO DRIVE A:"
40 PRINT"PUT THE FORMATTED DATA DISK INTO DRIVE B:"
50 PRINT"PRESS RETURN WHEN READY TO CONTINUE"
60 A$=INKEY$
70 IF A$<>CHR$(13) THEN GOTO 60
80 INPUT "WHAT IS THE NAME OF THE DATAFILE";E$
90 E$="A:"+E$+".DAT"
100 F$=E$
110 MID$(F$,1,3)="B:P"
120 OPEN E$ FOR INPUT AS #1
130 OPEN F$ FOR OUTPUT AS #2
140 FOR X=1 TO 4 'PASS OVER THE FIRST TWO HEADER LINES
150 INPUT #1,B$
160 NEXT X
170 P=1 'INITIALIZE COUNTER
180 A=0:B=0:C=0
190 FOR X=1 TO 128 'INPUT RAW DATA
200 INPUT #1,B$
210 IF X>2 THEN A=1
220 IF X>13 THEN B=1
230 IF X>125 THEN C=1
240 FOR Y=4+(A+B+C) TO 53+(A+B+C) STEP 7
250 C$(P)=MID$(B$,Y,7)
260 P=P+1
270 NEXT Y
280 NEXT X
290 FOR X=1 TO 1024
300 PRINT #2, USING "##### ";X;VAL(C$(X))
310 NEXT X
320 CLOSE
330 END

```

Fig. A3. Program TNCONV.

```

      SUBROUTINE NORMAL (TD,M)
      DOUBLE PRECISION M(1024),W(1024),TD(1024)
      INTEGER IT
C     THIS PROGRAM COMPUTES THE SPECTRAL EMITTANCE M(I)
C     OF A BLACK BODY AT TEMPERATURE T AND THEN
C     NORMALIZES M(I) BY ITS LARGEST COMPONENT, TYPICALLY
C     THE LAST. ACTUAL CALIBRATION DATA IS THEN PASSED
C     INTO THIS SUBROUTINE (TD(I)) AND M(I) IS RECOMPUTED
C     IN ITS FINAL INCARNATION AS THAT VECTOR WHICH, WHEN
C     MULTIPLIED BY RAW DATA RETURNS DATA FREED OF ALL
C     INSTRUMENT RESPONSE PROBLEMS.
      C0=3.7418317E-16
      C1=0.014387863
      C3=2.704260E-11
C     ENTER THE TEMPERATURE OF THE BLACK BODY
      WRITE(*,900)
900    FORMAT(1X,'PLEASE ENTER BLACK BODY TEMP (DEG K)')
      READ(*,1000) IT
1000   FORMAT(I4)
C     ENTER THE CENTRAL WAVELENGTH OF THE ARRAY IN METERS
      WRITE(*,1100)
1100   FORMAT(1X,'Enter the array central wavelength')
      WRITE(*,1120)
1120   FORMAT(1X,'in meters to five decimal places.')
      WRITE(*,1150)
1150   FORMAT(1X,'Example---3.34148E-7')
      READ(*,1200) BBWL
1200   FORMAT(E10.5)
      T=FLOAT(IT)
      CT1=C1/T
      W(1024)=BBWL+C3*511
      M(1024)=C0/(W(1024)**5*(DEXP(CT1/W(1024))-1.))
      DO 10 I=1,1024
      W(I)=BBWL+C3*FLOAT(I-512)
10     M(I)=C0/(M(1024)*W(I)**5*(DEXP(CT1/W(I))-1.))
      TMAX=0
      DO 30 J=1,1024
30     IF (TD(J).GT.TMAX) TMAX=TD(J)
      DO 40 J=1,1024
      TD(J)=TD(J)/TMAX
40     M(J)=M(J)/TD(J)
      WRITE(*,45)
45     FORMAT(1X,'Save instrument response filter to disk
+ 'with format B IRF .DAT when prompted.')
      WRITE(*,48)
48     FORMAT(1X,'Swap out disks in drive B now if needed')
      OPEN(4,FILE=' ',ACCESS='SEQUENTIAL',STATUS='NEW')
      WRITE(4,50) (M(K),K=1,1024)
50     FORMAT(3D21.15)
      CLOSE(4)
      RETURN
      END

```

Fig. A4. Program NORMAL.


```

      SUBROUTINE CALCDAT
      INTEGER WA,PD(1024),IPD(1024)
      DOUBLE PRECISION IR(1024),DPD(1024)
C     This subroutine reads TN data off 5" disk files of
C     type P_WTAG_.DAT and a selected instrument re-
C     sponse filter of type IRF_.DAT. The datafiles are
C     converted where necessary to double precision and
C     multiplied together to create an array of corrected
C     data. The corrected data and a channel counter are
C     saved to a new disk as files of type I_WTAG_.DAT.
C     Read in the raw data.
      WRITE(*,10)
10     FORMAT(1X,'Put data disk in drive B.')
      WRITE(*,15)
15     FORMAT(1X,'At prompt, enter the complete data',
+ ' filespec including the drive letter.')
      OPEN(4,FILE=' ',ACCESS='SEQUENTIAL',STATUS='OLD')
      READ(4,20) (WA,PD(K),K=1,1024)
20     FORMAT(I7,I8)
      CLOSE(4)
C     Now read in the instrument response filter.
      WRITE(*,30)
30     FORMAT(1X,'Be sure your instr response filter is',
+ ' handy.')
      WRITE(*,35)
35     FORMAT(1X,'At prompt, enter the complete filespec',
+ ' with the drive letter, of the filter.')
      OPEN(5,FILE=' ',ACCESS='SEQUENTIAL',STATUS='OLD')
      READ(5,40) (IR(K),K=1,1024)
40     FORMAT(3D21.15)
      CLOSE(5)
C     Convert negative numbers, and the enormous positive
C     numbers the TN1710 often interprets negative numbers
C     as, into proper positive numbers by upconverting
C     all the data.
      TMIN=0.
      DO 43 J=1,1024
      IF(PD(J).GT.1040000) PD(J)=PD(J)-1048576.
43     IF(PD(J).LT.TMIN) TMIN=PD(J)
      IF(TMIN.LT.0) TMIN=ABS(TMIN)
      DO 46 L=1,1024
      PD(L)=TMIN+PD(L)
46     IF(PD(L).LT.10) PD(L)=10
C     Convert the data (PD) to double precision (DPD).
      DO 50 I=1,1024
50     DPD(I)=DBLE(PD(I))
C     Generate the corrected data from DPD and IR.
      DO 60 J=1,1024
60     DPD(J)=DPD(J)*IR(J)

```

Fig. A5. Program CALCDAT. Continued on next page.

```

C      Convert DPD to an INTEGER*4 array, IPD, with IDNINT
C      so that the numbers will be rounded.
      DO 70 I=1,1024
      IPD(I)=IDNINT(DPD(I))
C      Do not let IPD get bigger than 1048570.
      IF(IPD(I).GT.1048570) THEN
        IPD(I)=1048570
      ENDIF
70    CONTINUE
C      Save IPD and a channel counter to disk to make a
C      plottable file of type I_WTAG_.DAT.
      WRITE(*,75)
75    FORMAT(1X,'Remove old data disk from drive B.')
      WRITE(*,78)
78    FORMAT(1X,'Insert a new, formatted disk into B',
+ ' to receive the corrected data.')
      WRITE(*,80)
80    FORMAT(1X,'At prompt, enter a complete filespec to',
+ ' save data, including drive letter.')
      OPEN(6,FILE=' ',ACCESS='SEQUENTIAL',STATUS='NEW')
      WRITE(6,90) (K,IPD(K),K=1,1024)
90    FORMAT(I7,1X,I7)
      CLOSE(6)
      RETURN
      END

```

Fig. A5. Program CALCDAT.

```

                                PROGRAM DATARED
      INTEGER I,J,C,F,TN(1024)
      DOUBLE PRECISION M(1024),TD(1024)
C      This program reads raw data converted into channel-
C      count format on Z-100 disks.  Its purpose is to 1)
C      calculate an instrument response filter for the
C      spectroscopy system in rm 66C, and to 2) remove
C      the instrument response from raw data taken on that
C      system using the previously computed instrument
C      response filter.
C      Ask the user which of the two paths he wishes to
C      follow.
5      WRITE(*,10)
10     FORMAT(1X,'Do you wish to 1.reduce data or 2.compute',
+       ' a filter "enter 1 or 2"?')
      READ(*,15) I
15     FORMAT(I2)
      IF(I.NE.2) GOTO 100
      WRITE(*,20)
20     FORMAT(1X,'Place the disk with the instrument res-',
+       ' ponse data PIR .DAT in drive B and then')
      WRITE(*,22)
22     FORMAT(1X,'strike any key.')
      READ(*,25) J
25     FORMAT(I2) J
      WRITE(*,26)
26     FORMAT(1X,'When prompted to enter a filename, be sure',
+       ' to specify drive B explicitly.')
      OPEN(3,FILE=' ',ACCESS='SEQUENTIAL',STATUS='OLD')
      READ(3,30) (C,TN(K),K=1,1024)
30     FORMAT(2I7)
C      Correct for possible negative numbers or the huge
C      numbers near 1040000 the TN1710 sometimes turns
C      negative numbers into.
      TMIN=0.
      DO 33 J=1,1024
      IF(TN(J).GT.1040000) TN(J)=TN(J)-1048576.
33     IF(TN(J).LT.TMIN) TMIN=TN(J)
      IF(TMIN.LT.0) TMIN=ABS(TMIN)
      DO 36 L=1,1024
      TN(L)=TMIN+TN(L)
36     IF(TN(L).LT.10) TN(L)=10.
      DO 40 K=1,1024
40     TD(K)=DBLE(TN(K))
      CLOSE(3)

```

Fig. A6. Program DATARED. Continued on next page.

```

        CALL NORMAL(TD,M)
        GOTO 200
100     CALL CALCDAT
200     WRITE(*,210)
210     FORMAT(1X,'Work completed on selected task.')
        WRITE(*,220)
220     FORMAT(1X,'Do you wish to continue? 1=YES ')
        READ(*,230) F
230     FORMAT(I2)
        IF(F.EQ.1) GOTO 5
        STOP
        END

```

Fig. A6. Program DATARED.

BIBLIOGRAPHY

1. Allen, J. W. "Energy Levels of Transition Metal Impurities in Semiconductors." Physics of Semiconductors, Proceedings of the 7th International Conference, 781-787. New York: Academic Press, 1964.
2. Arpiarian, N. "The Centenary of the Discovery of Luminescent Zinc Sulfide." Proceedings of the International Conference on Luminescence, 1966, 903-906. Budapest: Akademiai Akaido, 1968.
3. Aven, M. and J. S. Prener. Physics and Chemistry of II-VI Compounds. New York: John Wiley and Sons, Inc., 1967.
4. Baars, J. W. "The Fundamental Reflectivity of ZnS Single Crystals with 3C, 2H, 4H, 6H, 10H Structures." II-VI Semiconducting Compounds: 1967 International Conference, 631-638. New York: W. A. Benjamin, Inc., 1967.
5. Baczewski, A. "Epitaxial Growth of ZnSe on GaAs." Journal of the Electrochemical Society, 112: 577-580 (1965).
6. Baldereschi, A. and N. O. Lipari. "Spherical Model of Shallow Acceptor States in Semiconductors." Physical Review B, 8: 2697-2709 (15 Sept 1973).
7. Ibid. "Cubic Contributions to the Spherical Model of Shallow Acceptor States." Physical Review B, 9: 1525-1539 (15 Feb 1974).
8. Baltrameyunas, R., et al. "Edge Luminescence of ZnS Single Crystals Under Strong Photoexcitation Conditions." Soviet Physics-Solid State Physics, 22: 589-591 (April 1980).
9. Baltrameyunas, R., et al. "Photoluminescence of ZnS with Ion-Implanted Ne Impurity." Journal of Applied Spectroscopy, 30: 110-112 (Jan 1979).
10. Bergh, A. A. and P. J. Dean. Light Emitting Diodes. Oxford: Clarendon Press, 1976.
11. Besomi, P. and B. W. Wessels. "Deep Level Defects in Polycrystalline CdS." Applied Physics Letters, 37: 955-958 (1980).

12. Bhargava, R. N. "The Role of Impurities in Refined ZnSe and Other II-VI Semiconductors." Journal of Crystal Growth, 59: 15-26 (Sep 1982).
13. Bir, G. L., et al. "Exciton Piezoreflectance of Cubic Zinc Sulphide Crystals." Soviet Physics-Solid State Physics, 12: 926-928 (1970).
14. Birman, J. L. "Theory of Luminescent Centers and Processes in ZnS-Type Compounds." Proceedings of the International Conference on Luminescence, 1966: 919-960. Budapest: Akademiai Kiado, 1968.
15. Birman, J. L., H. Samelson, and A. Lempicki. "Reflection and Emission of Polarized Light in ZnS and CdS." GT E Research and Development Journal, 1: 2-15 (Jan 1961).
16. Birman, J. L. "Simplified LCAO Method for Zincblende, Wurtzite, and Mixed Crystal Structures." Physical Review, 115: 1493-1505 (1959).
17. Bishop, H. E. "Electron-Solid Interactions and Energy Dissipation." In Quantitative Scanning Electron Microscopy, edited by D. B. Holt, M. D. Muir, P. R. Grant, and I. M. Boswara. New York: Academic Press, 1974.
18. Blessinger, D. "High Resolution Cathodoluminescence of Yellow and Waterclear Polycrystalline cvd ZnS." Unpublished MS thesis. AFIT School of Engineering, Wright-Patterson AFB, Ohio, August 1983.
19. Bochkov, et al. "Photoluminescence of ZnS with Ion-Implanted Ne Impurity." Journal of Applied Spectroscopy, 30: 179-182 (Feb 1979).
20. Ibid. "Recombination Radiation of ZnS." Optics and Spectroscopy, 22: 356-357 (Apr 1967).
21. Bonfiglioli, G. and A. Suardo. "Cu Reprecipitation and Electroluminescence in ZnS Single Crystals." Physics Letters, 13: 197-198 (Dec 1964).
22. Brafman, O. and I. T. Steinberger. "Optical Band Gap and Birefringence of ZnS Polytypes." Physical Review, 143: 501-505 (Mar 1966).
23. Broser, et al. "Luminescence of an M Center in ZnS?" Journal of the Physics and Chemistry of Solids, 41: 101-107 (1980).

24. Bryant, F. J. and P. S. Manning. "The Effect of Zn Displacement on the Luminescence of ZnS." Solid State Communications, 10: 501-504 (1972).
25. Bryant, F. J. and S. A. Hamid. "Electron-Irradiation and Trapping Centers in ZnS Single Crystals." Physica Status Solidi (A), 2: 597-605 (1970).
26. Bryant, F. J. and S. A. Hamid. "Heat Treatment of Trapping Centres in Zinc Sulfide Single Crystals." Physica Status Solidi (A), 2, no 3: 607-618 (1970).
27. Carter, D. B. "Zinc Sulphide." Report EPIC-DS-135-(2-ED), Hughes Aircraft Co., Culver City, California, Electronic Properties Information Center, Nov 1966. AD Number 803 885.
28. Catalano, et al. "Spontaneous and Stimulated Luminescence in CdS, ZnS Excited by Multiphonon Optical Pumping." Physical Review B, 8: 1488-1492 (Aug 1973).
29. Conversations with Mr. Donald Evans of the Optics Branch, Materials Laboratory, Wright-Patterson AFB, Ohio. (November 1982-March 1983).
30. Data sheets provided by CVD, Inc.
31. Datta, S., et al. "The Shape of the Self-Activated Cathodoluminescence Band in ZnS:Cl Crystals." Journal of Luminescence, 21: 53-73 (Dec 1979).
32. Datta, S., B. G. Yacobi, and D. B. Holt. "Scanning Electron Microscope Studies of Local Variations in Cathodoluminescence in Striated ZnS Platelets." Journal of Materials Science, 12: 2411-2420 (1977).
33. Davidson, S. M. and C. A. Dimitriadis. "Advances in the Electrical Assessment of Semiconductors Using the Scanning Electron Microscope." Journal of Microscopy, 118: 275-284 (1980).
34. Dean, P. J., et al. "Optical Properties of Undoped Organometallically Grown ZnSe and ZnS." Journal of Crystal Growth, 59: 301-306 (Sept 1982).
35. Dean, P. J. "Photoluminescence as a Diagnostic for Semiconductors." Crystal Growth Characterization, 5: 89-174 (1982).

36. Dean, P. J., et al. "Donor Bound-Exciton States in ZnSe." Physical Review B, 23: 4888-4901 (Aug 1981).
37. Dean, P. J., et al. "Study of Donor Species in ZnSe and ZnTe with a New Photoluminescent Technique." Journal of the Physical Society of Japan, Supplement A, 49: 185-188 (1980).
38. Dean, P. J., et al. "Valence Band Contribution to Photoluminescent Excitation Spectra of Tightly Bound Holes in Zincblende Semiconductors." Journal of Luminescence, 21: 193-205 (Apr 1980).
39. Dean, P. J. "Inter-Impurity Recombination in Semiconductors." In Progress in Solid State Chemistry, Volume 8; McCaldin and Somorjai, editors. New York: Pergamon Press, 1973.
40. Dexter, D. L. "Interpretation of Urbach's Rule." Physical Review Letters, 19: 1383-1385 (1967).
41. Dow, J. D. and D. Redfield. "Toward a Unified Theory of Urbach's Rule and Exponential Absorption Edges." Physical Review B, 5: 594-610 (1972).
42. Egee, M. "Spectral Distribution of the Green Emission Band of ZnS:Cu in Dependence on the Localization Diversity of the Radiative Recombination Process." Physica Status Solidi (A), 35: 361-370 (May 1976).
43. Egorov, V. Yu., et al. "Luminescence and Raman Scattering in ZnS-Mn Crystals." Optical Spectroscopy, 44: 354-356 (Mar 1978).
44. Era, K. and D. W. Langer. Journal of Luminescence, 1/2: 514-518 (1970).
45. Etienne, et al. "Photoluminescence of ZnSe:Ga and ZnSe:As." Materials Research Bulletin, 10: 1365-1372 (Dec 1975). In French.
46. Fan, X. W. and J. Woods. "Free Exciton Emission in Forward Biased ZnSe MIS Diodes." Journal of Physics C, 14: 1863-1871 (1981).
47. Fisher, A. G. "Preparation and Properties of ZnS-Type Crystals from the Melt." Journal of the Electrochemical Society, 106: 838-839 (1959).

48. Flesch, U., R.-A. Hoffmann, and R. Rass. "Exciton Luminescence of Cubic ZnS Crystals." Journal of Luminescence, 3: 137-142 (1970).
49. Franz, W. "Influence of an Electric Field on an Optical Absorption Edge." Zeitschrift Naturforschung, 13a: 484-489 (1958). In German.
50. Fukushima, et al. "Luminescence of Bound Excitons in Te-Doped ZnS Crystals." Japanese Journal of Applied Physics, 12: 549-556 (Apr 1973).
51. Gezci, S. and J. Woods. "Edge Emission in ZnS." Journal of Applied Physics, 51: 1866-1867 (1980).
52. Gill, R. W. A. and S. Rothschild. Enlarged Abstracts, Electrochemical Society Meeting, Chicago, 1960 and Indianapolis, 1961 (unpublished).
53. Goldstein, J. J., et al. Scanning Electron Microscopy and X-Ray Microanalysis. New York: Plenum, 1981.
54. Grasser, R., A. Scharmann, and W. Schwedes. "Further Effects of High Temperature Annealing on the Photoluminescence of an Ultra High Purity ZnS Crystal." Zeitschrift fur Physik B, 28: 247-253 (1977).
55. Grebe, et al. " Cr^{2+} Excitation Levels in ZnSe and ZnS." Journal of Physics C-Solid State Physics, 9: 4511-4516 (Dec 1976).
56. Greene, L. C. and V. Swaminathan. "Photoluminescence in Polycrystalline ZnSe Laser Window Material." Air Force Materials Laboratory Technical Report AFML-TR-79-4039. AD Number B038963. Apr 1979.
57. Gross, et al. "Spectrum of Exciton Complexes in Hexagonal ZnS Crystals." Soviet Physics-Solid State Physics, 10: 818-820 (Oct 1968).
58. Gumlich, H. E., R. Moser, and E. Neumann. "On the Mn-Mn Interaction and the Structure of Optical Spectra of ZnS (Mn)." Physica Status Solidi, 24: K13 (1967).
59. Holt, D. B. and F. M. Saba. "The Cathodoluminescence Mode of the SEM: A Powerful Microcharacterization Technique." In Scanning Electron Microscopy/1985, edited by O. Johari. Chicago: SEM Inc, Vol. III, 1985.

60. Holt, D. B. and S. Datta. "The Cathodoluminescent Mode as an Analytical Technique: Its Development and Prospects." In Scanning Electron Microscopy/1980, edited by O. Johari. Chicago: SEM Inc., Vol I, 1980.
61. Holt, D. B. and M. Culpan. "Scanning Electron Microscope Studies of Striations in ZnS." Journal of Materials Science, 5: 546-556 (1970).
62. Holton, W. C., R. K. Watts, and R. D. Stinedurf. "Synthesis and Melt Growth of Doped ZnSe Crystals." Journal of Crystal Growth, 6: 97-100 (1969).
63. Hovel, H. J. and A. G. Milnes. "The Epitaxy of ZnSe on Ge, GaAs, and ZnSe by an HCl Close-Spaced Transport Process." Journal of the Electrochemical Society, 116: 843-848 (1969).
64. James, J. R., et al. "Donor-Acceptor Nature of the Blue Self-Activated Emission in ZnS Crystals." Solid State Communications, 17: 969-972 (1975).
65. Jaszczyn-Kopec, P., et al. "High Pressure Action on the SA and Mn Emission in the Cubic, Faulted, and Hexagonal ZnS Crystals." Solid State Communications, 32: 473-477 (Jun 1979).
66. Jaszczyn-Kopec, P., et al. "The Boron Center: A New Luminescence Center in ZnS Crystals." Journal of Luminescence, 18/19: (Jan 1979).
67. Jaszczyn-Kopec, P. and B. Lambert. "Red Luminescence of ZnS:Fe Crystals." Journal of Luminescence, 10: 243-260 (1975).
68. Johnson, S. L. "Cathodoluminescence of Ion-Implanted ZnS." Unpublished MS thesis. AFIT School of Engineering Wright-Patterson AFB, Ohio, 1973.
69. Kanaya, K. and S. Okayama. "Penetration and Energy-Loss Theory of Electrons in Solid Targets." Journal of Physics D, 5: 43-58 (1972).
70. Kawai, H. and T. Hoshina. "Exciton Structure in Luminescence Excitation Spectra of ZnS Phosphors." Solid State Communications, 22: 391-394 (1977).
71. Kawai, H., et al. "Cathodoluminescent Properties of ZnS:Ce, Li Phosphor." Japanese Journal of Applied Physics, 20: 1241-1247 (Jul 1981).

72. Kimura, H. and H. Komiya. "Melt Composition of II-VI Compounds during Crystal Growth in a High Pressure Furnace." Journal of Crystal Growth, 20: 283-291 (1973).
73. Klein, W. "Excitonenemission von Hexagonalem ZnS Bei Anregung mit 50-keV-Elektronen." Journal of the Physics and Chemistry of Solids, 26: 1517-1521 (1965).
74. Klein, C. A. and R. N. Donadio. "Infrared-Active Phonons in Cubic ZnS." Journal of Applied Physics, 51: 797-800 (1980).
75. Kobayashi, H., et al. "Excitation Mechanism of Electroluminescent ZnS Thin Films Doped with Rare-Earth Ions." Japanese Journal of Applied Physics, 13: 1110-1114 (Jul 1974).
76. Kuboniwa, S., H. Kawai, and T. Hoshina. "Cathodoluminescence Saturation and Decay Characteristics of ZnS:Cu,Al Phosphor." Japanese Journal of Applied Physics, 19: (Sept 1980).
77. Kukimoto, H., S. Oda, and T. Nakayama. "Preparation and Characterization of Low-Voltage Cathodoluminescent ZnS." Journal of Luminescence, 18/19: 365-368 (1979).
78. Kynov, K., et al. "Afterglow of Mn Centers in Pulse-Excited ZnS:Mn." Journal of Luminescence, 27: 199-205 (Aug 1982).
79. Lambert, B., T. Buch, and A. Geoffrey. "Optical Properties of Mn^{2+} in Pure and Faulted Cubic ZnS Single Crystals." Physical Review B, 8: 863-869 (Jul 1973).
80. Langer, D. "Pressure Effects on the Band Structure of II-VI Compounds with Zincblende Structure." Physics of Semiconductors: Proceedings of the 7th International Conference, 241-244. New York: Academic Press, 1964.
81. Langer, D. and I. Sumiaki. "Zero-Phonon Lines and Phonon Coupling in ZnS:Mn." Physical Review, 138, no 3A: A809-A815 (3 May 1965).
82. Leamy, H. J. "Charge Collection Scanning Electron Microscopy." Journal of Applied Physics, 53: R51-R62 (1982).

83. Lewis, K. L., D. J. Cook, and P. B. Roscoe. "The Structure and Optical Properties of Polycrystalline $\text{ZnS}_x\text{Se}_{1-x}$ Prepared by Chemical Vapor Deposition." Journal of Crystal Growth, 56: 614-620 (1982).
84. Lohnert, K. and E. Kubalek. "Characterization of Semiconducting Materials and Devices by EBIC and CL Techniques." In Microscopy of Semiconducting Materials. Oxford: Oxford, 1983. Institute of Physics Conference Series No. 67.
85. Lorenz, M. R. "Crystal Growth of II-VI Compounds." II-VI Semiconducting Compounds: 1967 International Conference, 215-243. New York: W. A. Benjamin, Inc., 1967.
86. Mahr, H. "Ultraviolet Absorption of KI Diluted in KCl Crystals." Physical Review, 125: 1510-1512 (1962).
87. Matsukura, N. and Y. Machi. "Preparation and Optical Properties of ZnSe Epitaxial Layers by a Close-Spaced Technique." Japanese Journal of Applied Physics, 18: 233-238 (1979).
88. Miloslavskii, V. K., E. N. Naboikina, and T. S. Kiyan. "Effect of Structure Defects on the Optical Properties of Thin ZnS Films in the Fundamental Absorption Edge Region." Soviet Physics-Semiconductors, 1: 527-532 (Nov 1967).
89. Mita, Y. and K. Sugibuchi. "Luminescence Centres in Zinc Sulfide Activated with Group IV Elements." Proceedings of the International Conference on Luminescence, 1966: 1158-1163. Budapest: Akademiai Akaido, 1968.
90. Morozova, N. K., et al. "On the Nature of SAL Bands in the Emission of ZnS." Journal of Applied Spectroscopy, 23: 933-936 (Jul 1975).
91. Morozova, N. K., M. M. Malov, and O. I. Korolev. "Presence of Oxygen in ZnS Single Crystals." Inorganic Materials, 8: 199-201 (Feb 1972).
92. Nemchenko, A. M. "Emission Spectra of ZnS:Cu Single Crystals." Journal of Applied Spectroscopy, 19: 930-933 (Jul 1973).
93. Nilsen, W. G. "Raman Spectrum of Cubic ZnS." Physical Review, 182: 838-842 (1969).

94. Nolle, E. L., et al. "UV Luminescence of ZnS Under Electron Excitation." Optics and Spectroscopy, 23: 144-145 (Aug 1967).
95. Norris, C. B., C. E. Barnes, and W. Beezhold. "Depth-Resolved Cathodoluminescence in Undamaged and Ion-Implanted GaAs, ZnS, and CdS." Journal of Applied Physics, 44: 3209-3221 (Jul 1973).
96. Otomo, Y. and H. Kusumoto. "Donor-Acceptor Pair Luminescence in Self-Activated ZnS Phosphors." Proceedings of the International Conference on Luminescence, 1966: 1177-1185. Budapest: Akademiai Akaido, 1968.
97. Ozawa, L., R. Huzimura, and Y. Ato. "Dependence of Luminescence in ZnS-Mn Phosphor on the Concentration of Mn^{2+} Determined by ESR." Proceedings of the International Conference on Luminescence, 1966: 798-800. Budapest: Akademiai Akaido, 1968.
98. Patel, J. L., et al. "Copper-Associated Donor-Acceptor Recombination in ZnS in the Far Blue Region." Solid State Communications, 43: 385-389 (Aug 1982).
99. Ramsdell, L. S. American Mineralogist, 32: 64-68 (1947).
100. Ray, B. II-VI Compounds. New York: Pergamon Press, 1969.
101. Redfield, D. "Effect of Defect Fields on the Optical Absorption Edge." Physical Review, 130: 916-918 (1963).
102. Riehl, N. "On the Investigation of Trap and Other Disorder Structures in ZnS Phosphors." Proceedings of the International Conference on Luminescence, 1966: 9074-987. Budapest: Akademiai Akaido, 1968.
103. Rizakhanov, M. A., M. M. Khamidov, and I. Y. Abramov. "Explanation of the Characteristics of the Green-Blue Luminescence of ZnS on the Basis of a New Model of Luminescence Centers." Soviet Physics-Semiconductors, 12: 1301-1304 (1978).
104. Roberts, S. H. and J. W. Steeds. "High Resolution in Scanning Cathodoluminescence of ZnS Edge Emission." Journal of Crystal Growth, 59: 312-316 (1982).

105. Rossler, U. and M. Lietz. "Band Structure of Cubic and Hexagonal ZnS (APW)." Physica Status Solidi, 17: 597-604 (1966).
106. Ryskin, A. L., et al. "Excitons in ZnS Crystals with Stacking Faults." Physica Status Solidi (B), 49: 875-884 (1972).
107. Ryzhikov, D. and E. F. Chaikovskii. "Development of New AII-BVI Compound-Based Scintillator Materials with Isovalent Activator." Izvestiya Akademii Nauk USSR, 43, no 6: 1150-1154 (1979).
108. Samelson, H. and A. Lempicki. "Fluorescence of Cubic ZnS:Cl Crystals." Physical Review, 125: 901-909 (1962).
109. Satoh, S. and K. Igaki. "Photoluminescent Properties of ZnS Grown from Te Solution." Japanese Journal of Applied Physics, 18: 705-706 (Mar 1979).
110. Scharmann, A., D. Schwabe, and D. Weyland. "Properties of the Pb-Luminescence Centre in ZnSe, ZnS, and Some $\text{ZnSe}_{1-x}\text{S}_x$ Single Crystals." Journal of Luminescence, 18/19: 833-836 (1979).
111. Schiller, C. and M. Boulou. "Investigation of Crystal Defects by Cathodoluminescence." Phillips Technical Review, 35: 239-243 (1975).
112. Schwenkenbecher, K., et al. "Optical Transitions at Ag Centers in ZnS Crystals." Physica Status Solidi (B), 101: 215-220 (Sep 1980).
113. Shalimova, K. V., N. K. Morozova, and M. M. Malov. "UV Spectra of Donor-Doped Single Crystals of ZnS." Inorganic Materials, 11: 530-533 (Apr 1975).
114. Shalimova, K. V., et al. "Temperature Dependence of the UV Radiation of ZnS." Soviet Physics Journal, 15: 1598-1604 (Nov 1972).
115. Shalimova, K. V., N. K. Morozova, and I. A. Karetnikov. "Luminescence of ZnS Thin Films." Optics and Spectroscopy, 30: 573-576 (Jun 1971).
116. Shalimova, K. V., et al. "Edge Emission of Zinc Sulfide." Proceedings of the International Conference on Luminescence, 1966: 1196-1200. Budapest: Akademiai Akaido, 1968.

117. Sharma, R. R. and S. Rodriguez. "Exciton-Donor Complexes in Semiconductors." Physical Review, 159: 649-651 (15 Jul 1967).
118. Shionoya, S. "Review of Luminescence in II-VI Compounds." Journal of Luminescence, 12: 17-38 (1970).
119. Shionoya, S., K. Era, and Y. Washizawa. "Time Resolved Spectra of the Green-Copper Luminescence in ZnS." Proceedings of the International Conference on Luminescence, 1966: 1164-1168. Budapest: Akademiai Akaido, 1968.
120. Shionoya, S., et al. "Nature of the Red-Copper Luminescence Centre in ZnS Crystals as Elucidated by Polarization Measurements." Journal of the Physics and Chemistry of Solids, 27: 865-869 (1966).
121. Shionoya, S., H. P. Kallmann, and B. Kramer. "Behavior of Excited Electrons and Holes in Zinc Sulfide Phosphors." Physical Review, 121: 1607-1619 (Mar 1961).
122. Smith, R. A. Wave Mechanics of Crystalline Solids (Second Edition). London: Chapman and Hall Ltd, 1969.
123. Stutius, W. "Nitrogen as Shallow Acceptor in ZnSe Grown by Organometallic Chemical Vapor Deposition." Applied Physics Letters, 40: 246-248 (Feb 1982).
124. Suslina, L. G. and E. B. Shadrin. "Excitation of Exciton States in ZnS Crystals Containing Stacking Faults." Soviet Physics-Solid State Physics, 14: 243-244 (1972).
125. Sweet, M. A. S. and D. Urquhart. "Shallow Traps in ZnS Single Crystals." Physica Status Solidi (A), 54: K81-K84 (1979).
126. Taguchi, T., T. Yokogawa, and H. Yamashita. "Excitonic and Time-Resolved Edge Emissions of Iodine-Doped Cubic ZnS Crystals Excited by an Excimer Laser." Solid State Communications, 49: 551-554 (1984).
127. Taguchi, T., et al. "Luminescence Properties of Iodine-Doped Cubic ZnS Crystals and the Effect of Ion Implantation of N, P, and Ag." Journal of Crystal Growth, 59: 317-322 (1982).

128. Takagi, K. "Blue Luminescence in Copper-Activated Zinc Sulfide Phosphor." Proceedings of the International Conference on Luminescence, 1966: 1265-1270. Budapest: Akademiai Akaido, 1968.
129. Taylor, R. L., M. J. Lefebvre, P. E. Price, and M. M. Maderazzo. "Erosion Resistant FLIR Windows: Colorless ZnS". AF Wright Aeronautical Laboratories Report AFWAL-TR-84-4034, 1984.
130. Taylor, R. L. and M. Lefebvre. "Recent Progress in the Development of a Rain Erosion Resistant Water-clear ZnS (Cleartran)." Unpublished report, Contract F33615-81-C-5076, Air Force Aeronautical Systems Division, Wright-Patterson AFB, Ohio. May 1983.
131. Taylor, R. L. and R. N. Donadio. "An Infrared Alternative: Vapor-Deposited Materials." Laser Focus, 17: 41-44 (Jul 1981).
132. Tripathi, L. N., G. R. Chaubey, and C. P. Mishra. "Luminescence in ZnS:(Cu,Tb) and ZnS:(Ag,Tb) Phosphors." Physica Status Solidi (A), 60: 185-192 (1980).
133. Tsujimoto, Y., Y. Onoderf, and F. Fukai. "Preparation of a Large Single Crystal of ZnSe from the Melt." Japanese Journal of Applied Physics, 5: 636 (1966).
134. Tunitskaya, V. F., et al. "The Temperature Properties of the Individual Blue Bands of Self-Activated ZnS and the Nature of the Common Radiative Center." Journal of Applied Spectroscopy, 14: 182-186 (Feb 1971).
135. Urabe, K., S. Shionoya, and A. Suzuki. "Polarization of the Blue-Copper Luminescence in ZnS Crystals." Journal of the Physical Society of Japan, 25: 1611-1617 (1968).
136. Urbach, F. "The Long-Wavelength Edge of Photographic Sensitivity and the Electronic Absorption of Solids." Physical Review, 92: 1324-1328 (1953).
137. Van Doorn, C. Z. "Temperature Dependence of the Energy Gap in ZnS." Physica (Utr.), 20: 1155-1156 (1954).
138. van Gool, W. and A. P. Cleirin. "Self-Activated and Cu-Activated Fluorescence of ZnS." Phillips Research Reports, 15: 238-242 (1960).

139. Varni, J. G. G. "The Optical Properties of ZnSe and ZnS: Special Report." Unpublished report. AFIT School of Engineering, Wright-Patterson AFB, Ohio, 1983.
140. Vim, W. M. and E. J. Stofko. "Vapor-Phase Epitaxial Growth of CdSe on Sapphire and CdS." Journal of the Electrochemical Society, 121: 965-967 (1974).
141. Vohl, P., W. R. Buchan, and J. E. Genthe. "Thick Epitaxial Films of Cubic ZnSe and ZnS by Vapor Phase Transport." Journal of the Electrochemical Society, 118: 1842-1847 (1971).
142. Wheeler, R. G. and J. C. Miklosz. "Exciton Structure and Zeeman Effects in Zinc Sulphide." Physics of Semiconductors, Proceedings of the 7th International Congress. Paris: Dunod, 1964.
143. Williams, P. M. and A. D. Yoffe. "Bombardment of Zinc Sulphide Single Crystals with 30 keV Electrons: Light Emission." Radiation Effects, 1: 61-64 (1969).
144. Ibid. "Physical Properties of Radiation-Induced and Growth Defects in II-VI Semiconductors." In Radiation Effects in Semiconductors, edited by J. W. Corbett and G. D. Watkins. New York: Gordon and Breach, 1971.
145. Yacobi, B. G. and D. B. Holt. "Cathodoluminescence Scanning Electron Microscopy of Semiconductors." Journal of Applied Physics, 59: R1-R24 (Feb 1986).
146. Yacobi, B. G. "Temperature Shift of the Emission Edge." Physical Review B, 22: 1007-1009 (July 1980).
147. Yacobi, B. G., et al. "Phonon-generated Microfields and Temperature Dependence of the Absorption Edge in II-VI Compounds." Physical Review B, 11: 2990-2998 (Apr 1975).
148. Koda, T. and S. Shionoya. "Nature of the Self-Activated Blue Luminescence Center in Cubic ZnS:Cl Single Crystals." Physical Review, 136: A541-A543 (1964).
149. Haynes, J. R. "Experimental Proof of the Existence of a New Electronic Complex in Silicon." Physical Review Letters, 4: 361-363 (Apr 1960).

150. Merz, J. L., H. Kukimoto, K. Nassau, and J. W. Shiever. "Optical Properties of Substitutional Donors in ZnSe." Physical Review B, 6: 545-556 (Jul 1972).

VITA

Jamie Varni was born on 11 April 1955 in Sonora, California. Upon graduation from the University of Southern California in 1977, he received a Bachelor of Science degree in Physics and a commission in the United States Air Force. He received his Master of Science degree in Engineering Physics from the Air Force Institute of Technology in 1978. He has served as a Physicist and Project Officer for both the Pulsed Laser Systems Branch and the Airborne Laser Laboratory project at the Air Force Weapons Laboratory, Kirtland AFB, New Mexico. He entered the Doctoral Program in Physics at the Air Force Institute of Technology in July, 1982. He is currently Instructor of Physics, Course Director, and Laser Laboratory Director in the Department of Physics, US Air Force Academy, Colorado, 80840.

Permanent Address:

32628 Pacific Coast Highway
Malibu, California 90265

REPORT DOCUMENTATION PAGE

Form Approved
OMB No. 0704-0188

1. REPORT SECURITY CLASSIFICATION UNCLASSIFIED			1b. RESTRICTIVE MARKINGS		
2a. SECURITY CLASSIFICATION AUTHORITY			3. DISTRIBUTION / AVAILABILITY OF REPORT Approved for public release; distribution unlimited.		
2b. DECLASSIFICATION / DOWNGRADING SCHEDULE					
4. PERFORMING ORGANIZATION REPORT NUMBER(S) AFIT/DS/ENP/86-2			5. MONITORING ORGANIZATION REPORT NUMBER(S)		
6a. NAME OF PERFORMING ORGANIZATION School of Engineering		6b. OFFICE SYMBOL (If applicable) AFIT/ENP		7a. NAME OF MONITORING ORGANIZATION	
6c. ADDRESS (City, State, and ZIP Code) Air Force Institute of Technology Wright-Patterson AFB, OH 45433				7b. ADDRESS (City, State, and ZIP Code)	
8a. NAME OF FUNDING / SPONSORING ORGANIZATION		8b. OFFICE SYMBOL (If applicable)		9. PROCUREMENT INSTRUMENT IDENTIFICATION NUMBER	
8c. ADDRESS (City, State, and ZIP Code)				10. SOURCE OF FUNDING NUMBERS	
				PROGRAM ELEMENT NO.	PROJECT NO.
11. TITLE (Include Security Classification) UNCLASSIFIED THE CATHODOLUMINESCENCE OF CLEARTRAN: A NOVEL FORM OF POLYCRYSTALLINE ZnS					
12. PERSONAL AUTHOR(S) Amie G.G. Varni, B.S., M.S., Ph.D., Capt, USAF					
13a. TYPE OF REPORT PhD Dissertation		13b. TIME COVERED FROM _____ TO _____		14. DATE OF REPORT (Year, Month, Day) 1986 December	
15. PAGE COUNT 174					
16. SUPPLEMENTARY NOTATION					
17. COSATI CODES			18. SUBJECT TERMS (Continue on reverse if necessary and identify by block number) Cathodoluminescence, Luminescence, ZnS, Zinc Sulphide, Single Crystal, cvd, Exciton, Polycrystalline, Microfield, Cubic Crystal		
FIELD	GROUP	SUB-GROUP			
20	12				
19. ABSTRACT (Continue on reverse if necessary and identify by block number) Title: THE CATHODOLUMINESCENCE OF CLEARTRAN: A NOVEL FORM OF POLYCRYSTALLINE ZnS Thesis Chairman: Robert L. Hengehold Professor and Head, Dept of Engineering Physics Continued on reverse.					
20. DISTRIBUTION / AVAILABILITY OF ABSTRACT <input checked="" type="checkbox"/> UNCLASSIFIED/UNLIMITED <input type="checkbox"/> SAME AS RPT <input type="checkbox"/> DTIC USERS				21. ABSTRACT SECURITY CLASSIFICATION UNCLASSIFIED	
22a. NAME OF RESPONSIBLE INDIVIDUAL Dr. Robert L. Hengehold, Prof., AFIT/ENP				22b. TELEPHONE (Include Area Code) 513-255-4498	
				22c. OFFICE SYMBOL AFIT/ENP	

END

5-87

DTIC